Aus dem Institut für Pharmakologie und Toxikologie

(Prof. Dr. med. W.-H. Zimmermann)

der Medizinischen Fakultät der Universität Göttingen

The role of tubulin acetylation in cardiac fibroblasts

INAUGURAL-DISSERTATION

zur Erlangung des Doktorgrades

der Medizinischen Fakultät der

Georg-August-Universität zu Göttingen

vorgelegt von

Felicitas Clara Johanna Mügge

aus

Halle an der Saale

Göttingen 2018

Dekan:	Prof. Dr. rer. nat. H.K. Kroemer
Referent/in	…….
Ko-Referent/in:	……..
Drittreferent/in:	…….

Datum der mündlichen Prüfung: ……

Hiermit erkläre ich, die Dissertation mit dem Titel

"The role of tubulin acetylation in cardiac fibroblasts"

eigenständig angefertigt und keine anderen als die von mir angegebenen Quellen und Hilfsmittel verwendet zu haben.

Göttingen, den 27.04.2018

Table of contents

I. List of abbreviations

2D	Two-dimensional
3D	Three-dimensional
3T3-L1	Standard fibroblast line cultured from mouse embryo fibroblasts
AC	Adenylyl cyclase
acetyl CoA	Acetyl Co-enzyme A
ACTR3	Actin-related protein 3
ADPKD	Autosomal dominant polycystic kidney disease
Akt	Protein kinase B
ALMS1	Alstrom syndrome 1
AMCF	Adult mouse cardiac fibroblast
APS	Ammonium persulfate
ATAT1	α-Tubulin-N-acetyl-transferase
BBS	Bardet-Biedl-syndrome
bHLH	Basic helix loop helix
BrDU	Bromodeoxyuridine
BSA	Bovine serum albumin
CC-RCC	Renal cancer of the clear cell type
CD31	Cluster of differentiation 31
C.elegans	*Caenorhabditis elegans*
CEE	Chicken embryo extract
CBFHH	Calcium and bicarbonate-free Hanks´ solution with HEPES
DAPI	4´,6-diamidino-2-phenylindole
ddH2O	Double distilled water
Dido3	Death inducer obliterator 3
DMEM	Dulbecco´s modified eagle medium
DPBS	Dulbecco´s phosphate-buffered saline
ECM	Extracellular matrix
ECT	Engineered connective tissue
EDTA	Ethylenediaminetetraacetic acid
EHM	Engineered heart muscle tissue

EMT	Epithelial-mesenchymal transition
EndMT	Endothelial-mesenchymal transition
FAP	Fibroblast activation protein
FCS	Fetal calf serum
FSP-1	Fibrolast-specific protein 1
HDAC6	Histone deacetylase 6
HEF1	Human enhancer of filamentation 1
HEPES	4-(2-hydroxyethyl)-1-piperazineethanesulfonic acid
HIF-1α	Hypoxia-inducible factor 1 alpha
HVCF	Human ventricular cardiac fibroblast
IF	Immunofluorescence
IFT	Intraflagellar transport
IL-4	Interleukin 4
IMPase	Inositol monophosphatase
FITC	Fluorescein isothiocyanate
KD	Human lip fibroblasts (Karen Day)
KIF3A	Kinesin-like protein 3A
MDCK	Madin Darby canine kidney
MEF	Mouse embryonic fibroblast
NEAA	Non-essential amino acids
NHCF-V	Normal human ventricular cardiac fibroblasts
NKM	Non-cardiomyocyte medium
NMCF	Neonatal mouse cardiac fibroblasts
NMCM	Neonatal mouse cardiomyocytes
NRCF	Neonatal rat cardiac fibroblast
PAGE	Polyacrylamide gel electrophoresis
PC1/2	Polycystin-1/2
PDGF	Platelet-derived growth factor
PDGFR-α	Platelet-derived growth factor receptor α
Pen/Strep	Penicillin/streptomycin
PFA	Paraformaldehyde
PHD	Prolyl hydroxylases

PI3K	Phosphatidylinositol-4,5-biphosphate 3-kinase
PKD	Polycystic kidney disease
Pod1	Transcription factor 21
pVHL	Product of Von-Hippel-Lindau tumour suppressor gene
rhFGF-β	Recombinant human fibroblast growth factor beta
RPE-1	Immortalized cells from the pigmented epithelium of the retina
SDS	Sodium dodecyl sulfate
SEM	Standard error of the mean
siRNA	Small interfering ribonucleic acid
TBST	Tris-buffered saline with tween 20
TCF-21	Transcription factor 21
TEMED	Tetramethylethylendiamine
TGF-β1	Transforming growth factor beta 1
Tris	Tris (hydroymethyl) aminomethane
TRITC	Tetramethylrhodamine
TRP	Transient receptor potential channel
TRPV	TRP of the vanilloid family
TubA	Tubastatin A

II. List of figures

III. List of tables

1 Introduction

1.1 Heart failure and cardiac fibrosis

Heart failure and cardiac fibrosis are two pathological processes, that cannot be assessed isolated from one another. Heart failure can be either cause or consequence of cardiac fibrosis and *vice versa*. Depending on the initial condition cardiac fibrosis can be divided into a reactive and a reparative type. In case of myocardial infarction reparative cardiac fibrosis occurs to prevent ventricular rupture. The sudden death of a huge amount of cardiomyocytes causes the release of growth factors and cytokines, such as transforming growth factor β1 (TGF-β1) and interleukin 4 (Il-4) (Peng et al. 2015), thus leading to the initiation of reparative fibrosis, which can be considered as a replacement fibrosis at the previous site of the necrotic cardiomyocytes. This process aims to maintain the structural integrity of the injured heart. However, the formation of fibrotic tissue subsequently causes an impairment of the contractile cardiac function (Segura et al. 2014).

In contrast, in response to pressure overload, for example due to hypertension or aortic stenosis, the overt neuro-humoral stimulation of cardiac cells induces reactive cardiac fibrosis (Kong et al. 2014). Over time the accumulation of extracellular matrix (ECM) in the myocardium triggers cardiomyocyte death and thus systolic heart dysfunction due to an insufficient perfusion of the muscle. This then drives reparative fibrotic processes. The imbalance between ECM production and degradation leads to an increase in cardiac stiffness thus additionally causing diastolic dysfunction. Since perfusion of the myocardium mainly takes place during relaxation in diastole, it is seriously compromised. Consequently, more cardiomyocytes decay and the inflammation and the consecutive remodelling continue in a vicious circle. A further consequence of the replacement of cardiomyocytes by extracellular matrix is the uncoupling of neighbouring cardiomyocytes and therefore the disruption of the syncytium by uncoupling. As propagation of the electrical excitation and the coordinated contraction is disturbed by the presence of the isolating matrix, arrhythmias can occur (Berk et al. 2007; Stein et al. 2010).

So far cardiac fibrosis cannot be halted or reversed. The interplay in this process between the different cardiac cells is complex and is currently a matter of intense research. In particular, fibroblasts residing in the myocardium are in the spotlight of many investigations.

1.2 Cardiac fibroblasts

The healthy adult heart contains a considerable number of quiescent fibroblasts. Due to their dynamic phenotype and their different developmental origins, the determination of exact numbers is difficult. More recent studies suggest that, after endothelial cells, cardiac fibroblasts account for the second most abundant non-myocyte cell type in the heart (Pinto et al. 2016).

Cardiac fibroblasts are embedded in a mesh of interstitial cardiac matrix and react to chemical and mechanical stimuli, making them sentinel cells in the myocardium. The surrounding matrix contains, in addition to structural components, bioactive molecules such as proteases and growth factors, which are secreted by cardiac fibroblasts and other cardiac cells. Cardiac fibroblasts can be activated quickly after cardiac damage due to manifold changes in their environment. This induces their transdifferentiation into myofibroblasts and subsequently the fibrotic process (Kong et al. 2014). Myofibroblasts can be distinguished by different features and are termed myofibroblasts due to similarities with smooth muscle cells. Myofibroblasts possess prominent microfilaments and expresses α-smooth muscle actin, the typical actin isoform in vascular smooth muscle cells (Bochaton-Piallat et al. 2016). By this myofibroblasts gain the ability to develop contractile forces. Thus, myofibroblast activation and reaction leads to wound contraction and results in a collagen-based scar for example following myocardial infarction.

It has been suggested, that the main source of myofibroblasts during tissue repair after myocardial infarction are proliferating resident fibroblasts (Yano et al. 2005). However, other origins may also contribute to the myofibroblast population. Bone marrow-derived cells, also called fibrocytes, are another well documented source of myofibroblasts (Möllmann et al. 2006; Chu et al. 2010). In addition, epicardial epithelial and vascular endothelial cells undergoing respectively an epithelial- and endothelial-mesenchymal transition (EMT, EndMT), and pericytes are also known sources of cardiac myofibroblasts (Zhou and Pu 2011; Wu et al. 2013; Montorfano et al. 2014).

Irrespective of their origin, myofibroblasts secrete more factors than quiescent cardiac fibroblasts. This includes not only structural components such as collagens, but also cytokines. The latter drive the intense inflammatory process and the recruitment of other cells, which finally contributes to the pool of cardiac myofibroblasts (Fig.1). As a consequence, the balance of ECM production and degradation is shifted towards its deposition (Brown et al. 2005).

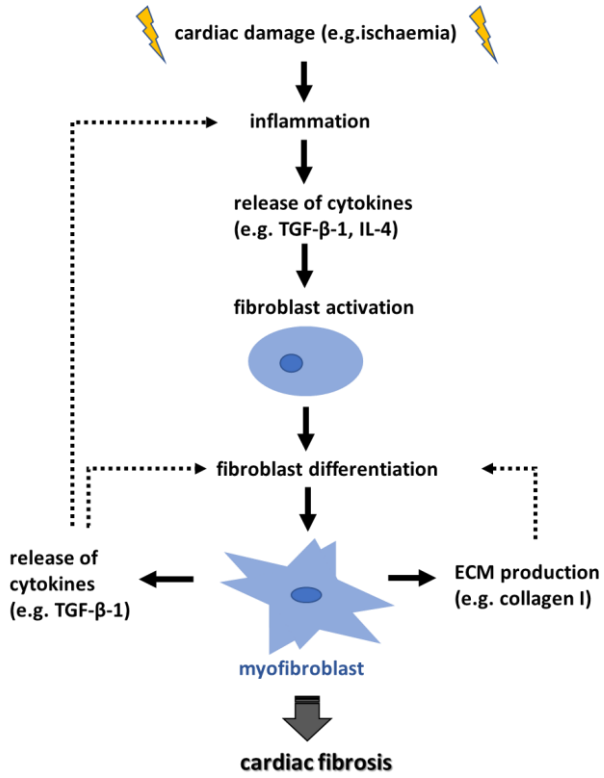

Figure 1: Schematic overview of cardiac fibrosis. Upon a stimulus associated with cardiac damage, an inflammatory reaction is triggered. Mediators such as TGF-β1 and Il-4 are released and stimulate the transdifferentiation of fibroblasts to myofibroblasts. The activated myofibroblasts produce extracellular matrix, contributing to fibrotic replacement of the dead cardiomyocytes and resulting in scar tissue and cardiac fibrosis.

One of the problems in analysing cardiac fibroblasts is the lack of specific markers. Various markers have been discussed, but so far none of them is well-established. The problem in finding an adequate marker has several reasons: cardiac fibroblasts can be derived from various sources and additionally, cardiac fibroblasts undergo significant changes upon their activation, as described before. This influences the proteome and thereby the pattern of marker expression (Matthijs Blankesteijn 2015). During development, signalling mediated via platelet derived growth factors (PDGF) α/β play an important role. The receptor PDGFR-α can be used as a marker for mesenchymal cells, to which fibroblasts belong (Olson and Soriano 2009). However, it was recently shown that the newly identified interstitial telocytes in the myocardium can be also characterised by PDGF receptor expression. Fibroblast activation protein alpha (FAP) has also been suggested as a marker for activated fibroblasts (Tillmanns et al. 2015) however quiescent fibroblasts would, in this case, not be detected. One further potential marker is fibroblast-specific protein 1 (FSP-1). But FSP-1 lacks specificity, since it has been detected in hematopoietic cells, endothelial cells, or vascular

smooth muscle cells as well. A more suitable marker is periostin, which marks cells morphologically compatible with myofibroblasts, but which was not detected in quiescent cardiac fibroblasts (Kong et al. 2013). Periostin was found to be expressed in connective tissue cells facing mechanical stress (Horiuchi et al. 1999). Accordingly, it can be found in activated cardiac fibroblasts. Transcription factor 21 (TCF-21; epicardin/Pod1/capsulin) belongs to the basic helix-loop-helix (bHLH) family of transcription factors and has been shown to be required for the epithelial-mesenchymal transition. It marks fibroblasts, but can also be found in coronary vascular smooth muscle cells (Acharya et al. 2012).

Identifying fibroblasts remains a critical topic, since the current known markers are either restricted to activated or quiescent fibroblasts, do not sufficiently detect fibroblasts from different origins or are not specific and expressed in other cells types as well. Hence, the identification of these cells is based on morphological criteria. They possess a spindle-shaped cell body, from which several processes branch out. In addition, fibroblasts are characterised by their Golgi apparatus and rough endoplasmic reticulum, which are very prominent (Souders et al. 2009). These traits are probably due to the high protein synthesis and secretion activity.

Their highly dynamic character and crucial role in the development of cardiac fibrosis make cardiac fibroblasts a prime target for research in the field of heart failure. A better understanding of cardiac fibroblast is the key to preventing unnecessary development of collagen scars, or even to reverse pathological cardiac remodelling.

1.3 Primary cilia

1.3.1 Microtubule structures form primary cilia

Primary cilia are cellular structures largely composed of a microtubule skeleton. In contrast to motile cilia, which are composed of 9 outer microtubule doublets and one doublet in the middle, primary cilia lack the core microtubule doublet and the surrounding proteins, which enable motile cilia, such as flagella, to produce motility (Satir et al. 2010). Thus, primary cilia are considered immotile microtubule structures, with the exception of primary cilia found at the embryonic node (Kim and Dynlacht 2013).

Figure 2 illustrates the structure of primary cilia, which emanate from the cell surface as solitary structures, covered by the plasma membrane. The primary cilium itself is built by vesicles which are transported from the Golgi apparatus to the cilium (Davis et al. 2006).

The primary cilium's axoneme extends from a basal body, that is derived from the mother centriole (Marshall 2007), which is prior to ciliogenesis part of the centrosome and microtubule organising centre. Several changes distinguish the basal body from the mother centriole. Among those basal body specific features are transition fibers, which aid the docking of the basal body to the ciliary membrane (Veland et al. 2014).

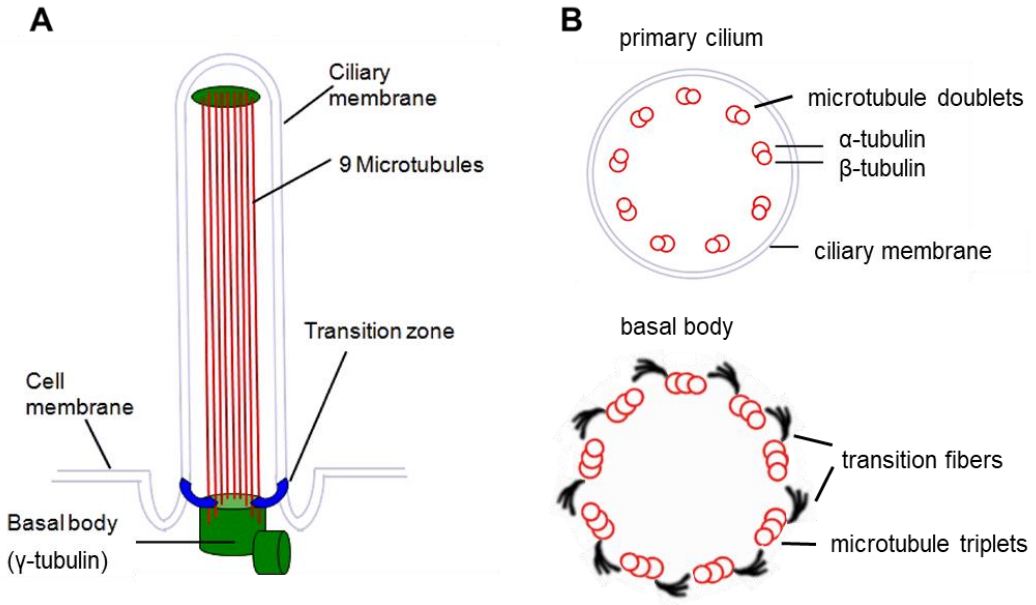

Figure 2: Schematic presentation of primary cilia structure. A) Schematic longitudinal section of a primary cilium. The primary cilium consists of a microtubule-based cytoskeleton covered by the ciliary membrane, which invaginates at the basis to form the ciliary pocket. Transition fibers connect the basal body to the ciliary pocket. B) Schematic horizontal section of microtubule structures of the ciliary axoneme (upper image) and of the basal body (below). The shaft of the cilium is composed of 9 outer microtubule doublets and transforms into 9 triplets in the basal body (adapted from Schimmack et al. 2016).

The microtubule doublets stabilising the ciliary shaft are composed of protofilaments. Thirteen protofilaments form a hollow microtubule cylinder and two of those cylinders build one microtubule doublet. The basis of the protofilaments are polymerised α- and β-tubulin dimers. As further described in section 1.4, α-tubulin undergoes various post-translational modifications, among them the intraluminal acetylation. Therefore, antibodies against acetylated α-tubulin can be used to visualise the primary cilium's shaft by immunofluorescence. A paralogue of α- and β-tubulin is γ-tubulin, which can be found in the basal body. In complexes with other proteins, γ-tubulin facilitates microtubule nucleation (Kollman et al. 2010). For primary cilia formation all three tubulin-isoforms and their correct

assembly are needed. To identify primary cilia structures the detection and characteristic co-localisation of α- and γ-tubulin in the shaft and the basal body, respectively, can be used.

1.3.2 Regulation of primary cilia formation and length

A substantial number of factors has been reported to contribute to primary cilia formation and length regulation.

One process that is crucial for primary cilia formation and maintenance, is intraflagellar transport (IFT) (Kozminski et al. 1993). Structures such as cilia and flagella are subjected to constant turnover. For this, a continuous input of α- and β-tubulin subunits is required to maintain length (Marshall and Rosenbaum 2001). In consequence, the assembly and disassembly of microtubule structures, such as the axoneme of cilia, demands the presence of soluble tubulin, which can be incorporated into the distal end of the cilium. Taxol, which inhibits depolymerisation of microtubules leads to a reduction of soluble tubulin subunits and thereby decreases length of cilia and flagella (Sharma et al. 2011).

Moreover, inhibition of actin polymerisation caused by cytochalasin D has been demonstrated to elongate cilia and support ciliogenesis. The actin-related protein ACTR3, which is required for actin polymerisation, was found to be an important regulator of ciliogenesis as its knockdown led to an elongation of primary cilia (Kim et al. 2010).

Primary cilia are regulated by environmental stimuli, for example by hypoxia. *In vivo* hypoxia can be caused by various different conditions, such as ischemia or injury. The processes of tissue impairment and reparation are complex, although hypoxia can be considered as one of the main factors contributing to the demise of cells. A change in primary cilia length has been documented for example upon tubular injury (Verghese et al. 2008). In this context it was demonstrated, that cobalt chloride, which stabilises hypoxia inducible factor alpha (HIF1-α), led to an elongation of primary cilia in Madin Darby canine kidney cells (Verghese et al. 2011). Which consequences this elongation of primary cilia under hypoxia has, remains to be elucidated.

Another substance that is known to increase primary cilia length is lithium chloride. The exact mechanism by which the mood stabiliser causes this effect, has yet to be elucidated. It is likely, that the mechanism is mediated via the glycogen synthase kinase 3β (GSK-3β) (Klein and Melton 1996). Various downstream pathways of GSK-3β inhibition are under discussion, e.g. the mobilisation of ATAT1 (Nakakura et al. 2015; see section 1.3.3). Other

factors have been shown to influence primary cilia length, but these will not be discussed further, as they are beyond the scope of this thesis.

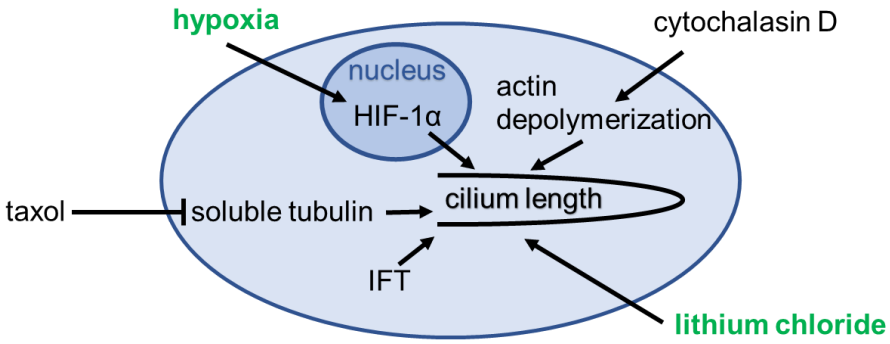

Figure 3: Factors that contribute to primary cilia length. Scheme of positive and inhibitory effects on the length of primary cilium. Hypoxia and LiCl are highlighted, both factors were analysed in the performed experiments.

1.3.3 The primary cilium as a sensory organelle

Primary cilia can fulfil a variety of functions, including a role as mechanosensors. A mechanical stimulus, e.g. fluid flow, first leads to a deflection of the cilium. For renal epithelium it has been shown that fluid flow initiates an intracellular calcium signal, which can also spread to surrounding cells, presumably via gap junctions (Praetorius and Spring 2001). The ability and sensitivity of primary cilia to react to fluid flow increases with enhanced ciliary length (Resnick and Hopfer 2007). On the other hand, flow was demonstrated to influence primary cilia formation. The endothelium, for example, carries primary cilia especially in regions with reduced or disturbed flow. These regions are susceptible to atherosclerosis (Conway und Schwartz 2013).

One of the channels thought to play a key role in the calcium signalling of primary cilia is polycystin-2 (PC2). It belongs to a subfamily of the transient receptor potential (TRP) channels and is mainly located at the membrane of the endoplasmic reticulum (Koulen et al. 2002). Another example for TRP channels can be found in primary cilia of neurons in *Caenorhabditis elegans* (*C. elegans*). Here TRPV (TRP of the vanilloid family) channel proteins were found to be important for sensory transduction and adaptation. In addition to their mechanosensory function, TRP channels in cilia of sensory neurons in *C. elegans* react to chemical stimuli such as high osmolarity (Tobin et al. 2002). Besides their role in mechanosensing, primary cilia also serve as environmental sensors for light and odorant detection (Berbari et al. 2009).

1.3.4 Primary cilia play a role in different tissues and their dysfunction plays a role in various diseases

The importance of primary cilia becomes especially obvious by the variety of tissue and organ deficiencies associated with ciliary defects.

One example for a genetic ciliopathic disorder in humans is the Bardet-Biedl-Syndrome (BBS). It is caused by defects in the genes encoding the BBS proteins, which are important for the function of cilia and the basal body (Ansley et al. 2003). The BBS comprises a variety of symptoms, including retinopathy, obesity, polydactyly, hypogonadism, cognitive impairment and polycystic kidneys. The involvement of other organ systems has also been reported, e.g. congenital heart defects (Elbedour et al. 1994).

In respect to the classification as ciliopathy, the proteins BBS-7 and BBS-8 have been shown to play key roles in the process of IFT and their loss of function results in cilia defects (Blacque et al. 2004). In addition, mutations in BBS-genes have been shown to lead to defects in mechano- and thermosensation in mice, probably caused by the dysfunction of cilia in sensory neuron of the skin (Tan et al. 2007).

Another rare genetic disorder, which belongs to the group of ciliopathies and shows similarity in its symptoms to the BBS, is the Alstrom syndrome. The underlying defect is a mutation of the ALMS1 gene. The encoded protein localises to ciliary basal bodies and a mutation in the ALMS1 gene has been shown to cause impaired cilia in kidney epithelial cells in mice (Li et al. 2007). Interestingly, autopsies of patients with Alstrom syndrome revealed fibrosis of various organs, for example of liver and kidney (Marshall et al. 2005). This raises the question of a potential role of defect cilia in the development of organ fibrosis.

Other proteins, localised to primary cilia, are polycystin-1 (PC1) and -2 (PC2). Defects in those proteins lead to autosomal dominant polycystic kidney disease (ADPKD). Primary cilia on kidney epithelial cells are important for a downright tissue morphogenesis. Hence, a defect of PC1 or PC2 leads to an impaired mechanosensation and results in the development of multiple renal cysts (Nauli et al. 2003).

Loss of function of primary cilia has also been related to tumorigenesis, such as the development of ovarian cancer (Egeberg et al. 2012), cholangiosarcoma (Gradilone et al. 2017) or pancreatic ductal adenocarcinoma (Schimmack et al. 2016).

1.3.5 Primary cilia in the heart

Primary cilia at the embryonic node are involved in the formation of the left-right body asymmetry by facilitating a laminar nodal flow (McGrath and Brueckner 2003). This asymmetry determines the distribution of whole organs, such as the liver and the stomach. It is also important for proper development of the heart, which is asymmetric in itself and in correlation to its connecting vessels (Koefoed et al. 2014).

In addition, primary cilia are involved in cardiomyocyte differentiation. Important components of the hedgehog signalling pathway, which plays a role in the development of various cell types, localise to the primary cilium, which thus contributes to cardiogenesis (Clement et al. 2009). Cardiac primary cilia also coordinate TGF-β signalling during cardiomyogenesis (Koefoed et al. 2014).

Apart from those findings referring to the developmental role of primary cilia in the heart, it can also be speculated that their versatile sensory abilities and involvements in signalling pathways may be of importance in the adult heart as well.

1.4 Tubulin acetylation

1.4.1 Post-translational acetylation of α-tubulin

After incorporation into microtubules, tubulin undergoes different post-translational modifications. Among them phosphorylation (Eipper 1974), detyrosination (Barra et al. 1973), glutamylation (Edde et al. 1990), glycylation (Redeker et al. 1994) and acetylation (L'Hernault und Rosenbaum 1983). The last one stands out since the α-tubulin-acetylation is the only modification which is located at the intraluminal side of the microtubules (Soppina et al. 2012).

This intraluminal acetylation takes place at the ε-amino-group of lysine 40 (K40) of α-tubulin and is catalysed by α-tubulin-N-acetyl-transferase (ATAT1) (Shida et al. 2010). ATAT1 transfers the acetyl group of acetyl Co-enzyme A to K40 of α-tubulin. The adversary of the acetyl-group transferring ATAT1 is the histone deacetylase 6 (HDAC6), which possesses the capacity to cleave acetyl groups from histones, but which is also the main deacetylase of α-tubulin.

Increased levels of acetylated tubulin can be detected in long-lived microtubules, that are found for example in axonemes and basal bodies of cilia and flagella (Piperno and Fuller 1985).

1.4.2 HDAC6 and its inhibition

There are 4 classes of histone deacetylases, grouped based on their sequence homology. Class I, II and IV HDACs gain their catalytic activity via a zinc-binding domain. HDAC6 is a class IIb histone deacetylase which is located in the cytoplasm and contributes to the regulation of tubulin stability and thus influencing mitosis (Hubbert et al. 2002). HDAC6 had been detected in higher density at the basal body of primary cilia and was found to be associated with their disassembly (Ran et al. 2015). Gradilone et al. have shown, that overexpression of HDAC6 in cholangiosarcoma cells induced deciliation in cholangiocytes, which in consequence led to a higher proliferation rate of those cells. This increased proliferation capacity could be reverted by the knockdown of HDAC6 and by HDAC6 inhibition with tubastatin A (Gradilone et al. 2013).

HDAC inhibitors have been used in cancer therapy for a while (Secrist et al. 2003). Using unspecific HDAC inhibitors bears a high risk of undesirable side effects. For this reason, the development of specific HDAC inhibitors is a current target in research. With tubastatin A, a highly specific HDAC6 inhibitor has been developed (Butler et al. 2010). Tubastatin A was shown to have neuroprotective (Zhang et al. 2014b) and anti-inflammatory effects (Vishwakarma et al. 2013) and is thought to be a promising therapeutic drug. Moreover, a certain role of HDAC6 in pathological cardiac remodelling can be assumed, since it has been demonstrated, that HDAC6 inhibition prevents the contractile dysfunction as a consequence to tachypacing (Zhang et al. 2014a).

The combination of the anti-proliferative and anti-inflammatory effect of HDAC6 inhibition by tubastatin A and its impact on the prevention of contractile dysfunction, directs the focus on the role of HDAC6 in cardiac fibroblasts, too.

1.4.3 ATAT1 and its mobilisation by lithium chloride

ATAT1 is the major acetyl-transferase in mammals (Kalebic et al. 2013). The enzymatic transfer rate of ATAT1 is relatively low due to the position of the enzymatic binding. Therefore, only stabile microtubule structures possess a considerable amount of acetylated α-tubulin (Szyk et al. 2014).

It has been shown in human fibroblast KD cells that ATAT1 can be mobilised by treatment with lithium chloride. Lithium chloride is used in the clinic as a mood stabiliser in prevention of bipolar disease. The mobilisation of ATAT1 is probably mediated via the inhibition of the glycogen synthase kinase 3β (GSK-3β) via excessive phosphorylation of this protein.

In consequence, the acetylation of α-tubulin is increased and primary cilia are elongated (Nakakura et al. 2015).

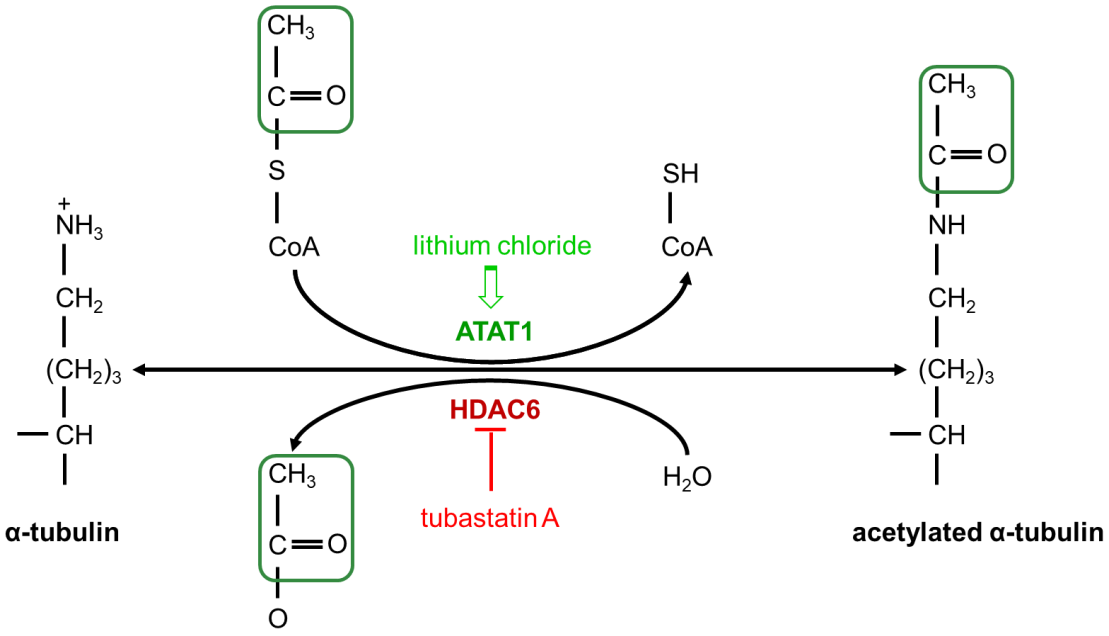

Figure 4: Acetylation of α-tubulin. ATAT1 transfers an acetyl group from acetyl-CoA to the ε-Amino-group of lysine 40 (K40) of α-tubulin. HDAC6 catalyses the split-off of the acetyl-group from α-tubulin.

1.5 Aim of the project

Cardiac fibrosis impairs cardiac function and leads to heart failure. Understanding its pathogenesis and the mechanisms behind the pathological cardiac remodelling will help to identify targets for anti-fibrotic treatment and thus improve quality of life and prognosis of patients with heart failure.

Cardiac fibroblasts play a central role in cardiac fibrosis and thus are the key to new therapeutic approaches. They possess the ability to react to chemical and mechanical stimuli. As sensory organelles, primary cilia contribute to such environmental adaptations in other cells.

The first part of the project was to investigate whether cardiac fibroblasts from different species and maturation states possess primary cilia in 2D cultures. If so, we then wished to address whether primary cilia are present in homogenous and heterogeneous 3D cultures of cardiac fibroblasts.

Acetylated α-tubulin marks stabilised microtubule structures and an increase in acetylated α-tubulin, either as consequence of a knockdown of the monomeric GTPase RhoA or induced by inhibition of HDAC6 with tubastatin A, had been found in cardiac fibroblasts in former studies of the group of Professor Lutz (Jatho et al. 2015). Hence, the regulation of tubulin acetylation in cardiac fibroblasts and its impact on primary cilia regulation were studied more intensely during this project. For this, in addition to the effect of tubastatin A as a specific HDAC6 inhibitor, the influence of lithium chloride was elucidated. In addition, as an important environmental change occurring in the diseased heart, the effect of hypoxia on primary cilia regulation was part of the proposed project.

Finally, the changes in tubulin acetylation and primary cilia regulation on a biological process should be evaluated. For this, proliferation assays were performed.

2 Materials

2.1 Animals

Wistar-Kyoto Rats, Charles River, Sulzfeld

NMRI mice, Zentralinstitut für Versuchstierzucht, Hannover

Wild type C57BL/6J adult mice, Charles River, Sulzfeld

2.2 Cells

Neonatal rat cardiac fibroblasts (NRCF), see method section 3.1.1 and 3.1.2 for detailed isolation procedure

Neonatal mouse cardiac fibroblasts (NMCF), see method section 3.1.1 and 3.1.3 for detailed isolation procedure

Adult mouse cardiac fibroblasts (AMCF), see method section 3.1.4 for detailed isolation procedure

Normal human cardiac fibroblasts (ventricle, NHCF-V), Cat. No. CC-2904, Lonza

2.3 Chemicals, reagents and consumables

Table 1: Fine chemicals and reagents

Reagent	**Company**
10% Triton X-100	Carl Roth
Acrylamide solution rotiphorese gel 30	Carl Roth
Ascorbic acid	AppliChem
BrDU	
DAPI (4',6-diamidino-2-phenylindole)	Sigma-Aldrich
Fluoromount	Sigma-Aldrich
Igepal CA-630	Sigma-Aldrich
Lithium chloride	Sigma-Aldrich
Lumi-LightPLUS western blotting substrate	Roche
Neonatal heart dissociation kit, mouse and rat	Miltenyi Biotec
Paraformaldehyde (PFA)	Sigma-Aldrich
PhosphoSTOP phosphatase inhibitor cocktail tablets	Roche Applied Science
Ponceau-S	Sigma-Aldrich
Protein marker „Roti-Mark Standard“	Carl Roth
Roti-Block (blocking reagent)	Carl Roth
Sodium dodecyl sulfate (SDS)	AppliChem

Tetramethylethylenediamine (TEMED)	Merck
TRITC-phalloidin	Sigma-Aldrich
Triton X-100	Carl Roth
Tubastatin A	Sigma-Aldrich
Tween-20	Carl Roth

Table 2: Consumables

	Specification	**Company**
Cell culture flasks	T25, T75, T175	Sarstedt
Cell culture plates	6 cm, 10 cm, 15 cm	Sarstedt
Cell culture multi well plates	6 well, 12 well	Sarstedt
Cell culture multi well plates	24 well	Greiner Bio One
Cell scraper	1.7 cm blade	Sarstedt
Microscope slides	24 x 50 mm, Menzel	Thermo Scientific
Cover slips	18 mm Ø, Menzel	Thermo Scientific
Filter Tips	10 µl, 100 µl, 1000 µl	Greiner Bio One
gentleMACS	C tubes	Miltenyi Biotec
Microscope cover glasses	22 mm	Thermo Scientific
Multi tips	2 ml, 5 ml, 10 ml	Eppendorf
Nitrocellulose membrane, Protran	Pore size 0.2 µM	Whatman, GE Healthcare
Pipette tips	10 µl, 100 µl, 1000 µl	Sarstedt
Rat EHM/ECT molds	Inner diameter 8 mm, outer diameter 16 mm, depth 5 mm, 2 moulds per 50 mm glass dish	Internal production of the Institute of Pharmocology and Toxicology, UMG
Sterile pipettes	2 ml, 5 ml, 10 ml, 25 ml	Sarstedt
Reaction and centrifuge tubes	15 ml, 50 ml	Greiner Bio One
Wide opening, serological pipettes	10 ml	Falcon

2.4 Devices

Table 3: Devices

Device	Type	Company
Autoclave	VX-150	Systec
Automated multiparameter cell analysis machine	Cellavista	SynenTec
Blotting chamber	Mini Trans-Blot Cell	Bio-Rad Laboratories
Cell counter and analyzer	CASY Model TTC	Roche
Cell counting chamber	Neubauer	Labor Optik
Cleanbench	Hera Safe KS 12	Thermo Electron
Centrifuges	Centrifuge 5804R	Eppendorf
	Megafuge 3.OR	Heraeus Sepatech
Chemiluminescence imager	ChemiDoc MP	Biorad
Confocal microscope Microscope objective 10x Microscope objective 20x Microscope objective 63x	LSM 710 EC Plan-Neofluar|0.3 EC Plan-Neofluar|0.5 Plan-Apochromat|1.4 oil	Zeiss Zeiss LSM 710 Zeiss LSM 710 Zeiss LSM 710
gentleMACS	Dissociator	Miltenyi Biotec
Gel electrophoresis chamber	Mini-Protean Tetra	Bio-Rad Laboratories
Inverted fluorescence microscope Microscope camera Microscope filter blue Microscope filter red Microscope filter green Microscope objective 4x Microscope objective 10x Microscope objective 20x Microscope objective 40x Microscope objective 60x	IX81 XM10 350 DAPI 575 TxRed 485 FITC UPlanFLN4xPh UPlanFLN10xPh LUCPlanFLN20xPh LUCPlanFLN20xPh PlanApo N60x|1.42 oil	Olympus Olympus Olympus Olympus Olympus Olympus Olympus Olympus Olympus Olympus
Heating block	Thermomixer comfort Thermomixer compact	Eppendorf

Heating plate (magnetic)	RCT basic	Janke u. Kunkel IKA Labortechnik
Incubators	Cell culture, 37°C, 5% CO_2	Labotec
	CB159	Binder, Tuttlingen
Large scale shaker	Innova 4300	Eppendorf
Oxygen-controlled workstation	Sci-tive	Baker Ruskin Technologies, Bridgeend, UK
pH meter	Inolab pH	Wtw
Rotation shaker	Reax 3	Heidolph
Shaker	3016	GFL
Sterile hood	Telstar Bio II A	Prettl
Table centrifuge	Centrifuge 5415D	Eppendorf
Vibratome	Leica VT1000S	Leica
Vortexer	VF2	W. Krannich

2.5 Cell culture media and additives

Table 4: Additives for cell culture

Reagent	**Company**
10x DPBS (Dulbecco's phosphate buffered saline), w/o calcium and magnesium chloride	Life Technologies
CASYton	OLS OMNI Life Science
Chicken embryo extract (CEE)	Self-made
Collagen I (rat tail)	own production
DMEM (Dulbeccos modified eagle medium) powder 10x	BD Biosciences
DMEM/F12 Glutamax, Cat-No. 31331-028	Life Technologies
DMEM GlutaMAX 1 g/l glucose, pyruvate Cat-No. 21068-028	Life Technologies
DMEM GlutaMAX, 1 g/l glucose Cat-No. F 04150	Biochrom
DMEM GlutaMAX 4.5 g/l glucose Cat-No. 42430-025	Life Technologies
DPBS (Dulbecco's phosphate buffered saline), w/o calcium and magnesium chloride	Life Technologies

Fetal bovine serum (FBS)	Life Technologies
Fibroblast growth medium-3 (FGM-3) BulletKit (CC-3131 & CC-4525)	Lonza
Horse serum	Life Technologies
Matrigel basement membrane matrix	BD Biosciences
Non-essential amino acids (NEAA), 100x	Life Technologies
Penicillin-streptomycin (P/S), 100x (10000 U/ml penicillin, 10000 µg/ml streptomycin)	Life Technologies
Trypan blue (0.4%)	Fluka
TrypLE Express	Life Technologies
Trypsin-EDTA (0.05%)	Life Technologies

Table 5: Cell culture media and solutions

Isolation of neonatal cardiac cells	
Calcium and bicarbonate free Hank's with HEPES (CBFHH)	40 ml NaCl stock (200 g/l) 10 ml $MgSO_4$ stock (20 g/l) 10 ml KH_2PO_4 stock (6 g/l) 10 ml Na_2HPO_4 2 H_2O (5.95 g/l) 10 ml Glucose dehydrate stock (100 g/l) ddH_2O up to 1l, sterile filtered, pH 7.4 with NaOH
Heat-inactivated FBS	50 ml FBS were incubated in a water bath at 56°C for 30 min
Non-cardiomyocyte medium (NCM)	DMEM GlutaMAX 1 g/l glucose 10% FBS (v/v, heat-inactivated) 1% P/S (v/v)
Neonatal heart dissociation kit, mouse and rat (Miltenyi Biotec)	Buffer X Buffer Y Enzyme A (reconstituted with 1 ml buffer A) Enzyme D (reconstituted with 3 ml DMEM) Enzyme P (ready to use)

Neonatal mouse cardiomyocyte medium (NMCM)	DMEM GlutaMAX 1 g/l glucose, 3.7 g/l $NaHCO_3$ 10% FBS (v/v) 1% P/S (v/v) 1% BrDU
NRCF/NMCF culturing	
Growth medium	DMEM GlutaMAX 4.5 g/l glucose 10% FBS active (v/v) 1% P/S (v/v) 1% NEAA (v/v)
Serum-depleted medium	DMEM GlutaMAX 1 g/l glucose 1% P/S (v/v) 1% NEAA (v/v)
Generation of engineered cardiac fibroblast tissue from NRCF (ECT)	
2x DMEM	20% 10x DMEM 20% FBS (v/v) 2% P/S (v/v) in ddH_2O, sterile filtered
Generation of engineered heart muscle from NRCF (EHM)	
EHM medium	DMEM, 1g/l glucose, NaHCO3 11.6% Horse serum 2.3% CEE 1% P/S (v/v)
AMCF culturing	
Growth medium	DMEM/F12 GlutaMAX 10% FCS active (v/v) 1% P/S (v/v) 100 µM Ascorbic acid
HVCF culturing	
Growth medium	FGM-3 basal medium 0.1% rhFGF-β (r-human FGF- β) 0.1% Insulin 0.1% GA-1000 (Gentamycin, Amphotericin) 10% FCS

2.6 Buffers and solutions

Table 6: Buffers and solutions

Immunofluorescence	
4% Paraformaldehyde (PFA)	40 g Paraformaldehyde 200 µl 10 N NaOH 100 ml 10x DPBS pH 7.0 with HCl, ddH_2O to 250 ml
0.2% Triton X-100	1 ml 10% Triton X-100 DPBS to 50 ml
1x Roti block	5 mL Roti-Block ddH_2O to 50 ml
Blocking and permeabilization buffer for immunostaining of samples on cover slips	5 ml FCS 1 ml 10% Triton X-100 DPBS to 50 ml
Blocking and permeabilization buffer for immunostaining of vibratome sections	5 ml Roti-block 1 ml 10x Triton X-100 ddH_2O to 50 ml
SDS-PAGE and immunoblot	
Lysis buffer (GST-Fish)	50 mM Tris 150 mM NaCl 2 mM $MgCl_2$ 10% Glycerol (v/v) 1% Igepal CA-630 (v/v) pH 7.4 with HCl dd$H_2$0 to 1 l Phosphatase inhibitor cocktail added prior to use
4x SDS-PAGE sample buffer w/o glycerol	1% β-Mercaptoethanol (v/v) 200 mM Tris (7.4) 5.7 g SDS 0.2 g Bromophenol blue in ddH2O, pH 7.4
10% APS	1 g APS ddH_2O to 10 ml

10% SDS	10 g SDS ddH_2O to 100 ml
5x SDS-PAGE buffer	30.2 g Tris 188 g Glycine 10 g SDS pH 8.3 with HCl ddH_2O to 2 l
1x SDS-PAGE buffer	400 ml 5x SDS-PAGE buffer ddH_2O to 2 l
1x Immunoblot buffer	6 g Tris 28.8 g Glycine 400 ml Methanol H_2O to 2 l, pH 8.4
10x Tris-buffered saline (TBS)	24.2 g Tris 175.3 g NaCl pH 7.4 with HCl ddH_2O to 2 l
1 x TBS with tween-20 (TBST)	200 ml TBS 2 ml Tween-20 ddH_2O to 2 l
Ponceau-S solution	0.2 g Ponceau-S 3 ml Acetic acid ddH_2O to 100 ml

2.7 Antibodies

Table 7: Primary antibodies for immunoblot and immunofluorescence analysis

Primary Antibody against	**Dilution**		**Species**	**Clone**	**Company**
	WB	IF			
β-actin	1:5000	-	Mouse	AC-47	Sigma-Aldrich

Caveolin-3	-	1:500	Rabbit	Polyclonal, ab2912	Abcam
CD31	-	1:100	Rabbit	Polyclonal, ab28364	Abcam
α-Tubulin	1:5000	-	Mouse	monoclonal B-5-1-2, T5168	Sigma-Aldrich
Acetylated α-tubulin	1:2000	1:1000	Mouse	monoclonal/ 6-11B-1, T6793	Sigma-Aldrich
γ-Tubulin	1:100	1:500	Rabbit	Polyclonal/T3559	Sigma-Aldrich

Table 8: Secondary antibodies for immunoblot analyses

Secondary antibody against	Dilution	Species	Cat No./Company
anti-mouse-IgG-horse-radish peroxidase conjugate	1:10000	Goat	031M4752 Sigma-Aldrich
anti-rabbit-IgG-horse-radish peroxidase conjugate	1:40000	Goat	119K4815 Sigma-Aldrich

Table 9: Secondary antibodies for immunofluorescence analyses

Secondary antibody against	Dilution	Species	Cat No./Company
AlexaFluor 488 anti-mouse conjugate	1:500	Goat	115-545-003, Jackson Immuno Research
AlexaFluor 594 anti-rabbit conjugate	1:500	Goat	111-475-144, Jackson Immuno Research

2.8 Software

Table 10: Software

Analyses	Software
Confocal images	Zen 2012 (Zeiss)
Image processing & analyses	ImageJ/Fiji
Immunoblot	ImageLab 5.1 (Biorad Laboratories)
Immunofluorescence	Xcellence pro (Olympus)
Proliferation assay	Cellavista
Statistical calculations/ graphical drawing	GraphPad Prism 5.0

3 Methods

3.1 Cell biology methods

3.1.1 Preparation of cardiac cells from neonatal rats and mice

Cardiac fibroblasts were isolated from neonatal Wistar rat hearts (postnatal day 0 to 3) and neonatal NMRI mouse hearts (postnatal day 2 to 4) using the neonatal heart dissociation kit, mouse and rat (gentleMACS, Miltenyi Biotec). The isolation was performed according to the protocol provided by the manufacturer.

First, neonatal rats and mice were sacrificed by decapitation, thoracotomy was performed and the complete hearts were taken out and transferred into a 10 cm cell culture dish containing ice-cold CBFHH buffer (rat hearts) or DPBS-buffer (mouse hearts). The following steps were performed on ice and under sterile conditions. To extract ventricular cells only the vascular pedicles and the atria were removed.

The ventricles were washed twice to remove dispensable blood and afterwards cut into pieces of 1-2 mm^3 size and washed again using CBFHH or DPBS buffer for rat and mouse hearts, respectively.
Enzyme mix 1 and 2 were prepared (Table 11), enzyme mix 1 was pre-warmed at 37°C for 5 min and afterwards added to enzyme mix 2.

Table 11: Preparation of enzyme mixes for digestion of neonatal cardiac cells

Number of neonatal rats/mice	**Total volume**	**Enzyme mix 1**		**Enzyme mix 2**		
		Enzyme P	Buffer X	Buffer Y	Enzyme A	Enzyme D
1	0.125 ml	3.125 µl	160 µl	1.25 µl	0.625 µl	5 µl
40	5 ml	125 µl	4600 µl	50 µl	25 µl	200 µl
60	7.5 ml	187.5 µl	6900 µl	75 µl	37.5 µl	300 µl

The ventricular tissue was transferred to gentleMACS C tubes with tissue of 20 up to 30 hearts per tube. Afterwards the appropriate enzyme mix was added, e.g. 2.5 ml for 20 hearts, and the samples were incubated without agitation at 37°C for 12 min (mouse hearts) or 15 min (rat hearts). Then, the C tubes were attached onto the sleeve of the gentleMACS dissociator and the program htumor3.01 was used for the subsequent dissociation of the tissue. Incubation and dissociation were repeated 3 times alternately.

3.1.2 End of digestion process and separation of cardiac fibroblasts and cardiomyocytes of neonatal rat hearts

The digestion process was stopped by resuspending the cells in 7.5 ml of NCM medium. The suspension was strained with a mesh of stainless steel (250 µm pores) and centrifuged for 20 min at 60 x g at 4°C. The supernatant was discarded and the cell pellet resuspended in 20 ml NCM medium. To determine the number of viable cells 10 µl of the cell suspension was mixed with 0.4% trypan blue solution 1:1 and a Neubauer counting chamber was used for counting of neonatal rat cells.

Per 15 cm cell culture dish an amount of 8 x 10^6 cardiac cells was seeded. To separate fibroblasts from cardiomyocytes NCM medium was added and the dishes were incubated for 45 min under humidified condition at 37°C with 5% CO_2. After incubation, the NCM medium containing most of the cardiomyocytes was removed, the plate washed two times with NRCF growth medium and NRCF growth medium was added to the adherent fibroblasts on the dish. Medium was changed on the first day after the preparation and afterwards every second day. NRCF were cultured until they reached confluency at 37°C and 5% CO_2.

3.1.3 End of digestion process and separation of cardiac fibroblasts and cardiomyocytes of neonatal mouse hearts

The digestion process of neonatal mouse hearts was performed analogue to the rat hearts with only small modifications. Before filtering the cells, the digested mouse heart cells were resuspended in 10 ml NMCM medium. The cell suspension was centrifuged for 20 min at 60 g at 4 °C. The supernatant was discarded and the pellet resuspended in 10 ml NMCM medium. The preplating was performed for 50 min with 15 ml cell suspension. During this time most of the fibroblasts adhered. The cultivation of NMCF was carried out analogue to the cultivation of NRCF as described above.

3.1.4 Isolation of adult mouse cardiac fibroblasts

Adult mouse cardiac fibroblasts used for the experiments were kindly provided by Sebastian Pasch, Institute of Pharmacology, University Medical Centre Göttingen. The cell isolation was performed via Langendorff perfusion, a method in the first instance used to obtain cardiomyocytes, during which in addition cardiac fibroblasts can be isolated by using the supernatant. After centrifugation and resuspension in AMCF growth medium the fibroblasts were seeded on cell culture surfaces and cultivated until they reached confluency at 37°C and 5% CO_2.

3.1.5 Culturing and passaging of primary cells

Cardiac fibroblasts were kept in growth medium on cell culture surfaces and cultivated at 37°C with 5% CO_2 in a humidified incubator. To prepare the plates for passaging the medium was removed and the cells were washed with pre-warmed DPBS. Likewise, pre-warmed 0.05% trypsin-EDTA was used to detach the cells from the plate. The detachment of the cells from the plate surface took about 3 - 5 min. The process was controlled by observation of the cells under the light microscope. To stop the digestion activity of trypsin, medium containing 10% serum was added and the dish was rinsed several times to collect the majority of cells. The cell suspension was centrifuged for 5 min at 300 x g and the cell pellet was resuspended in the respective growth media. Using the CASY cell counter system the cell viability and the number of cells in suspension were measured in the isotonic CASYton buffer. Cells were seeded in different density and on different cell culture surfaces depending on the experiment (see section 3.1.7).

3.1.6 Culturing and passaging of human ventricular cardiac fibroblasts

The NHCF-V were thawed and afterwards cultured in Fibroblast growth medium-3 (FGM-3) under humidified conditions at 37°C with 5% CO_2 as recommended by the manufacturer.

For passaging the medium was removed, the cells were washed with DPBS and incubated with TrypLE Express reagent for 3-5 min at 37°C and the detachment process was assessed by light microscopy and stopped by adding FGM-3. The cell suspension was centrifuged for 5 min at 300 g, the cell pellet was resuspended in FGM-3 and the cell number was evaluated using the CASY cell counter. The cells were seeded on cell culture plates in appropriate numbers depending on the experiment.

3.1.7 Treatment with lithium chloride and tubastatin A

To study α-tubulin acetylation and primary cilia formation, appropriate media containing serum and serum-free media were supplemented with either lithium chloride or tubastatin A.

The lithium chloride stock solution contained 2.12 g of lithium chloride powder (Molecular weight: 42.39 g/mol) in 10 ml sterile water. The solution was filtered under a sterile work bench. Thereby a 5 M lithium chloride stock solution was generated, which was stored at 4°C until further use. For the experiments a final concentration of 50 mM of lithium chloride was used.

The 3 mM tubastatin A stock solution was prepared under a sterile work bench by dissolving 5 mg tubastatin A in 2 ml sterile water and subsequent sterile filtering of the suspension. Aliquots of 20 µl of this 3 mM stock solution were prepared and stored at -20°C until they were needed. For the experiments a final concentration of 6 µM tubastatin A was used.

3.1.7.1 Preparation of samples for immunofluorescence analysis

To prepare samples for immunofluorescence analysis cells were seeded into 12 well plates. For immunostaining on plastic approximately 30.000 cells were seeded per well. The samples for imaging with the confocal microscope were prepared seeding 25.000 cells per well on collagen-coated glass slides. For this, glass cover slips were cleaned with 70% Ethanol and afterwards autoclaved. The sterile cover slips were placed in a 12 well plate and in cold DPBS diluted rat tail collagen I (1:100) was added to each well in a laminar flow hood. The cover slips were incubated there for 30 min. Then, excessive collagen solution was removed and the cells were directly seeded on the cover slips.

The cells were cultured for 24 h in growth medium in a humidified incubator at 37°C and 5% CO_2. After that, cells were divided into two groups: serum-containing and no serum condition. For the first group only the growth medium was renewed. The cells in the second group were washed twice with pre-warmed serum-free medium and afterwards cultured in this medium for another 24 h.

In the next step, the treatment was performed. For this, the medium was exchanged for either lithium chloride or tubastatin A containing medium (see chapter 4.1.7) in the presence or absence of serum and the incubation was carried out for 24 h at 37°C and 5% CO_2.

After the treatment was completed the medium was removed and the cells were washed once with DPBS. For fixation 4% PFA was added to the cells and incubated for 15 min at room temperature. Three washing steps with DPBS followed. The fixed cells were either directly used for immunofluorescence staining (3.2.1) or stored at 4°C until further use.

3.1.7.2 Preparation of samples for protein isolation

To prepare samples for protein isolation cells were seeded onto 6 well-plates. The cells were cultured in growth medium in a humidified incubator at 37°C and 5% CO_2 until they reached 80% confluency. Thereafter, incubation was continued with serum-free medium for at least 24 h before the treatment was started. For this, after another change of medium, either lithium chloride or tubastatin A was added to the medium as described in chapter 3.1.7 and the incubation was continued for further 24 h before cell lysis was carried out.

For cell lysis, cell scraper and lysis buffer were kept on ice until they were needed. The medium was removed from the plates and the cells were washed twice with DPBS. After complete removal of residual medium, 500 µl of ice-cold lysis-buffer was added and the cells were scraped off the plate. The homogenates were centrifuged for 30 min at 14.000g and 4°C. Samples for immunoblotting were prepared by addition of an appropriate volume of 4x SDS-PAGE sample buffer and subsequent incubation for 5 min at 95°C for protein denaturation. The remaining lysates were frozen in liquid nitrogen and stored at -80°C until further use.

3.1.8 Establishment of hypoxic conditions

NRCF were seeded into 12 well and 6 well plates for immunofluorescence and protein isolation, respectively. The hypoxia experiments were performed with neonatal rat cardiac fibroblasts obtained by the isolation procedure described in sections 3.1.1 and 3.1.2. NRCF were cultivated and after the first passaging incubated in growth medium at 37°C in an incubator under humidified conditions with 20% O_2 and 5% CO_2 for another 24 h. To apply hypoxic conditions, an oxygen-controlled workstation was used. After placing the plates into the oxygen-controlled workstation, the growth medium was removed, the cells were washed with serum-free medium twice and afterwards kept in serum-free medium in the hypoxia chamber for 24 h at 1% O_2. Afterwards the medium was changed and the cells were treated with lithium chloride and tubastatin A as described in section 3.1.7. The cells were kept under those conditions for further 24 h. Then, the cells were washed with serum-free medium twice and afterwards removed from the hypoxia chamber.

To compare hypoxic and normoxic conditions, cells were treated the same way, but kept under normoxic conditions (20% O_2). Finally, the cells were either fixed with 4% PFA for subsequent immunofluorescence analysis, or the protein samples were obtained, as described in section 3.3.1.

3.1.9 Proliferation assay

To assess the proliferation capacity of NRCF and AMCF, the cells were trypsinised as described in section 3.1.5, and the number of cells determined using the CASY counting system. Afterwards, 24 well plates were prepared for the proliferation experiments by seeding 10.000 cells per well in growth medium. In total, 5 plates were prepared for each assay. For these experiments passage one cells only were used.

After seeding, the cells were cultivated in growth medium for 24 h. Then one of the plates was washed with pre-warmed DPBS and the cells were fixed (day 0). Every other plate was

divided into three sections for the three different conditions: daily change of growth medium without further supplements as control, and change of medium with addition of either lithium chloride or tubastatin A. Every 24 h the cells of one plate were fixed and on the other plates the medium was changed and the treatment renewed. On day 4 the last 24 well plate was fixed. For fixation the cells were incubated with 4% PFA for 15 min. After one washing step with DPBS, the cells were permeabilised with 0.2% Triton X-100 for 3 min and finally washed with DPBS again. Subsequently, the cell nuclei were stained with DAPI (final concentration 1 µg/ml) for 30 min in the dark and afterwards washed three times with DPBS. To evaluate the proliferation rate the number of cell nuclei was measured using the Cellavista system.

3.1.10 Generation of engineered heart muscles (EHM) from primary neonatal rat cardiac cells

Table 12: Composition of one EHM

Components	**Volume**
Rat tail collagen type I (~3.5 mg/ml)	280 µl (~1 mg per EHM)
2x DMEM	280 µl
Matrigel	100 µl
0.1 N NaOH	App. 20 µl
Cell suspension (2.5 x 10^6 cells, containing cardiomyocytes and cardiac fibroblasts)	220 µl
Total	900 µl

The generation of EHM was carried out using a modified protocol of Zimmermann et al. 2002. All steps were performed on ice with pre-cooled components and materials. Depending on the number of EHM a multiple of the volumes given in table 12 was used. First, collagen I and 2x DMEM containing phenol red were mixed in equal parts. Afterwards Matrigel was added and the pH adjusted using 0.1 N NaOH to neutralise the mixture, indicated by a change of colour from yellow to red. The cell suspension, containing 2.5 x 10^6 cells in 220 µl EHM medium was added to the buffered ECM proteins, carefully mixed and casted into circular moulds. The EHM mixture was incubated at 37°C for 45 min to let the tissues consolidate. Then, EHM medium was added. The medium was renewed the following day and afterwards every second day. EHM were then transferred on phasic stretchers after 5 days and stretched at a frequency of 1 Hz for 24 h. Phasic stretching was continued for 12 more days at 2 Hz before EHM were fixed.

3.1.11 Generation of engineered connective tissue (ECT) from primary neonatal rat cardiac fibroblasts

Table 13: Composition of one ECT

Components	Volume
Rat tail collagen type I (~3.5 mg/ml)	400 µl (~1.4 mg per ECT)
2x DMEM	400 µl
0.1 N NaOH	App. 50µl
Cell suspension (1.5 x 10^6 cells/ECT)	App. 50µl (depending on volume of NaOH)
Total	900µl

To prepare ECT, NRCF were cultured in NRCF medium containing 10% serum for 24 h. The cells were digested and transferred into a reaction tube. After cells were counted using the CASY Cell Counter, the cell suspension was centrifuged, the supernatant discarded and the pellet resuspended in appropriate volume of growth medium (see section 3.1.5).
The following steps of ECT preparation were performed on ice. First, equal volumes of collagen and 2x DMEM were mixed and NaOH was added to neutralise pH by titration. About 1.5 million cells were added per ECT in an appropriate volume of medium, resulting in 900 µl of mixture per ECT. The mixture was pipetted into circular casting moulds and incubated for consolidation for 45 min at 37°C. Then 7ml of 10% NRCF medium was added to each mould. The medium was changed after 24 h and then every second day. After five days the medium was changed to serum free medium and then cultured for another 48 hours. For lithium chloride treatment of ECT after 24 h lithium chloride was added to the serum free medium in a final concentration of 50 mM.

3.2 Histological methods

3.2.1 Fluorescence staining of cells in cell culture plates

The fixed cells in 12 well plates (see section 3.1.7.1) were permeabilised for 3 min with 0.2% Triton X-100. After three washing steps with DPBS, Roti-Block was added to the cells for 1 h to block unspecific binding of antibodies. Then, the cells were washed once and incubated with the diluted primary antibodies overnight at 4°C on a shaking plate. The dilutions of the antibodies are given in table 7. The next day, the cells were washed three times with DPBS and the secondary antibody together with 1 µg/ml DAPI and 0.5 µg/ml TRITC-Phalloidin in DPBS were incubated for 1 h at room temperature in the dark.
Finally, the cells were washed 3 times with DPBS and afterwards stored at 4°C in the dark until used for imaging.

3.2.2 Fluorescence staining of cells on glass cover slips

For confocal microscopy, the cells were cultured, treated and fixed on collagen-coated glass cover slips as described in section 3.1.7. Permeabilization and blocking was carried out simultaneously with blocking and permeabilisation buffer containing 10% fetal calf serum and 0.2% Triton X-100 in DPBS (see table 6) for 45 min. The primary antibodies were diluted in the same buffer as used for permeabilisation and blocking and incubated with the samples overnight. The dilutions of the antibodies are given in table 7. After three washing steps with blocking buffer, the secondary antibodies (see table 9) in blocking buffer were added and incubation was carried out in the dark for 4 hours. In the last 30 min 0.5 µg/ml TRITC-Phalloidin and 1 µg/ml DAPI were added. Next, the cells were washed with DPBS three times and the cover slips were mounted with Fluoromount on microscope slides and sealed with nail polish on the following day. The samples were stored at room temperature in the dark until further usage.

3.2.3 Preparation of vibratome sections of engineered tissue

EHM and ECT were fixed in 4% PFA in DPBS overnight. After washing with DPBS, the engineered tissue samples were embedded in 2% agarose dissolved in TAE buffer in 6 well plates. The embedded samples were kept at 4°C overnight for complete hardening. Cuboids of agarose containing the EHM or ECT were cut out and fixed on the vibratome surrounded by cold DPBS. Slices of 100 µm thickness were cut, transferred into a 6 well plate filled with DPBS and stored at 4°C until used for immunostaining.

3.2.4 Fluorescence staining of engineered tissue

The vibratome sections of engineered tissue were using a blocking and permeabilisation buffer containing Roti-Block and 0.2% Triton X-100 in aqua dest. (see table 6) at 4°C for 1 hour. The primary antibodies were added to the described buffer and the sections were incubated at 4°C overnight whilst shaking. The next day three washing steps with DPBS were performed and the secondary antibodies were incubated overnight in the dark whilst shaking. After three washing steps with DPBS the sections were incubated with 0.5 µg/ml TRITC-Phalloidin and 1 µg/ml DAPI for 45 min at room temperature in the dark. The agarose was removed and the tissue sections were mounted on glass slides using Fluoromount and cover slips to envelope the samples. Finally, the cover slips were sealed with nail polish on the following day. The glass slides were stored in the dark at room temperature until used for imaging.

3.3 Protein biochemical methods

3.3.1 Sodium dodecyl sulphate polyacrylamide gel electrophoresis (SDS-PAGE)

To separate proteins according to their size, SDS-PAGE was performed, using a 5% stacking gel and a resolving gel containing a 10% acrylamide/bisacrylamide concentration, see table 14.

Table 14: Components of stacking and resolving gel for SDS-PAGE

Reagent	**5% stacking gel**	**10% resolving gel**
ddH_2O	2.8 ml	1.9 ml
1.0 M Tris/HCl, pH 6.8	0.38 ml	-
1.5 M Tris/HCl, pH 8.8	-	1.3 ml
Acrylamide/bisacrylamide mix (29%/1%)	1.3 ml	1.7 ml
10% SDS	0.03 ml	0.05 ml
10% APS	0.03 ml	0.05 ml
TEMED	0.003 ml	0.003 ml
Total volume	3 ml	5 ml

Protein samples, prepared as described in section 3.1.7.2, were loaded onto the prepared gels and separated with constant 200 Volt in 1x SDS running buffer for approximately 45 min until the bromophenol blue of the sample buffer reached the end of the gel.

3.3.2 Immunoblotting

After the proteins had been separated by SDS-PAGE, they were transferred onto a nitrocellulose membrane. For this the gel and the membrane were layered between filter paper and soaked in 4°C cold immunoblotting buffer. 100 Volt were applied for 1 h, while the gel and membrane were kept in the cold immunoblotting buffer. Thereby the proteins were successfully transferred onto the membrane, which could be shown by Ponceau-S staining afterwards. After incubation in Ponceau-S solution for 5 min, the membrane was washed three times with distilled water until only the single bands stayed visible. Images of the staining were taken and the membrane was cut into strips for detection of the respective proteins. The remaining Ponceau-S staining was washed off using TBST. The cut membrane was incubated in 1x Roti-Block for 1 h at room temperature whilst shaking to prevent unspecific binding of the antibodies. Afterwards the strips were incubated over night

at 4°C with the respective primary antibody diluted in TBST on a shaking plate. The used antibody concentrations are given in table 7. The next day, the membranes were washed at room temperature three times with TBST, each washing step was carried out for 10 min, and afterwards the horseradish peroxidase (HRP)-conjugated secondary antibodies in TBST were applied to the membranes. The used antibody concentrations are given in table 8. The incubation was performed at room temperature whilst continuously shaking. The membrane strips were then washed three times for 10 min each with TBST and afterwards the HRP activity was detected with a chemoluminescence detection system using an enhanced chemoluminescence substrate (Lumi-LightPLUS). The following quantitative analysis was carried out with the help of ImageLab 5.1 analysis software.

3.4 Microscopy

Imaging was performed either using an inverted microscope for epifluorescence microscopy (Olympus IX81) or a confocal microscope (Zeiss, LSM 170).

3.4.1 Epifluorescence microscopy

For engineered tissue and for taking pictures for primary cilia measurement the inverted fluorescence microscope was used. Microscopy was carried out in the dark.

The following filters and objectives were used:

- filter DAPI BP 403/12 Olympus
- filter EGFP BP 470/20 Olympus
- filter Texas Red BP 572/23 Olympus
- objective 20x LUCPLFLN20xPH/ 0.45 Olympus
- objective 40x LUCPLFLN40xPH/ 0.60 Olympus
- objective 60x PlanApo N60x/ 1.42 oil Olympus

3.4.2 Confocal microscopy

For higher resolution images, z-stack-analysis and 3D reconstruction confocal laser scanning microscopy was performed.

The following objectives were used:

- objective 10x: EC Plan-Neofluar/ 0.3 (Zeiss LSM 710)
- objective 20x: EC Plan-Neofluar/ 0.5 (Zeiss LSM 710)
- objective 63x: Plan-Apochromat/ 1.4 oil (Zeiss LSM 710)
- objective 100x: EC Plan-Neofluar/ 1.3 oil (Zeiss LSM 710)

Laser intensity and gain were adjusted depending on the signal.

3.5 Quantitative and statistical analysis

3.5.1 Measurement of primary cilia length and percentage of cells with cilia

For measurement of the length of primary cilia of cardiac fibroblasts FIJI/ImageJ was used to analyse immunostainings. The pictures for length measurement were taken with an inverted fluorescence microscope (Olympus IX81) at a magnification of 320x. Besides acetylated α-tubulin the nuclei were imaged for better orientation. A stack of all images was prepared.

The information of the pixel size was manually added in the programme and the cilia were measured using the tool “free hand line”. The data of every stack was transferred to Prism to measure means and standard error and for graphical presentation.

In addition to the cilia length, the fraction of cells carrying primary cilia was determined. For this, images of acetylated α-tubulin and DAPI staining were taken with a magnification of 200x. Each 12 well plate contained 4 wells of each condition (control/TubA/LiCl) and per well 10 images were taken. With the help of the image stacks and FIJI/ImageJ, the total cell number was determined as well as the percentage of cells carrying primary cilia.

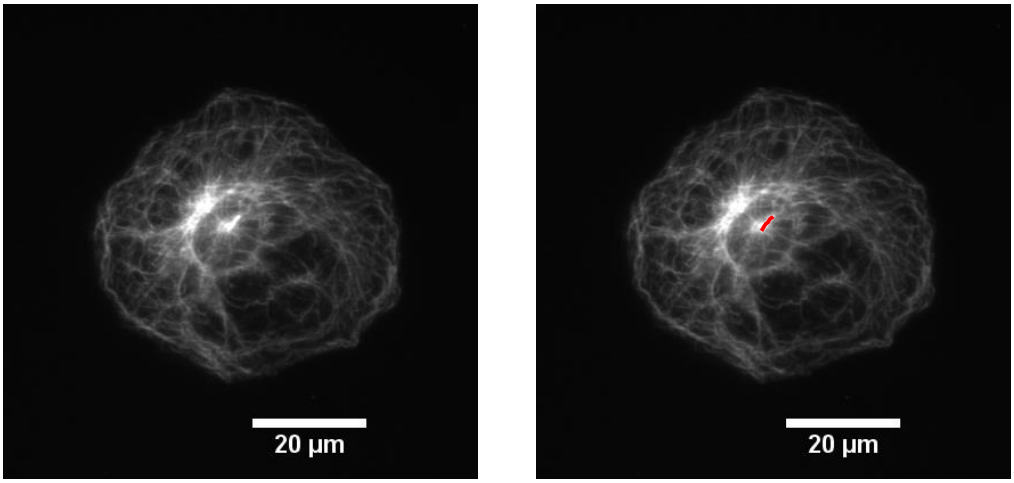

Figure 5: **Measurement of primary cilia length.** Immunofluorescence staining of acetylated tubulin of NRCF after treatment with lithium chloride under serum-starved conditions. The image was taken with an inverted fluorescence microscope at a magnification of 320x. The primary cilium length (red line) was measured with the “free hand line” tool of FIJI/ImageJ.

4 Results

4.1 Primary cilia in cardiac fibroblasts

4.1.1 Primary cilia are present in cardiac fibroblasts in 2 D culture

Since it was unknown whether cardiac fibroblasts possess primary cilia, cultured neonatal rat cardiac fibroblasts (NRCF) were used for immunofluorescence analysis. Acetylated α-tubulin and γ-tubulin were detected with specific antibodies and the nuclei were stained with DAPI. Confocal microscopy revealed that on top of NRCF nuclei, primary cilia could be detected characterised by their main structural shaft component acetylated α-tubulin and the main basal body component γ-tubulin (Fig. 6).

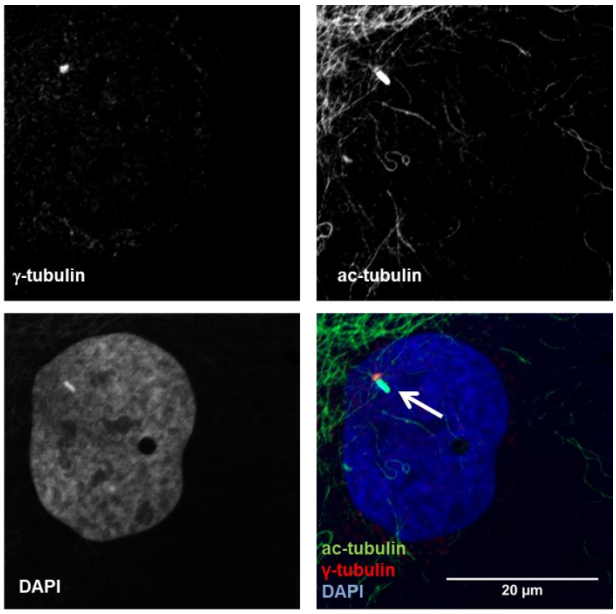

Figure 6: Confocal microscopy of a primary cilium in a serum-starved NRCF. Serum-starved 2D cardiac fibroblast cultures derived from neonatal rats (NRCF) were used for immunofluorescence analysis. Acetylated α-tubulin (green) and γ-tubulin (red) were detected with specific antibodies, the nuclei were stained with DAPI (blue), and confocal imaging was performed. Shown are the single channels in grayscale and the merge in color. The arrow indicates a primary cilium. A magnification of 1000x was used.

4.1.2 Primary cilia are present in cardiac fibroblasts of different species

To investigate if primary cilia are present in cardiac fibroblasts of different species, acetylated α-tubulin was detected by immunofluorescence in neonatal and adult mouse cardiac fibroblasts (NMCF and AMCF), in human ventricular cardiac fibroblasts (HVCF) and in addition for comparison in NRCF. For better orientation nuclei were stained with DAPI. In all investigated 2D cardiac fibroblasts cultures primary cilia were present on top or directly next to nuclei.

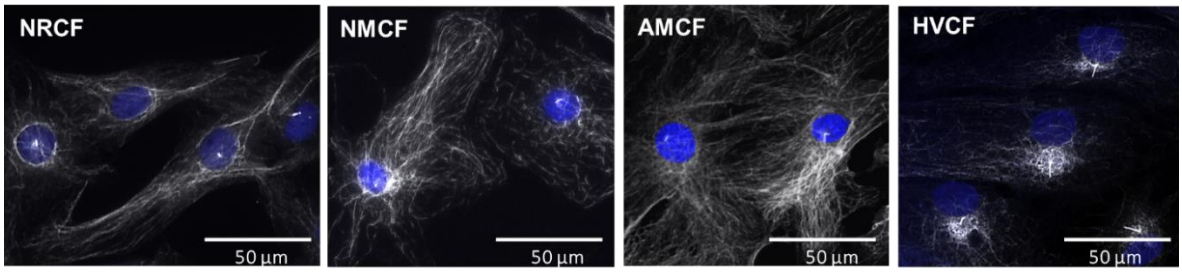

Figure 7: Fluorescence microscopy of primary cilia in serum-starved NRCF, NMCF, AMCF and HVCF. Serum-starved 2D cardiac fibroblast cultures derived from neonatal rats (NRCF), neonatal mice (NMCF), adult mice (AMCF) and humans (HVCF) were used for immunofluorescence analysis. Acetylated α-tubulin (grayscale) was detected with a specific antibody, the nuclei were stained with DAPI (blue) and fluorescence imaging was performed. Shown are the overlays. A magnification of 320x was used.

4.1.3 Primary cilia are present in engineered connective tissue

In the next step, the presence of primary cilia in 3D cardiac fibroblast cultures was examined. For this purpose, engineered connective tissues (ECT), composed of NRCF and collagen I, were prepared. After sectioning and staining of acetylated α-tubulin, confocal imaging was performed. In addition, F-actin was detected with TRITC-phalloidin to determine the cell borders. As shown in figure 8A, primary cilia can be found under control conditions, however, not all cells seem to possess these structures (left images vs. right images). The treatment of cells with lithium chloride had been demonstrated to influence primary cilia length (Nakakura et al. 2015). Therefore, ECT were treated in parallel for the last 24 h with 50 mM lithium chloride and primary cilia were detected. As shown in figure 8B, the length of primary cilia was increased and interestingly split primary cilia or pairs of primary cilia could be detected on some cells.

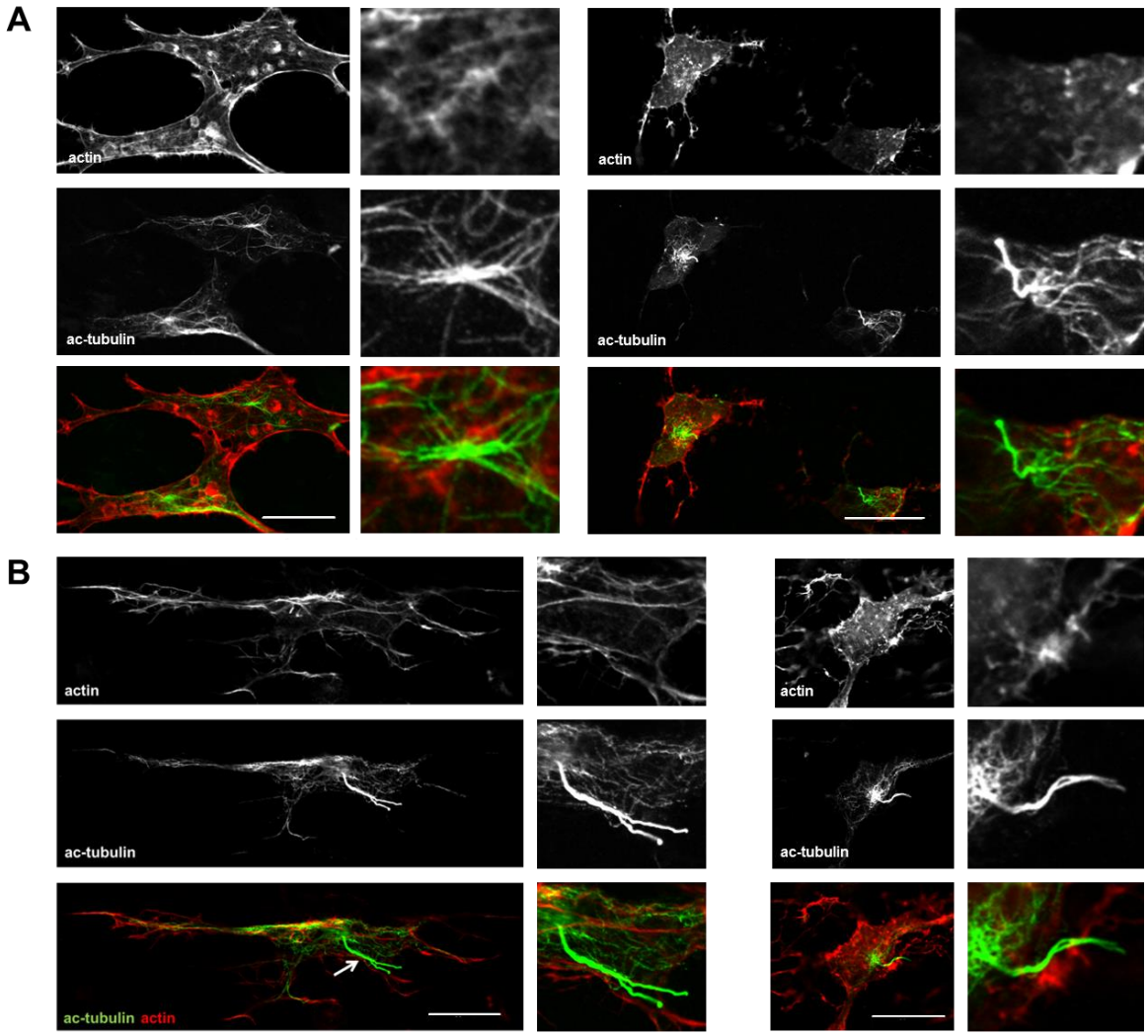

Figure 8: Confocal microscopy of primary cilia in engineered connective tissues. Engineered connective tissues (ECT) were generated from neonatal rat cardiac fibroblasts and collagen I. During the last 2 culture days, the ECT were either serum-starved (A) or serum-starved for 24 h and afterwards treated with 50 mM lithium chloride under serum-starved conditions for further 24 h (B). Vibratome sections of 100 µm thickness were prepared and acetylated α-tubulin (green) was detected with a specific antibody. In addition, F-actin was stained with TRITC-Phalloidin (red). Shown are the single channels and the merges of two examples each. Arrow indicates a primary cilium. A magnification of 630x was used. The white scale bars represent 20 µm. The rectangles mark the areas, which are shown in higher magnifications on the right hand side of each image.

4.1.4 Primary cilia are present in engineered heart muscles

The data so far shows that primary cilia can be detected in homogenous 2D and 3D cultures of cardiac fibroblasts. This raised the question whether primary cilia are also present in contractile heart muscle. The attempt to detect primary cilia in native myocardium, however, failed due to several reasons. First, in the adult myocardium cardiac fibroblasts are difficult to identify because of the lack of specific cell markers. Second, staining of myocardial tissue with an antibody against acetylated α-tubulin led to strong signals in neuronal cells. These cells stabilise their axons by acetylated α-tubulin. By sectioning of heart tissue, the meandering axons were occasionally cut and thus primary cilia-shaped artefacts were produced (data not shown). Therefore, engineered heart muscles (EHM) were used in the following to analyse the presence of primary cilia in a heterogenous and contractile environment. EHM were prepared of all cardiac cells isolated from neonatal rat hearts. The maturation of cardiomyocytes and syncytium formation was induced by phasic stretch. After 19 days in culture the EHM showed coherent spontaneous beating. To study the presence of primary cilia in EHM, the tissues were sectioned and immunofluorescence analysis of acetylated α-tubulin was performed. In addition, F-actin was stained to identify cardiomyocytes by their sarcomeric actin pattern as well as nuclei were detected to verify the presence of primary cilia due to their perinuclear localization. In figure 9, fluorescence images are presented of a less densely packed area in an EHM. The staining of acetylated α-tubulin suggested that in EHM ciliated cells are present. Especially cells without prominent F-actin possessed primary cilia.

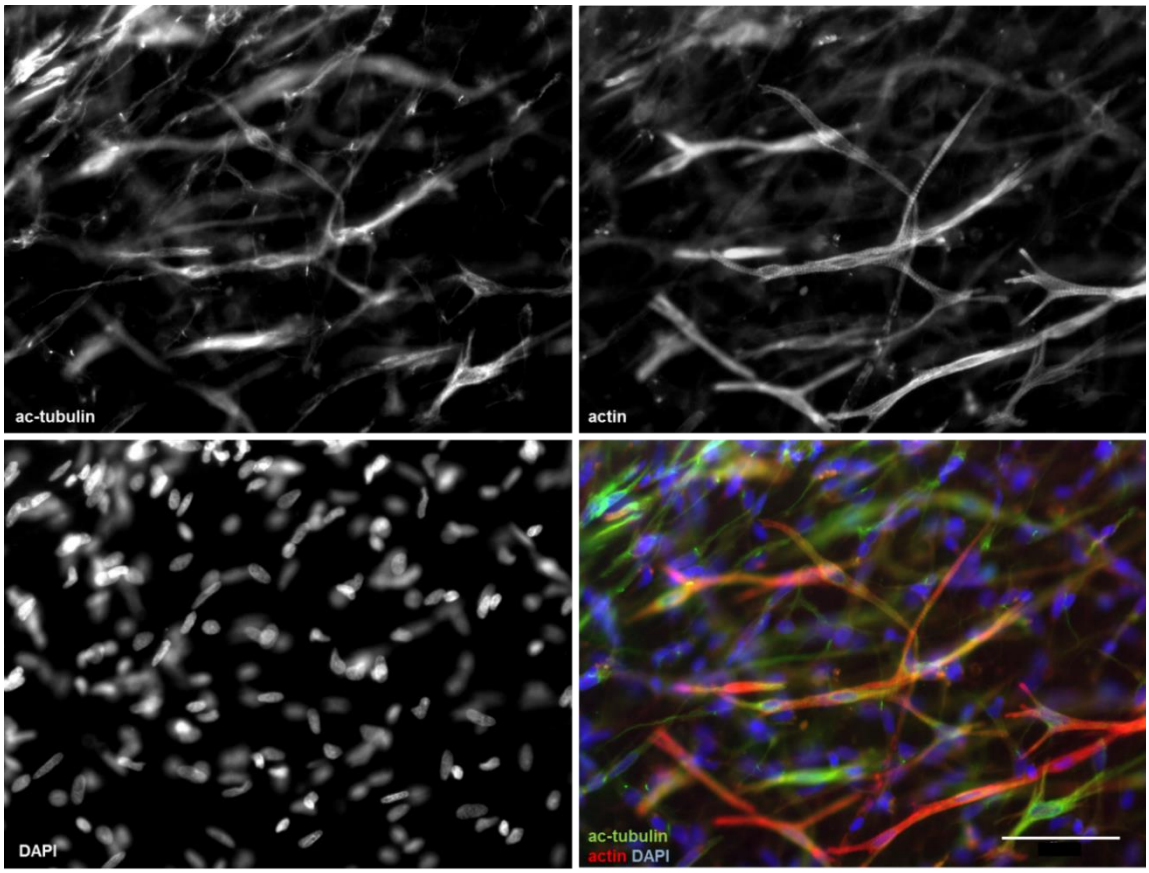

Figure 9: **Fluorescence microscopy of primary cilia in engineered heart muscle.** Engineered heart muscle (EHM) were generated from neonatal rat heart cells and collagen I. Shown is an immunostaining of acetylated α-tubulin (green) of a 100 µm thick vibratome section. F-actin was stained with TRITC-Phalloidin (red) and the nuclei with DAPI (blue). Imaging was performed by fluorescence microscopy. Single channels are shown in grayscale and the merge in color. A magnification of 320x was used. The white scale bar represents 50µm.

To further validate this finding, higher magnification images were taken. Again, cells with striated actin and strong acetylated α-tubulin signals were found to carry no primary cilia.

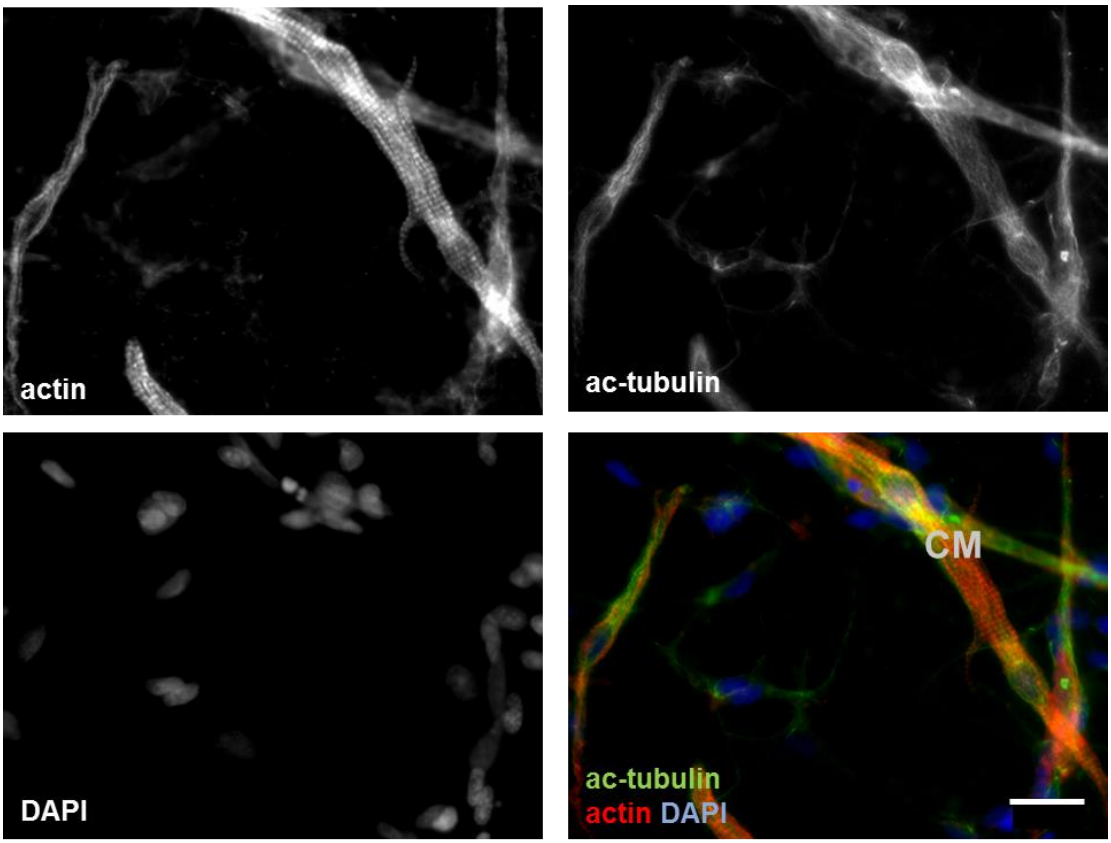

Figure 10: Fluorescence microscopy of cardiomyocytes (CM) in engineered heart muscle detected by F-actin staining. Engineered heart muscle (EHM) were generated from neonatal rat heart cells and collagen I. Shown is an immunostaining of acetylated α-tubulin (green) of a 100 µm thick vibratome section. F-actin was stained with TRITC-Phalloidin (red) and the nuclei with DAPI (blue). Imaging was performed by fluorescence microscopy. Single channels are shown in grayscale and the merge in color. The cardiomyocyte was identified by its actin striation and is labelled with CM. A magnification of 600x was used. The white scale bar represents 20 µm.

4.1.4.1 Primary cilia could not be found on cardiomyocytes in EHM

To more exactly characterise ciliated cardiac cells in EHM, immunofluorescence analysis of acetylated α-tubulin and specific cell markers was performed. First, cardiomyocytes were detected in addition to their unique actin pattern by caveolin-3 expression. This caveolin isoform is exclusively expressed in striated muscle cells. Two representative examples of striated and caveolin-3 positive cardiomyocytes in EHM are shown in figure 11. Although, acetylated α-tubulin could be detected in these cells, no primary cilia were present. This data suggests that cardiomyocytes in EHM, showing a certain degree of maturity, are not carrying primary cilia. Whether immature cardiomyocytes, with less organized sarcomeres, have primary cilia could not be answered by this approach.

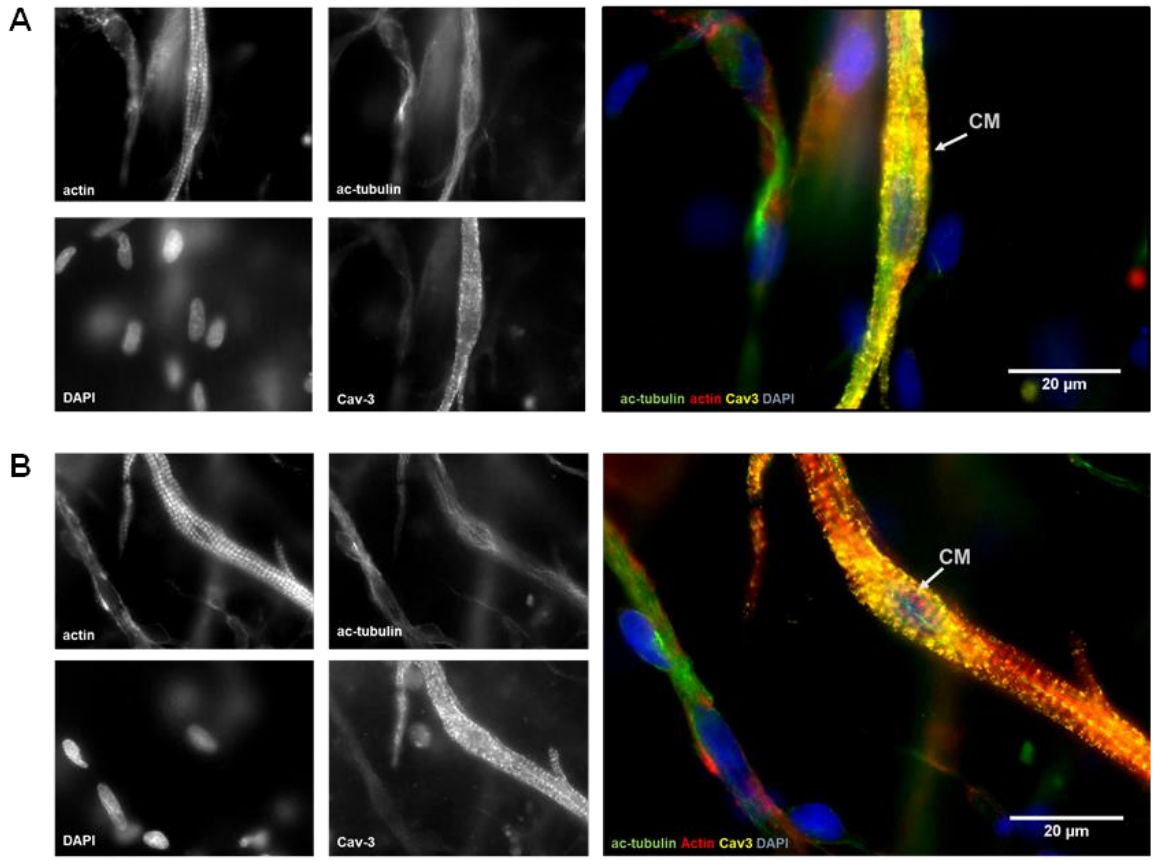

Figure 11: Fluorescence microscopy of cardiomyocytes (CM) in engineered heart muscle detected by F-actin and caveolin-3 staining. Engineered heart muscle (EHM) were generated from neonatal rat heart cells and collagen I. Shown are immunostainings of acetylated α-tubulin (green) and caveolin-3 (Cav-3, yellow) of two 100 µm thick vibratome sections. F-actin was stained with TRITC-Phalloidin (red) and the nuclei with DAPI (blue). Imaging was performed by fluorescence microscopy. Single channels are shown in grayscale and the merges in color. The cardiomyocytes were identified by their actin striation and Cav-3 expression and are labelled with CM. A magnification of 960x was used.

4.1.4.2 Primary cilia could be found on endothelial tube-like structures

As reported by Naito and colleagues (Naito et al. 2006) in rat engineered heart tissues tube-like structures develop, which are composed of endothelial cells. Endothelial cells had been described to carry primary cilia on their luminal side (Nauli et al. 2008). To test whether endothelial tubes could be detected in the used EHM, and more importantly whether endothelial cells possess primary cilia in EHM, the endothelial marker CD31 was stained together with acetylated α-tubulin, F-actin and DAPI. CD31, also known as platelet endothelial cell adhesion molecule-1 (PECAM-1), is a transmembrane protein located in the intercellular junctions of endothelial cells (Privratsky and Newman 2014).

By CD31 staining tube-like structures could be detected in EHM. These tubes were built of cells with elongated nuclei and were showing a punctured CD31 localisation, probably reflecting cell-cell junctions (Fig. 12A). Branched tubes could also be detected (Fig. 12B). The tube-forming, CD31-positive endothelial cells, were in addition positive for acetylated α-tubulin. Occasionally primary cilia could be detected on the outside of these tubes (Fig. 12B). Whether these are primary cilia of endothelial cells with a missing cell polarity or these primary cilia belong to the tube stabilizing pericytes, has to be elucidated further.

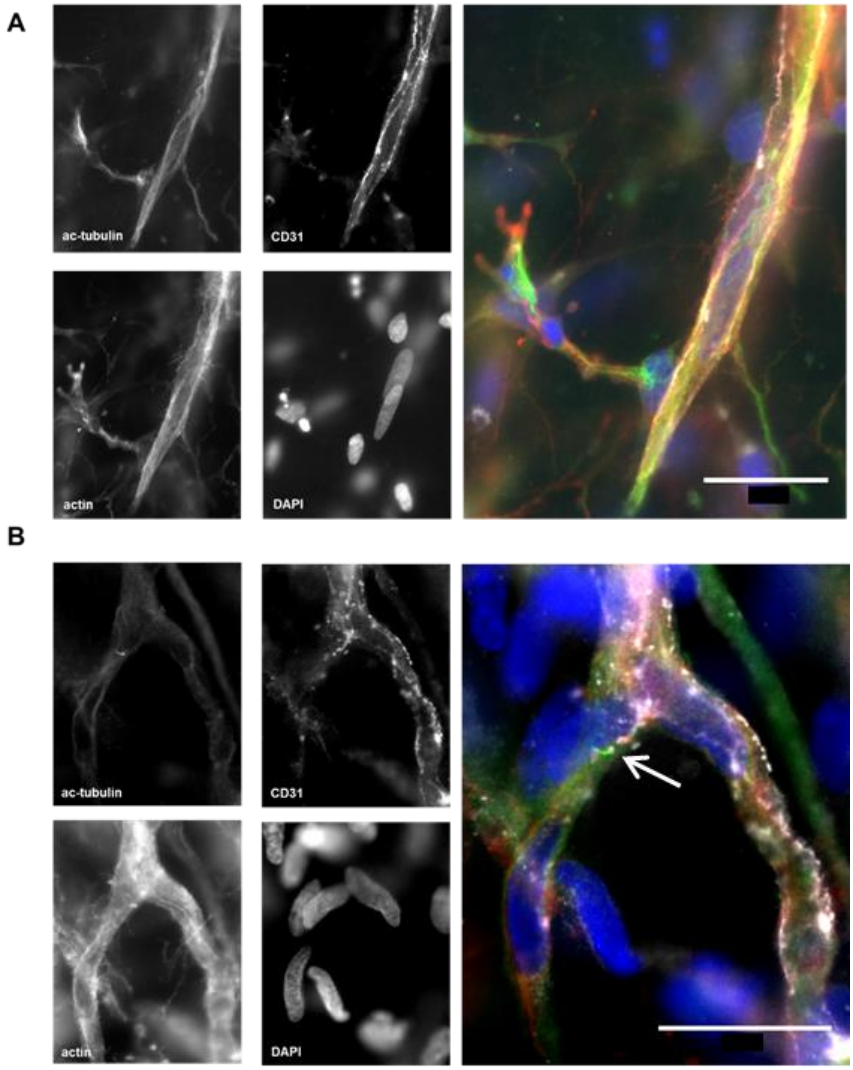

Figure 12: Fluorescence microscopy of endothelial cells (EC) in engineered heart muscle detected by CD31 staining. Engineered heart muscle (EHM) was generated from neonatal rat heart cells and collagen I. Shown are immunostainings of acetylated α-tubulin (green) and CD31 (grayscale) of a 100 µm thick vibratome section. F-actin was stained with TRITC-Phalloidin (red) and the nuclei with DAPI (blue). Imaging was performed by fluorescence microscopy. Single channels are shown in grayscale and the merges in color. The endothelial cells were identified by their CD31 expression and are labelled with EC. The arrow indicates a primary cilium. Magnification of 600x (A) and 960x (B) were used. The white scale bars represent 20 µm.

Next, caveolin-1 was stained in addition to acetylated α-tubulin, actin and DAPI. Caveolin-1 is the main structural caveolin isoform in cells others than striated muscle cells. The strongest caveolin-1 expression could be detected in elongated cells, which are most likely due to their elongated nuclei endothelial cells. Similar as shown for CD31-positive cells, these cells were positive for acetylated α-tubulin and carried in some cases on their outside primary cilia (Fig. 13).

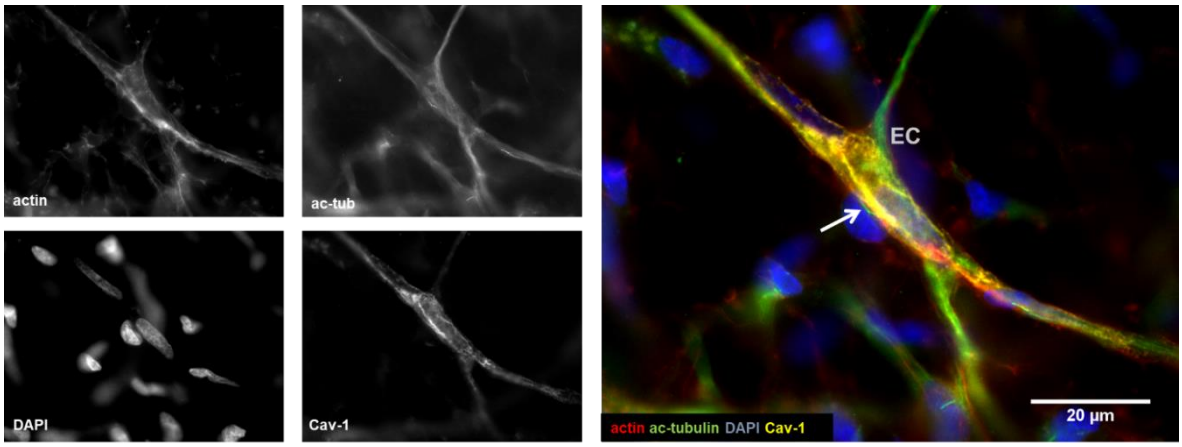

Figure 13: Fluorescence microscopy of endothelial cells (EC) in engineered heart muscle detected by caveolin-1 staining. Engineered heart muscle (EHM) were generated from neonatal rat heart cells and collagen I. Shown are immunostaining of acetylated α-tubulin (green) and caveolin-1 (Cav-1, yellow) of a 100 µm thick vibratome section. F-actin was stained with TRITC-Phalloidin (red) and the nuclei with DAPI (blue). Imaging was performed by fluorescence microscopy. Single channels are shown in grayscale and the merges in color. Endothelial-like cells were strongly positive for caveolin-1 and are labelled with EC. The arrow indicates a primary cilium. A magnification of 960x was used.

4.1.4.3 Primary cilia could be found on cardiac fibroblasts in EHM

In less densely packed regions of EHM, where no or only few cardiomyocytes could be detected, most cells carried primary cilia (Fig. 14A). These highly abundant cells were only faintly positive for F-actin and acetylated α-tubulin, and negative for CD31 (Fig. 14B). In addition, they were negative for caveolin-3 (not shown). The cells possessed ellipsoid nuclei and a branched cortical actin cytoskeleton. Taken together, these findings strongly argue that these ciliated cells are cardiac fibroblasts (Fig. 14C).

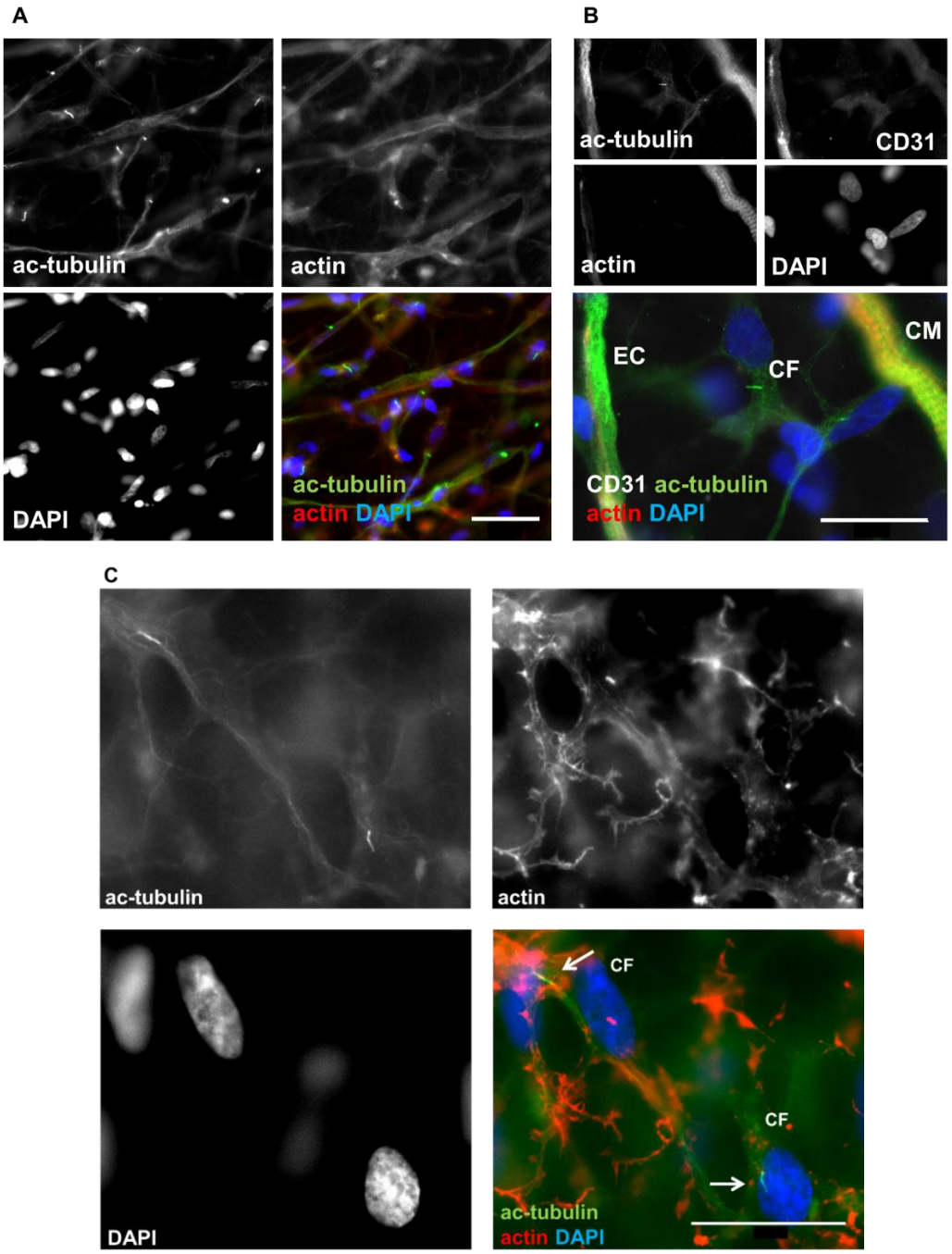

Figure 14: Fluorescence microscopy of cardiac fibroblasts (CF) in engineered heart muscle. Engineered heart muscle (EHM) were generated from neonatal rat heart cells and collagen I. Shown are immunostainings of acetylated α-tubulin (green) of two 100 µm thick vibratome section. F-actin was stained with TRITC-Phalloidin (red) and the nuclei with DAPI (blue). In B) CD31 was stained in addition. Imaging was performed by fluorescence microscopy. Single channels are shown in grayscale and the merges in color. The cardiac fibroblasts are labelled with CF. The arrows indicate primary cilia. The images were taken with magnifications of 200x (A), 600x (B) and 960x (C). The white scale bars represent 50 µm (A) or 20 µm (B, C).

4.1.4.4 Primary cilia are present in more densely packed muscle strands

Muscle strands responsible for the coherent beating of EHM are not uniformly distributed in engineered tissues. Since so far all ciliated cells were detected in less densely packed regions of EHM, next, areas containing muscle strands were analysed. Therefore, confocal z-stack analysis was performed. In figure 15 a 3D reconstruction of such a muscle strand is depicted. Interestingly, long thin fibre-like structures are connected to the muscle fibre, which are strongly positive for acetylated α-tubulin. Due their shape, these fibres are likely to be axons of neuronal cells in EHM, which had, however, not been described so far in engineered heart tissue.

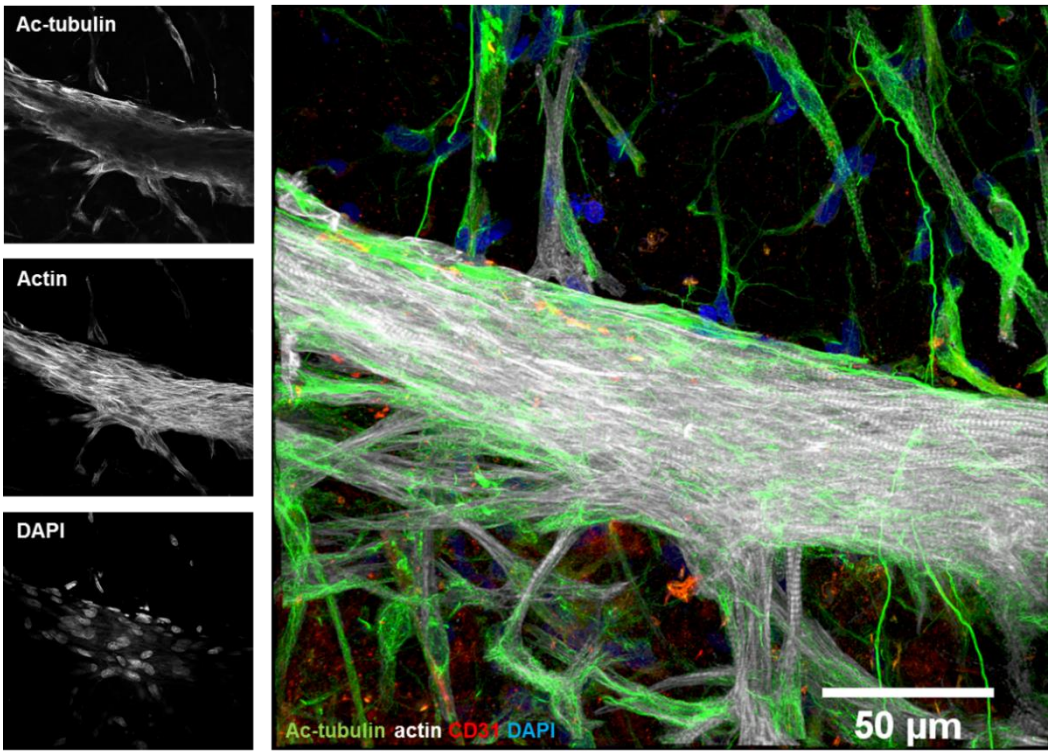

Figure 15: Confocal microscopy of densely packed muscle strands in engineered connective tissue. Engineered heart muscle (EHM) were generated from neonatal rat heart cells and collagen I. Shown is a 3D reconstruction of a confocal z-stack of immunostained acetylated α-tubulin (green) and CD31 (red, only shown in the merge) of a 100 µm thick vibratome section. F-actin was stained with TRITC-Phalloidin (grayscale) and the nuclei with DAPI (blue). Single channels are shown in grayscale and the merge in color. The 3D-reconstruction was generated of 44 z-slices representing a total z-depth of 14.5 µm.

By using higher magnifications, single cells could be located on the surface of muscle stands in EHM carrying primary cilia (Fig. 19). As these cells do not possess a very pronounced actin cytoskeleton, it can be assumed that they are cardiac fibroblasts.

However, future studies are needed to further discriminate between the different cells types in these complexly composed engineered tissues.

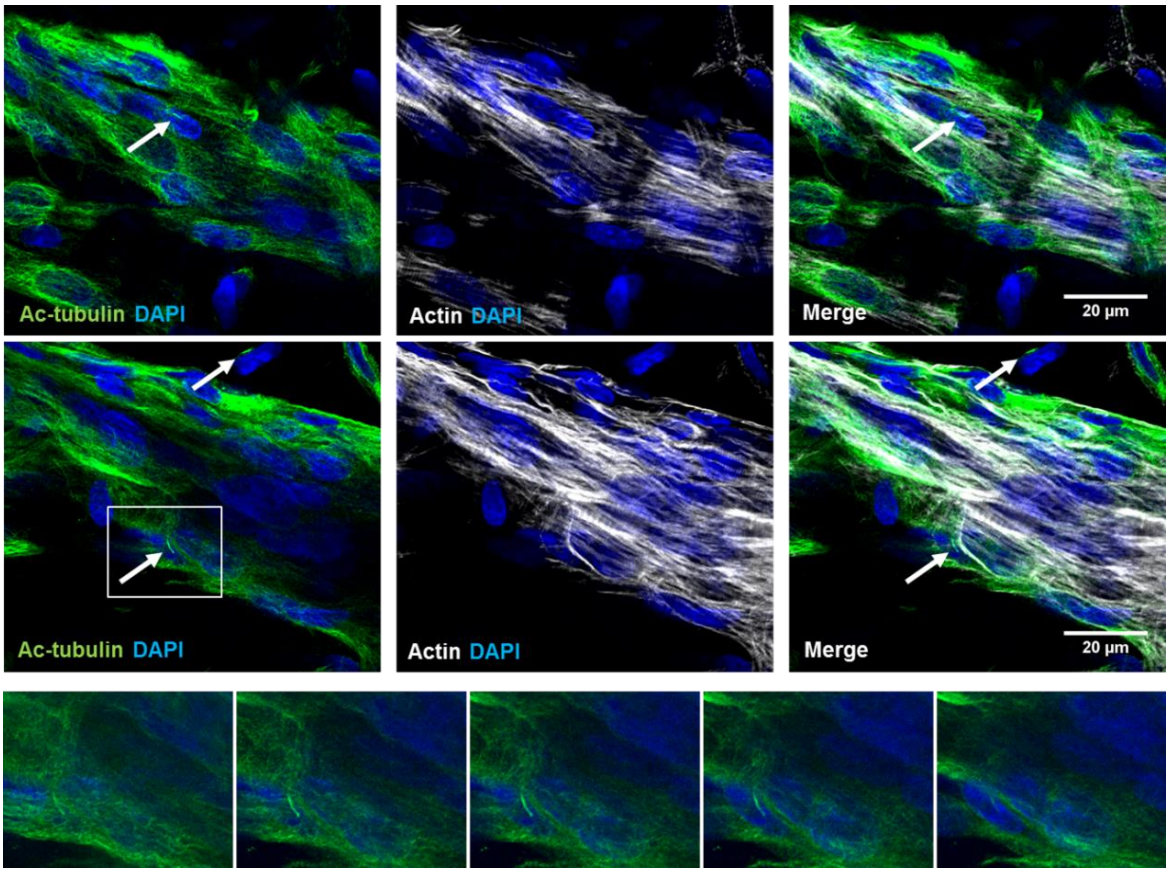

Figure 16: Confocal microscopy of primary cilia in densely packed muscle strands in engineered connective tissue. Engineered heart muscle (EHM) were generated from neonatal rat heart cells and collagen I. Shown are two slices of a z-stack (upper two rows) of immunostained acetylated α-tubulin (green) of a 100 µm thick vibratome section. F-actin was stained with TRITC-Phalloidin (grayscale) and the nuclei with DAPI (blue). Merges are shown of acetylated α-tubulin and DAPI, of actin and DAPI as well as of all tree channels. The arrows indicate primary cilia. In the bottom row a magnification of single z-stack images of the acetylated α-tubulin stain is shown. The region is demonstrated in the upper image by a white rectangle. The depths of the z-slices are 0.33 µm.

4.1.5 Neither serum-starvation nor treatment with tubastatin A and lithium chloride lead to a change of number of primary cilia

After the presence of primary cilia in cardiac fibroblasts in 2D and 3D cultures had been proven, the regulation of primary cilia by serum, tubastatin A and lithium chloride was assessed. First, the fraction of ciliated NRCF in 2D cultures treated with these substances was quantified in immunofluorescence images (Fig. 19A). Although it has been shown that 10% serum induces the proliferation rate of NRCF (Jatho et al. 2015), and thus less primary cilia could be expected (Plotnikova et al. 2009), no difference in the fraction of ciliated NRCF were found. In the absence of serum as well as in the presence of 10% serum around 60% of cells were ciliated. This was by trend diminished, when the cells were treated with 6 µM tubastatin A for 24 h (Fig. 17B). Tubastatin A is supposedly a specific inhibitor for HDAC6, the main α-tubulin deacetylase. By immunofluorescence analysis the effect of HDAC6 inhibition became apparent as an increase of acetylated microtubules spreading throughout the whole cell, instead of being confined to the perinuclear region. This effect of tubastatin A was not different between starved and serum-treated NRCF (Fig. 17A). In contrast to tubastatin A, application of 50 mM lithium chloride, which was demonstrated to mobilises the α-tubulin N-acetyltransferase 1 (Nakakura et al. 2015) had no effect on the number of ciliated cells and on the appearance of acetylated microtubules (Fig. 17B).

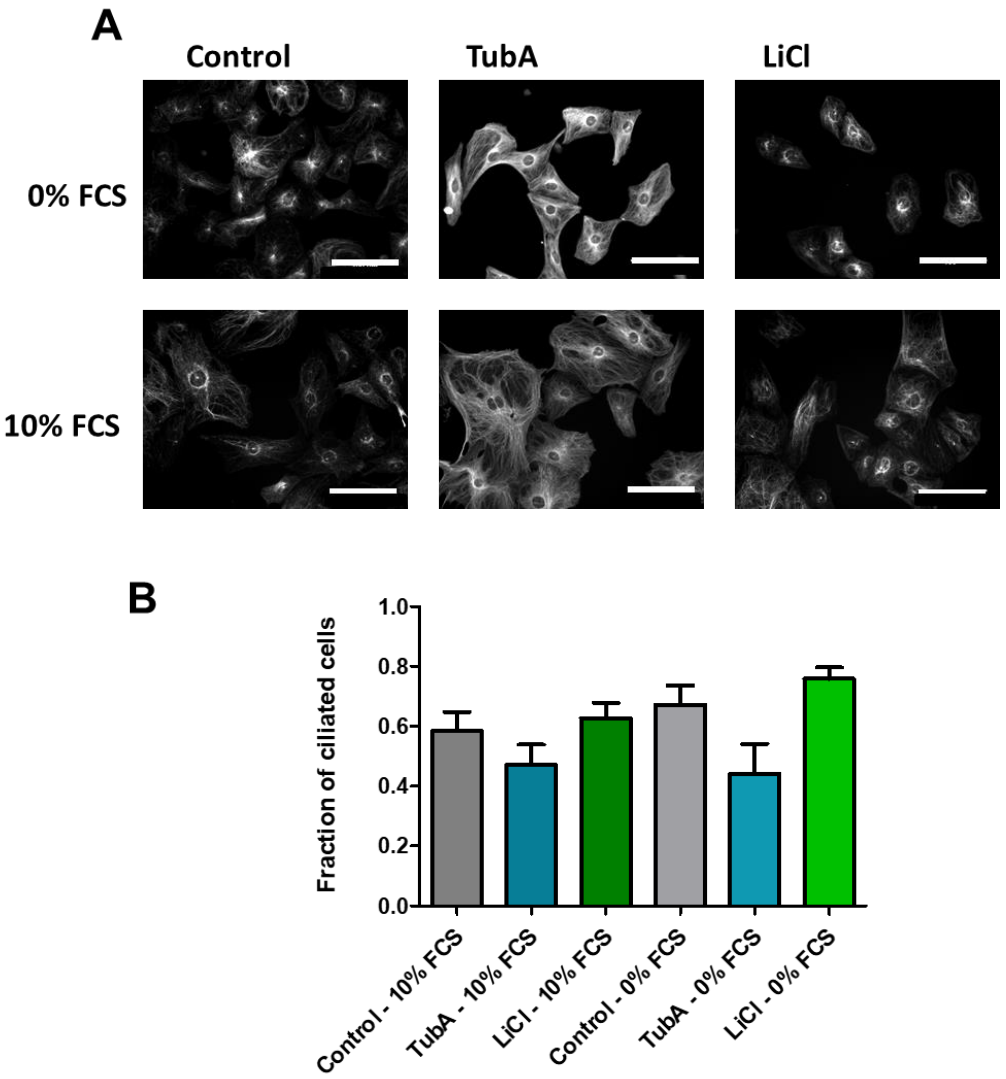

Figure 17: Fluorescence microscopy and quantification of primary cilia in NRCF after tubastatin A and LiCl treatment. 2D cardiac fibroblast cultures derived from neonatal rats (NRCF) were cultured for 24 h in the presence or absence of 10% serum.Afterwards, 6 µM tubastatin A (TubA) or 50 mM LiCl were added to both conditions as indicated and the cells were cultured for further 24 h. Acetylated α-tubulin (grayscale) was detected with a specific antibody, and fluorescence imaging was performed. **A)** Shown are representative images with a magnification of 200x. The white scale bars represent 100µm. **B)** The number of ciliated cells was counted and is given as fraction of all cells. Shown are the means±SEM of three independent experiments (n=3). In each experiment a minimum of 252 cells per condition were analysed.

4.1.6 Primary cilia length increases under serum-starvation and after treatment with lithium chloride

Next, the effect of serum, tubastatin A and lithium chloride on the length of primary cilia was analysed. As already demonstrated for the ECT model, lithium chloride treatment could elongate primary cilia in NRCF (see Fig. 8). As shown in the confocal microscopy images in figure 18, this seemed to be also the case in 2D NRCF cultures, when the cells were serum-starved beforehand. In contrast, tubastatin A showed no obvious effect on primary cilia length.

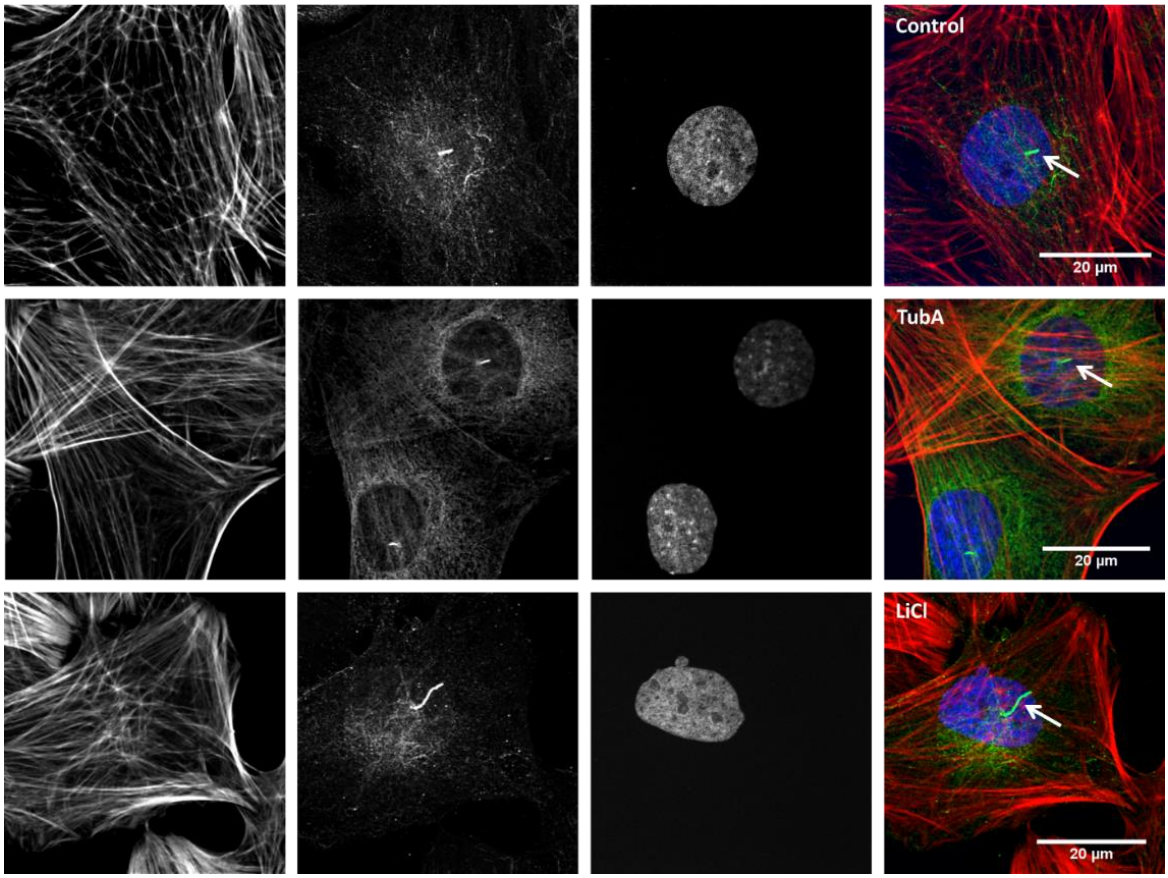

Figure 18: Confocal microscopy of primary cilia in NRCF after tubastatin A and LiCl treatment. 2D cardiac fibroblast cultures derived from neonatal rats (NRCF) were cultured for 24 h in the absence of serum and afterwards 6 µM tubastatin A (TubA) or 50 mM LiCl in serum-free medium was added. The cells were cultured for further 24 h. Acetylated α-tubulin (green) was detected with a specific antibody, F-actin was stained with TRITC-Phalloidin (red) and the nuclei with DAPI (blue). Confocal imaging was performed. Single channels are shown in grayscale and the merges in color. The arrows indicate primary cilia. A magnification of 630x was used.

For quantification of primary cilia lengths, fluorescence microscopy images were used and the lengths were determined with the freehand line tool of Image J. The withdrawal of serum generally increased the length of primary cilia independent of the additional treatment. The

mean primary cilium length in the presence of serum was 1.6 µm and by withdrawal of serum it increased to 2.72 µm. Under both conditions the application of 50 mM lithium chloride led to an elongation of primary cilia, resulting in lengths of 2.4 µm and 4.6 µm in the presence and absence of serum, respectively. In contrast, no effect could be detected in response to tubastatin A.

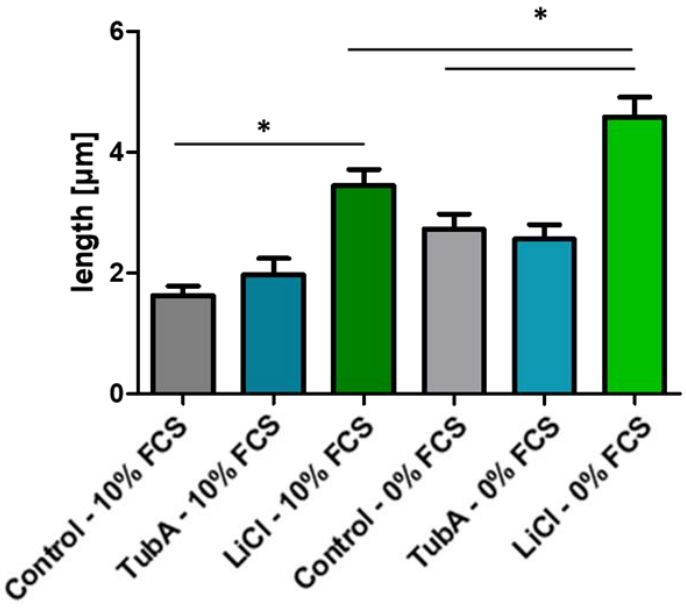

Figure 19: Quantification of primary cilia length in NRCF after tubastatin A and LiCl treatment. 2D cardiac fibroblast cultures derived from neonatal rats (NRCF) were cultured for 24 h in the presence or absence of serum and afterwards 6 µM tubastatin A (TubA) or 50 mM LiCl in serum-containing or serum-free medium was added. The cells were cultured for further 24 h. Acetylated α-tubulin (green) was detected with a specific antibody. Fluorescence imaging was performed and the length of primary cilia was measured with the freehand line of Image J. Given are the means±SEM of three independent experiments (n=3). In each experiment a minimum of 23 cells per condition were analysed, *p<0.05 assessed by one-way ANOVA.

4.2 Primary cilia regulation in hypoxia

During pathological processes such as myocardial infarction cardiac fibroblasts are exposed to hypoxia. To elucidate how hypoxia influences α-tubulin acetylation and importantly primary cilia formation in cardiac fibroblasts, NRCF were kept in culture at 1% O_2 and 20 % O_2, representing hypoxia and normoxia, in parallel. In addition, the cells were again treated with tubastatin A and lithium chloride to see, if hypoxia interferes with these substances. By immunofluorescence analysis of acetylated α-tubulin, no obvious differences in cell morphology could be detected with respect to oxygen levels. Under control conditions, as well as in the presence of lithium chloride, acetylated α-tubulin was

mainly detected around the nucleus, after tubastatin A treatment acetylated microtubules where evenly distributed in the cells (Fig. 20).

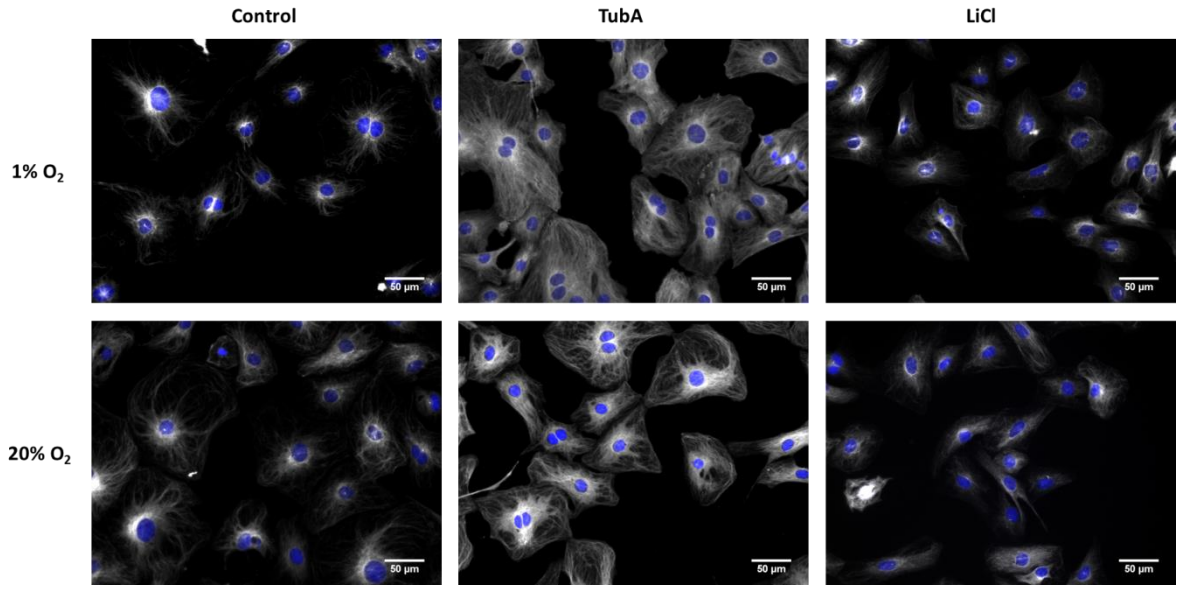

Figure 20: Fluorescence microscopy of primary cilia in serum-starved NRCF under hypoxic and normoxic condition with additional TubA or LiCl treatment. 2D cardiac fibroblast cultures derived from neonatal rats (NRCF) were cultured for 48 h in the absence of serum either under normoxic (20% O_2) or hypoxic (1% O_2) conditions. In the last 24 h 6 µM tubastatin A (TubA) or 50 mM LiCl was added. Acetylated α-tubulin (grayscale) was detected with a specific antibody, the nuclei were stained with DAPI (blue) and fluorescence imaging was performed. Shown are the overlays. A magnification of 200x was used.

4.2.1 Hypoxia leads to no change in number of primary cilia in cardiac fibroblasts under control condition

The fraction of ciliated cells was measured after immunofluorescent staining of acetylated α-tubulin, comparing NRCF cultured with 20% O_2 and 1% O_2 under control condition and after treatment with tubastatin A and lithium chloride. Under normoxic conditions, tubastatin A treatment reduced the fraction of ciliated cells as described above. In this set of experiments, the decline was significant due to the lower variances of the data sets. And again lithium chloride showed no effect on the number of ciliated cells. In hypoxia compared to normoxia, a further decline after tubastatin A treatment was observed, whereas in the presence of lithium chloride by trend an increase in the number of ciliated cells was detected (Fig. 21).

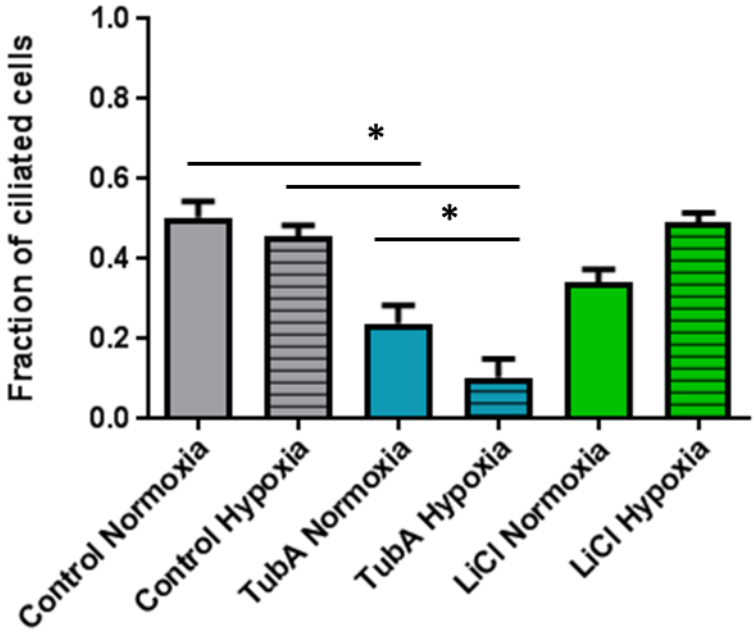

Figure 21: Quantification of ciliated, serum-starved NRCF under hypoxic and normoxic condition with additional TubA or LiCl treatment. 2D cardiac fibroblast cultures derived from neonatal rats (NRCF) were cultured for 48 h in the absence of serum either under normoxic (20% O_2) or hypoxic (1% O_2) conditions. In the last 24 h 5 µg/mL tubastatin A (TubA) or 50 mM LiCl was added. Acetylated α-tubulin was detected with a specific antibody and fluorescence imaging was performed. The number of ciliated cells was counted and is given as fraction of all cells. Shown are the means±SEM of three independent experiments (n=3). In each experiment a minimum of 414 cells per condition were analysed, *p<0.05.

4.2.2 Hypoxia increases primary cilia length in cardiac fibroblasts

Besides the fraction of ciliated cells, the length of cilia in normoxia and hypoxia was compared. It has been suggested, that hypoxia-inducible factor 1-alpha (HIF1-α) contributes to primary cilia length in renal epithelial cells upon renal injury (Verghese et al. 2011). The analysis of primary cilia length under normoxic and hypoxic conditions showed that hypoxia significantly increases primary cilia length in NRCF, under control conditions. Application of lithium chloride increased primary cilia length in normoxia and hypoxia. Tubastatin A, in contrast, had no effect on cilia length in normoxia and blunted the hypoxia-dependent increase (Fig. 22).

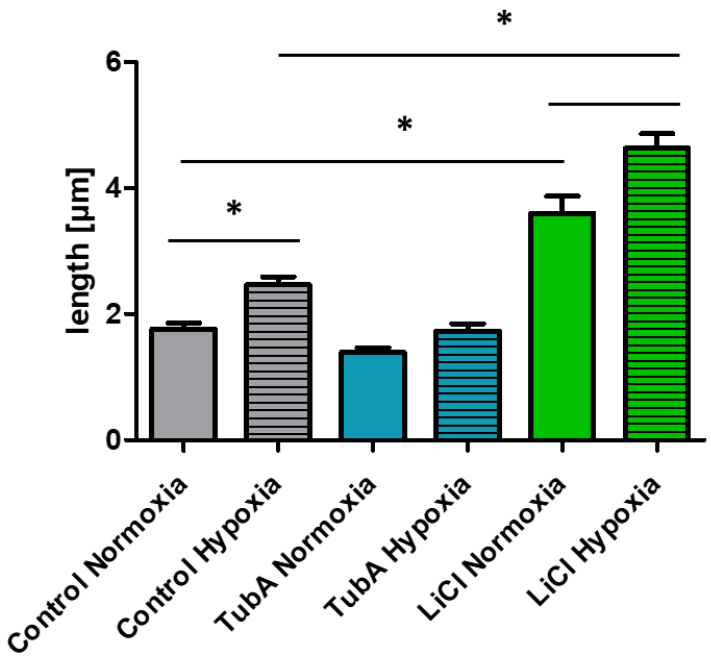

Figure 22: Quantification of primary cilia length in serum-starved NRCF under hypoxic and normoxic condition with additional TubA or LiCl treatment. 2D cardiac fibroblast cultures derived from neonatal rats (NRCF) were cultured for 48 h in the absence of serum either under normoxic (20% O_2) or hypoxic (1% O_2) conditions. In the last 24 h 6 µM tubastatin A (TubA) or 50 mM LiCl was added. Acetylated α-tubulin was detected with a specific antibody and fluorescence imaging was performed. The length of primary cilia were measured with the free hand tool of Image J. Given are the means±SEM of three independent experiments (n=3). In each experiment a minimum of 39 cells per condition were analysed, *p<0.05 assessed by one-way ANOVA.

4.2.3 Tubastatin A and lithium chloride increase α-tubulin acetylation under normoxic and hypoxic condition

To assess whether the induction of hypoxia in NRCF was successful and if hypoxia influences α-tubulin acetylation, immunoblot analysis for HIF1-α and acetylated α-tubulin was carried out. In addition, total α-tubulin, β-actin and vinculin were analysed as loading controls. As shown in figure 23, in lysates of cells, which had been exposed to hypoxia HIF1-α was stabilized proving the lowered oxygen levels during culture. In addition, a strong increase in acetylated α-tubulin was detected after tubastatin A treatment independent of the oxygen levels showing that HDAC6 inhibition was successful. In the same samples, the total α-tubulin signal was reduced compared to control. To ensure that this was not due to unequal total protein loading, β-actin and vinculin were analysed in addition. Both showed no differences between all samples. Finally, the acetylated α-tubulin signals in lysates of

cells treated with lithium chloride appeared to be slightly higher as in the corresponding controls.

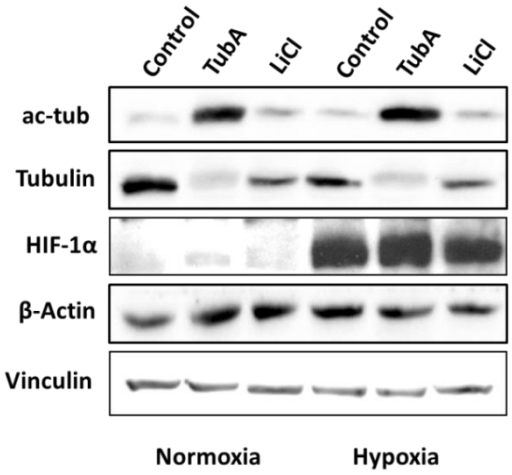

Figure 23: Immunoblot of α-tubulin acetylation in NRCF under normoxic and hypoxic conditions with additional tubastatin A or LiCl treatment. 2D cardiac fibroblast cultures derived from neonatal rats (NRCF) were cultured for 48 h in the absence of serum either under normoxic (20% O_2) or hypoxic (1% O_2) conditions. In the last 24 h 6 µM tubastatin A (TubA) or 50 mM LiCl was added. By immunoblot analysis acetylated α-tubulin, total α-tubulin, HIF-1α, β-actin and vinculin were detected with specific antibodies in cell lysates containing equal protein amounts. Shown are representative immunoblots.

4.3 Comparison of α-tubulin acetylation and primary cilia regulation in cardiac fibroblasts from different species

The data presented so far, demonstrate the effects of tubastatin A and lithium chloride on primary cilia number and length as well as on α-tubulin acetylation in NRCF. Analysis of cardiac fibroblast from other species suggested that the presence of primary cilia on cardiac fibroblasts is conserved over species and developmental stages (see Fig. 7). To analyse this in more detail, adult mouse cardiac fibroblasts (AMCF) were compared with NRCF first with respect to their levels of acetylated α-tubulin by immunoblot. In AMCF the ratio of acetylated α-tubulin to total α-tubulin was by trend higher than in NRCF (Fig. 24).

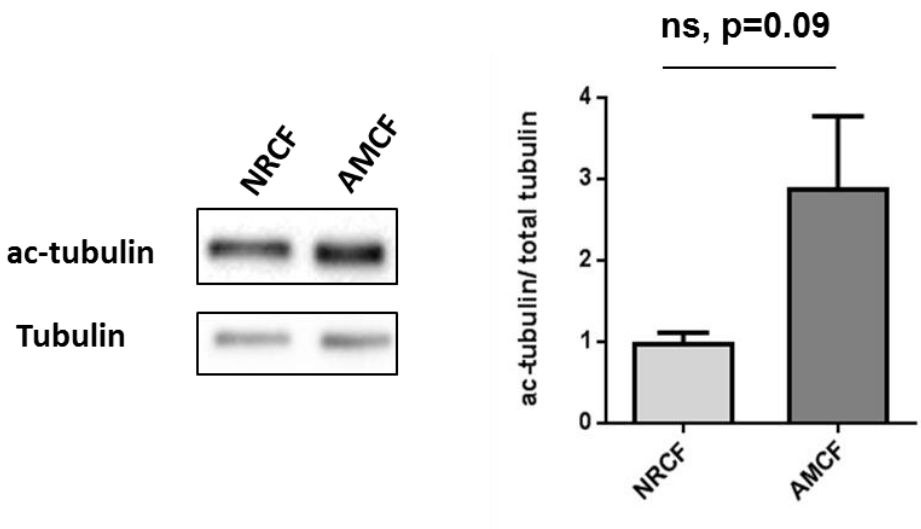

Figure 24: Comparison of α-tubulin acetylation in NRCF and AMCF by immunoblot analysis. Serum-starved 2D cardiac fibroblast cultures derived from neonatal rats (NRCF) and adult mice (AMCF) were used for immunoblot analysis. Acetylated α-tubulin and total α-tubulin were detected with specific antibodies in cell lysates containing equal protein amounts. Shown are representative immunoblots (left) and the analysis of acetylated α-tubulin normalized by α-tubulin. The values are given as means±SEM relative to NRCF, n=3, significance was tested vs. NRCF assessed by unpaired t-test.

4.3.1 Tubastatin A and lithium chloride increase α-tubulin acetylation

In the next step, the effects of tubastatin A and lithium chloride on α-tubulin acetylation was compared in NRCF and AMCF by immunoblot analysis. As already demonstrated in figure 17A, tubastatin A treatment led to a strong increase in acetylated α-tubulin in NRCF. By quantification a 22-fold and 12-fold increase was found for NRCF and AMCF, respectively. The treatment with lithium chloride increased α-tubulin acetylation only moderately and to the same extent in both cell types. In NRCF the increase was 2.2-fold and in AMCF 2.0-fold (Fig. 25).

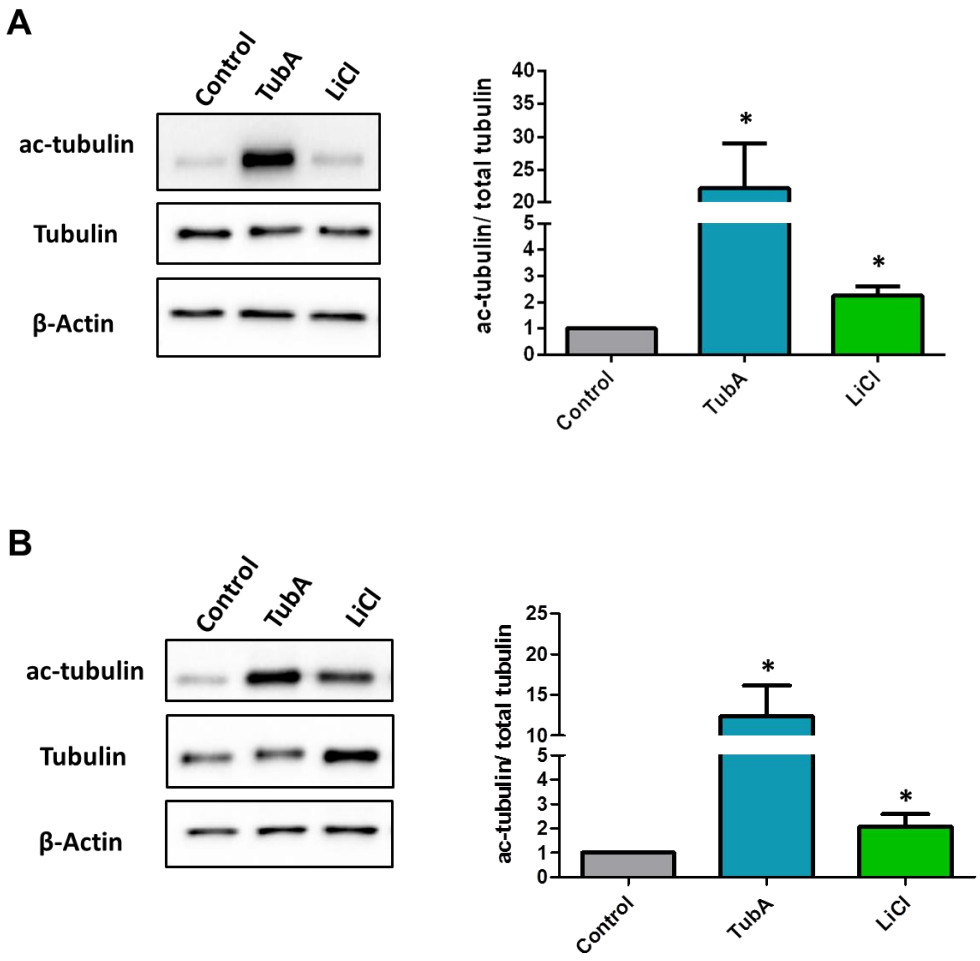

Figure 25: Quantification of α-tubulin acetylation by immunoblot analysis in NRCF and AMCF treated with tubastatin A and LiCl. 2D cardiac fibroblast cultures derived from neonatal rats (NRCF, shown in A) and adult mice (AMCF, shown in B) were cultured for 24 h in the absence of serum and afterwards 6 µM tubastatin A (TubA) or 50 mM LiCl in serum-free medium was added as indicated. The cells were cultured for further 24 h. By immunoblot analysis acetylated α-tubulin, total α-tubulin and β-actin were detected with specific antibodies in cell lysates containing equal protein amounts. Shown are representative immunoblots (left) and the analysis of acetylated α-tubulin normalized by α-tubulin. The values are given as means±SEM relative to untreated control, n=3, *p<0.05 vs. control assessed by one-way ANOVA.

Next, the frequency of ciliated AMCF and the length of primary cilia were analysed under basal conditions and after tubastatin A and lithium chloride treatment. Although the basal levels of acetylated α-tubulin were higher in AMCF compared to NRCF, the fraction of ciliated cells were lower. Only around 30% of AMCF were found to be ciliated under control condition (Fig. 26A). In contrast, the percentages of NRCF ranged from 50% to 60% (see Fig. 17 and Fig. 21). The mean primary cilium length was in addition shorter in AMCF

compared to NRCF. Under control condition a mean length in AMCF of 0.6 µm was found, whereas in NRCF the mean length in the absence of serum ranged between 1.7 µm and 2.7 µm (see Fig. 19 and Fig. 26). Similar as in NRCF, treatment of AMCF with tubastatin A resulted in a frequency reduction of ciliated cells and had no influence on primary cilia length. The decline in the number of ciliated cells was more pronounced in AMCF than in NRCF, although the relative effect of tubastatin A on the increase in acetylated α-tubulin was lower (see Fig. 25). Lithium chloride treatment had no effect on the number of ciliated AMCF as previously shown for NRCF and it increased the mean primary cilia length to 1.2 µm. The relative effect of lithium chloride on primary cilia length was similar in AMCF and NRCF. An around 2-fold increase could be detected in both cell types.

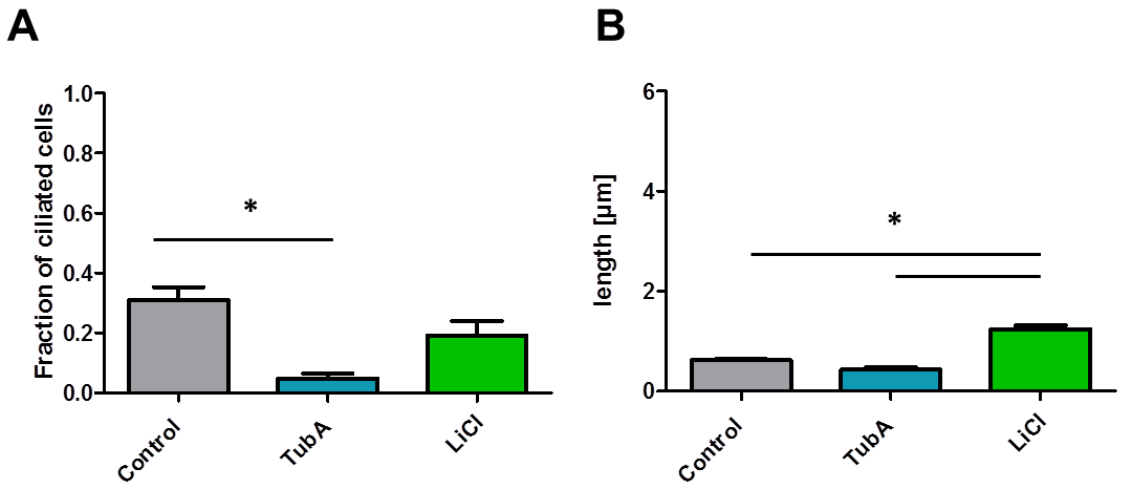

Figure 26: Quantification of primary cilia frequency and length in AMCF after tubastatin A and LiCl treatment. 2D cardiac fibroblast cultures derived from adult mice (AMCF) were cultured for 24 h in absence of serum and afterwards 6 µM tubastatin A (TubA) or 50 mM LiCl in serum-free medium was added. The cells were cultured for further 24 h. Acetylated α-tubulin was detected with a specific antibody. **A)** Fluorescence imaging was performed and the number of ciliated cells was counted and is given as fraction of all cells. **B)** The length of primary cilia was measured with the freehand line tool of Image J. Given are the means±SEM of three independent experiments (n=3). In each experiment a minimum of 507 cells and for length measurement a minimum of 16 cilia per condition were analysed, *p<0.05 assessed by one-way ANOVA.

The observed differences between NRCF and AMCF raised the question whether this was due to a difference in species or developmental stage. Therefore, neonatal mouse cardiac fibroblasts were investigated in addition. By immunoblot analysis a similar difference in the ratio of acetylated α-tubulin to total α-tubulin between NMCF and NRCF was found as compared to AMCF and NRCF. In both mouse cardiac fibroblasts 3-fold more α-tubulin was acetylated arguing for a species-specific difference in α-tubulin acetylation under basal conditions.

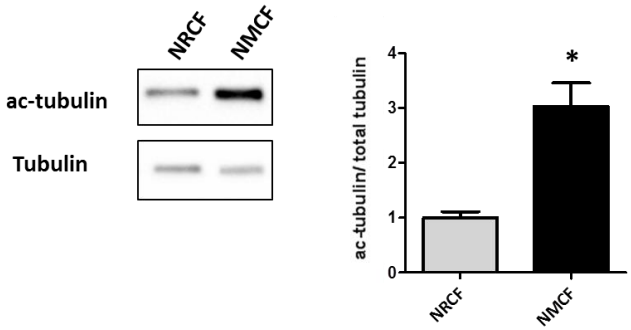

Figure 27: Comparison of α-tubulin acetylation in NRCF and NMCF by immunoblot analysis. Serum-starved 2D cardiac fibroblast cultures derived from neonatal rats (NRCF) and neonatal mice (NMCF) were used for immunoblot analysis. Acetylated α-tubulin and total α-tubulin were detected with specific antibodies in cell lysates containing equal protein amounts. Shown are representative immunoblots (left) and the analysis of acetylated α-tubulin normalized by α-tubulin. The values are given as means±SEM relative to NRCF, n=3, significance was tested vs. NRCF assessed by unpaired t-test.

Next, the NMCF were treated with tubastatin A and lithium chloride after starvation and α-tubulin acetylation as well as primary cilia regulation was investigated. Tubastatin A increased α-tubulin acetylation by 15-fold and lithium chloride by 2.2-fold, which is more similar to the observed changes in AMCF than in NRCF. The fraction of ciliated NMCF was under basal condition around 60%, and declined in the presence of tubastatin A to 30%. Similar as shown for NRCF and AMCF, lithium chloride had no effect on the number of ciliated cells. Thus, the fraction of ciliated NRCF and NMCF was rather comparable. The measured mean primary cilia length was 0.6 µm under basal conditions and thus it was identical to the mean cilium length in AMCF. Lithium chloride treatment increased the mean length to 0.84 µm.

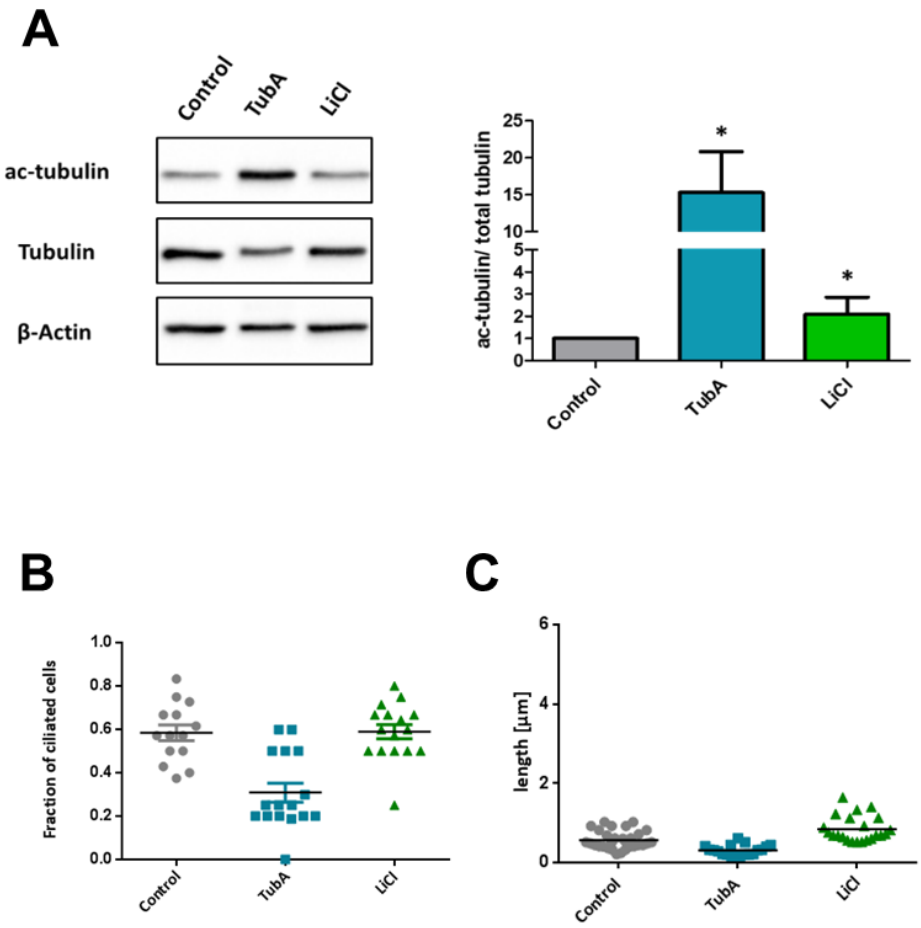

Figure 28: Quantification of α-tubulin acetylation and of primary cilia frequency and length in NMCF treated with tubastatin A and LiCl. 2D cardiac fibroblast cultures derived from neonatal mice (NMCF) were cultured for 24 h in absence of serum and afterwards 5 µg/mL tubastatin A (TubA) or 6 µM LiCl in serum-free medium was added as indicated. The cells were cultured for further 24 h. **A)** By immunoblot analysis acetylated α-tubulin, total α-tubulin and β-actin were detected with specific antibodies in cell lysates containing equal protein amounts. Shown are representative immunoblots (left) and the analysis of acetylated α-tubulin normalized by α-tubulin. The values are given as means±SEM relative to untreated control, n=3, *p<0.05 vs. control assessed by one-way ANOVA. **B)** Acetylated α-tubulin was detected with a specific antibody. Fluorescence imaging was performed and the number of ciliated cells was counted and is given as fraction of all cells. n=2, 7 to 8 images were analysed per experiment. Shown are the single measurements and the means. **C)** The length of primary cilia was measured with the freehand line tool of Image J. Given are the single measurements and the means of two independent experiments, n=2.

4.4 Increased α-tubulin acetylation interferes with proliferation capacity of cardiac fibroblasts

Primary cilia are post-mitotic cellular structures that are present in cells during G0/G1 and the beginning of S phase. They disassemble at late S to early G2 phase when the centriole in the basal body is used to organise the mitotic spindle (Rieder et al. 1979). Therefore, primary cilia regulation is tightly connected to cell cycle control. In order to investigate the effects of tubastatin A and lithium chloride on the ability of NRCF to divide, proliferation assays were performed. Under basal condition, the doubling time was around 70 hours in the presence of serum. Treatment with tubastatin A and lithium chloride both completely blocked cell proliferation. Four days of lithium chloride treatment resulted in a decline in cell number by around 30% compared to day 0 (Fig.29).

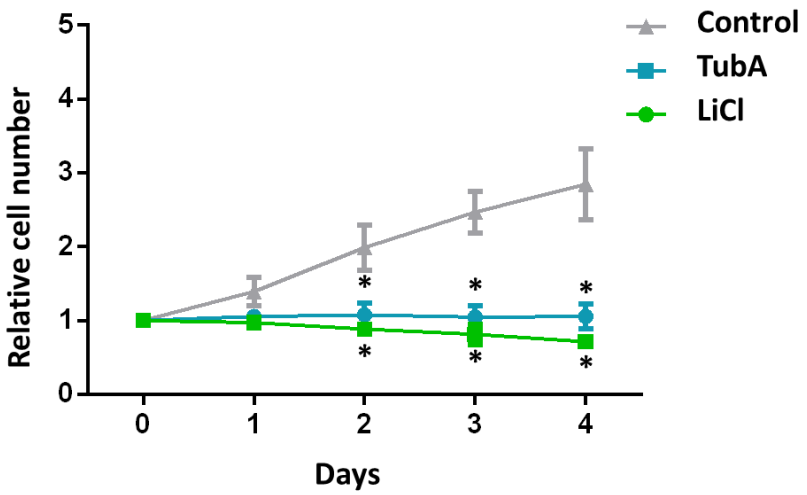

Figure 29*:* Analysis of proliferation of NRCF under control conditions and after treatment with tubastatin A or LiCl. 2D cardiac fibroblast cultures derived from neonatal rats (NRCF) were cultured in medium containing 10% FCS and additionally 5 µg/mL tubastatin A (TubA) or 50 mM LiCl as indicated for up to 4 days. Nuclei were stained with DAPI and quantified by automated counting. The change in cell numbers are given relative to day 0 of each group and are shown are means±SEM, n=3, *p<0.05 vs. control at the respective time point.

Next the proliferation capacity of AMCF was analysed. These cells grew very poorly even in the presence of serum and the estimated doubling time according to the data presented in figure 28 was around 200 hours. Treatment with tubastatin A and lithium chloride blocked cell proliferation. Four days of tubastatin A and lithium chloride treatment resulted in a decline in cell number by around 15% and 40%, respectively, compared to day 0 (Fig.30).

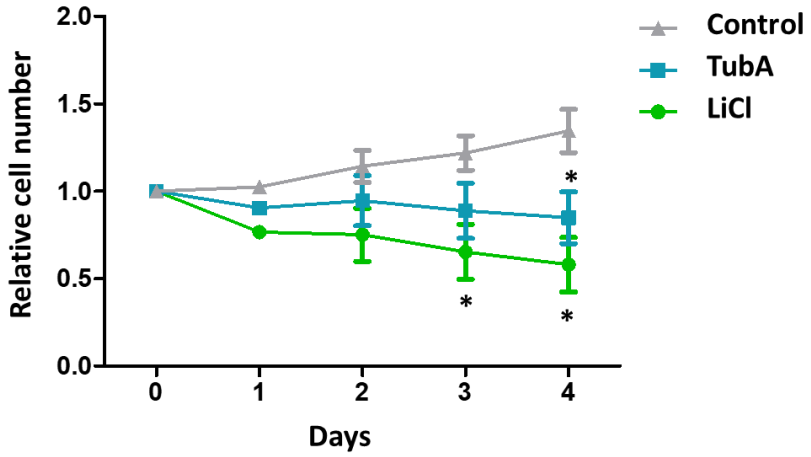

Figure 30: Analysis of proliferation of AMCF under control conditions and after treatment with tubastatin A or LiCl. 2D cardiac fibroblast cultures derived from adult mice (AMCF) were cultured in medium containing 10% FCS and additionally 6 µM tubastatin A (TubA) or 50 mM LiCl as indicated for up to 4 days. Nuclei were stained with DAPI and quantified by automated counting. The change in cell numbers are given relative to day 0 of each group and are shown as means±SEM, n=3, *p<0.05 vs. control at the respective time point.

5 Discussion

5.1 Do cardiac fibroblasts carry primary cilia?

Primary cilia have been shown to be present in most mammalian cells (Miyoshi et al. 2011) but no data is available, whether these structures can be found on cardiac fibroblasts or not. At the beginning of this thesis, several criteria were considered to reduce the risk of falsely identifying cytoskeletal structures as primary cilia. First, for immunofluorescence experiments, a specific antibody against acetylated α-tubulin and not against total α-tubulin was used to better visualise the axoneme of primary cilia. In addition, γ-tubulin, which is an indispensable part of the cilium's basal body (Kollman et al. 2010) was co-stained with acetylated α-tubulin. These stainings were then imaged by confocal microscopy to allow better resolution. By this, typical primary ciliary structures were found in neonatal rat cardiac fibroblasts (NRCF) located characteristically on top or close to the nucleus (Gerdes et al. 2009). Furthermore, the mean length of these structures in cardiac fibroblasts was 1.6 µm in the presence and 2.72 µm in the absence of serum, which resembles the typical primary cilia length of 1-3 µm (Deane et al. 2013). Moreover, by showing that lithium chloride treatment increased the length of these structures in cardiac fibroblasts, their presence in these cells can be regarded as proven.

Next, the dependence on species or maturation state was investigated by analysing human ventricular as well as neonatal and adult mouse cardiac fibroblasts (NMCF and AMCF) in addition. All of them were found to carry structures fulfilling the characteristics of primary cilia. Hence, it can be assumed, that the presence of primary cilia in cardiac fibroblasts in 2D cultures is species and maturation state independent. Therefore, some of the further experiments were carried out only on NRCF, as we assumed that phenomena observed in these cells could are shared with other cardiac fibroblasts.

Primary cilia and their presence as sensory organelles have been studied intensely in epithelial and endothelial cells, which are located on organ and vessel surfaces. In 2D cultures, cardiac fibroblasts were grown in a monolayer covered by the culture medium, which more resembles a surface environment than that of interstitial cells. Although primary cilia have been detected in other interstitial cells such as osteocytes (Spasic und Jacobs 2017) as well as in 3D culture models of chondrocytes (McGlashan et al. 2010), their presence in matrix-embedded cardiac fibroblasts had not been demonstrated. Therefore, NRCF were embedded in a mesh of collagen 1, cultured for 5 days and acetylated α-tubulin was then detected in slices of these tissues. This clearly revealed that primary cilia were

also present in collagen-embedded cardiac fibroblasts and were not only an artefact of the potentially developed pseudo-polarity in 2D cultures.

However, in this kind of engineered tissue, fibroblasts were not exposed to other cell types and thus conditions did not resemble those in the heart *in vivo*. Therefore, engineered heart muscles (EHM) composed of all cardiac cells were used as a heterogeneous 3D model. To assess the presence of primary cilia in EHM, the different cell types had to be distinguished from each other. The identification of cardiomyocytes is relatively uncomplicated. Their sarcomere structure can be easily identified by staining for F-actin and cell-specific markers, such as caveolin-3 (Song et al. 1996), which was used in the experiments of this thesis. The second most abundant cell type in the heart, endothelial cells (Pinto et al. 2016), could be differentiated using immunostaining for CD31. In the EHM endothelial cells formed tube-like structures exhibiting a dotted pattern of CD31, likely marking adherence junctions (Privratsky and Newman 2014). Finally, the identification of cardiac fibroblasts was based on the exclusion principle. Cells negative for caveolin-3 and CD31 were considered as cardiac fibroblasts. Using this method it is not possible to distinguish between cardiac fibroblasts and smooth muscle cells. However detailed analysis of the cell composition used for EHM preparation (Naito et al. 2006) revealed that the majority of used non-myocytes were cardiac fibroblasts, which allowed us to use this model. Although no numerical data is available on the fraction of ciliated cells in EHM, the stainings clearly demonstrated that cardiomyocytes, displaying a certain degree of maturity as evaluated by caveolin-3 expression (Lieu et al. 2009) did not carry primary cilia. This is in line with early findings on the presence of primary cilia in the human heart showing that in the embryonic myocardium primary cilia were detectable in myoblasts and rarely in defined cardiomyocytes, whereas in the adult heart, primary cilia were restricted to non-muscular cells of the myocardial layer (Myklebust et al. 1977). Cells forming the endothelial tubes or those which are attached to them were found occasionally to carry primary cilia in EHM. Endothelial cells of the aorta had been shown to carry primary cilia especially in areas of blood flow turbulences (Van der Heiden et al. 2008). These cilia, however, project into the vessel lumen and not towards the surrounding tissue as in case of the EHM. We were not able to show if this is because of the absence of flow in the EHM or because the cells which carry primary cilia are for example pericytes. Finally, the vast majority of the residual fraction of cells carried primary cilia in EHM. Although it is likely that most of these cells are indeed cardiac fibroblasts, future studies are needed to further characterise these cells e.g. by expression of periostin and TCF21 (Snider et al. 2008; Acharya et al. 2012). Moreover, the number of ciliated cells and the length of the cilia need to be quantified.

Our preliminary observations indicate that ciliary length seemed to be increased in embedded cells. This is in accordance with an observation of Xu and co-worker showing that type I collagen, which is the main component of the ECM in the heart and in the EHM, increased the primary cilia length of mouse embryo 3T3-L1 fibroblasts (Xu et al. 2017). Nevertheless, it needs to be taken into account that length measurements in 3D is a technical challenge. One possible methodological approach has been described by Saggese et al. which combines confocal imaging, deconvolution and Gaussian blurring to accurately measure the length of primary cilia in 3D culture (Saggese et al. 2012).

5.2 Primary cilia regulation in cardiac fibroblasts

5.2.1 HDAC6 inhibition reduces the number of primary cilia in cardiac fibroblasts

Histone deacetylase 6 (HDAC6) is a class IIb deacetylase, which regulates the deacetylation of α-tubulin in cells (Hubbert et al. 2002). To study the role of HDAC6, different inhibitors are available of which tubastatin A shows so far the highest selectivity (Butler et al. 2010). In this thesis tubastatin A was used to study the effect of HDAC6 inhibition on primary cilia formation in cardiac fibroblasts. Immunoblot analysis revealed an over 10-fold increase in tubulin acetylation in all investigated cardiac fibroblast types, it was surprising to see that this uniformly resulted in a reduction of the fraction of ciliated cells. This is in sharp contrast to other studies showing that tubastatin A treatment increased the fraction of ciliated cholangiocarcinoma (Gradilone et al. 2013) and chondrosarcoma cells (Xiang et al. 2017). Moreover, knockdown of HDAC6 in immortalised RPE-1 (Pugacheva et al. 2007), mouse embryo fibroblast 3T3-L1 (Xu et al. 2016) and chondrosarcoma cells (Xiang et al. 2017) prevented the reabsorption of primary cilia. *Vice versa*, the up-regulation of HDAC6, as for example found in osteoblasts treated with transforming growth factor β1 (TGF-β1), resulted in a reduced number of ciliated cells accompanied by a shortening and deformation of primary cilia (Ehnert et al. 2017). However, there are also studies showing on one hand that overexpression of HDAC6 in a human retinal pigment epithelial cell line led to a decrease in cilia length and number, but on the other hand neither the knockout nor the inhibition of HDAC6 by TubA had any influence on primary cilia formation (Ran et al. 2015). There is no data available demonstrating that HDAC6 inhibition decreases the number of ciliated cells. To further analyse this phenomenon, in this thesis the distribution of acetylated α-tubulin in cardiac fibroblasts was analysed. By immunofluorescence analysis, it was found that the acetylated α-tubulin was distributed all over the cells and not restricted to the perinuclear region as in control cells or after treatment with lithium chloride. A possible

explanation for this finding could lie in the distribution of HDAC6 itself. For RPE-1 cells it was shown that HDAC6 is distributed all over the cytoplasm and enriched at the basal body and the centrosome (Ran et al. 2015). The centrosomal distribution, however, depends on its regulation by the death inducer obliterator 3 (Dido3) (Sánchez de Diego et al. 2014). Whether HDAC6 indeed has a different localisation in cardiac fibroblasts, maybe due to its regulation by Dido3, has to be elucidated further.

5.2.2 LiCl increases primary cilia length in cardiac fibroblasts

Lithium salts are used in the clinics as mood stabilisers to treat e.g. bipolar disorders. On a cellular level lithium was found to increase the length of primary cilia in many different cell types (Miyoshi et al. 2009; Thompson et al. 2016; Spasic und Jacobs 2017). Whether this could explain its pharmacological action is not known. On a molecular level several targets of lithium have been identified including glycogen synthase kinase 3β (GSK-3β) (Klein and Melton 1996), several adenylyl cyclases (AC), preferentially AC5 (Mann et al. 2009), but also ACIII which resides in the primary cilium (Ou et al. 2012; Antal et al. 2017)), and the inositol monophosphatase (IMPase) (Shaldubina et al. 2001). With respect to bipolar disorders, there are several lines of evidences that the inhibitory effect of lithium on GSK-3β is responsible for its pharmacological action (Muneer 2017). The inhibitory mechanism of lithium on GSK-3β seems to be complex. On one hand a direct mechanism was proposed in which the lithium ion replaces the essential magnesium ion which may influence the phosphoryl transfer to substrates (Ryves und Harwood 2001). On the other hand lithium was demonstrated to increase phosphatidylinositol-4,5-bisphosphate 3-kinase (PI3K) activity, leading to an inhibition of GSK-3β by phosphorylation of serine 9 via Akt activation (Chalecka-Franaszek and Chuang 1999).

In line with several other publications demonstrating that lithium chloride increases the length of primary cilia in fibroblasts or fibroblasts-like cells (Nakakura et al. 2015; Spasic und Jacobs 2017), the treatment of cardiac fibroblasts with lithium chloride in 2D and 3D cultures resulted in an elongation of primary cilia by around 2-fold , independent of their source and whether serum was present or not. The open question which remains is how this elongation is regulated in detail. A potential mechanism is the lithium chloride-dependent inhibition of GSK-3β, which had been assessed in other cells not only by lithium chloride, but also by the use of more specific tools. For example, in N1 murine hypothalamic neuronal cells it had been demonstrated that the knockdown of GSK-3β by a specific siRNA resulted in primary cilia elongation (Kang et al. 2015). In human retinal pigmented epithelium RPE cells, the usage of the specific GSK-3β inhibitors CHIR99021 and the L803-

mts peptide inhibitor was found to increase ciliary length similar as lithium did (Ou et al. 2012). However, there are also contradictory findings showing e.g. that in contrast to lithium four different GSK-3β inhibitors (valproate, GSK-3β inhibitor II, VII and XI) did not have any effect on cilia length in human fibroblast-like synoviocytes (Ou et al. 2009). And in mouse embryonic fibroblasts and in murine NIH 3T3 fibroblasts the knockout of GSK-3β as well as its inhibition by CHIR99021 resulted even in an inhibition of primary cilia formation (Zhang et al. 2015).

The role of GSK-3β in the regulation of primary cilia formation and elongation is controversially discussed, and potential down-stream mechanisms are unclear. In N1 murine hypothalamic neuronal cells it was shown that overexpression of GSK-3β led to a down-regulation of ciliary genes such as KIF3A and several IFT-genes. (Kang et al. 2015). For human fibroblast KD cells it was suggested that inhibition of GSK-3β by lithium chloride mobilises the α-tubulin-N-acetyl-transferase (ATAT1), which leads to increased acetylation of α-tubulin and to elongation of primary cilia. However, this hypothesis mainly relies on data showing that the knockout of ATAT1 by a siRNA reduced α-tubulin acetylation whereas inhibition of GSK-3β increased it (Nakakura et al. 2015). In primary mouse embryonic fibroblasts (MEFs) it was shown that only the combined inactivation of the gene product of the Von-Hippel-Lindau tumour suppressor gene (pVHL) and of GSK-3β led to a reduction of the fraction of ciliated cells. The inactivation of only one of those two factors was not sufficient to affect cilia maintenance (Thoma et al. 2007).

Taken together, the data in this thesis clearly demonstrates that primary cilia elongation in cardiac fibroblasts is sensitive to lithium chloride treatment, however, whether or not this involves the inhibition of GSK-3β and/or the mobilisation of ATAT1 requires further investigation.

5.2.3 Hypoxia increases primary cilia length

Hypoxia is a pathologic condition which occurs in the heart either as an immediate consequence e.g. of a coronary artery occlusion or chronically as a result of cardiac fibrosis leading to an insufficient perfusion of the myocardium. Hypoxia affects all cells in the heart including cardiac fibroblasts, which transdifferentiate into myofibroblasts (Watson et al. 2014). This induces, in case of a myocardial infarction, the induction of reparative fibrosis in order to produce a stable scar.

The effect of hypoxia on cardiac fibroblast behaviour has been also studied in 2D culture models by which it was shown that hypoxia complexly change the behaviour of cardiac

fibroblasts. This e.g. includes the production of ECM proteins and cell proliferation (Gao et al. 2014; Ugolini et al. 2017). In this thesis, the elongation of primary cilia of cardiac fibroblasts as a consequence of hypoxia could be observed.

The central molecule in the transmission of hypoxia into a biological response is the transcription factor HIF-1α. Under normoxic conditions HIF-1α is hydroxylated by prolyl hydroxylases (PHD), leading to binding of pVHL and consequently to its ubiquitination and proteasomal degradation (Metzen und Ratcliffe 2004). As already mentioned above, pVHL plays a role in the regulation of primary cilia formation. Patients having mutations in pVHL are predisposed to certain cancer types, including renal cancer of the clear cell type (CC-RCC), thus pVHL acts in addition as a tumour suppressor gene. Interestingly, established cancer cell lines from CC-RCC patients are missing primary cilia and are often used to study the role of pVHL in this context. In these cell lines it was further shown that loss-of-function mutations in pVHL led to the accumulation of HIF-1α (Esteban et al. 2006; Xu et al. 2010), raising the question whether HIF-1α is needed for primary cilia regulation. By induction of hypoxia and by the use of specific siRNAs against HIF-1α or by its overexpression in normoxia most studies could establish a role of this transcription factor in primary cilia regulation, not only in RCC cells, but also in other cell types including mouse embryonic fibroblasts and mesenchymal stem cells (Esteban et al. 2006; Xu et al. 2010; Proulx-Bonneau und Annabi 2011; Troilo et al. 2014). However, these studies uniformly show that HIF-1α inhibits primary cilia formation, in sharp contrast to the finding in this current thesis. There was no difference in the proportion of ciliated cells under normoxic and hypoxic control conditions eitherin the presence or absence of lithium chloride. Only when HDAC6 was inhibited, less cells were found to carry primary cilia in hypoxia. This data argues for a link between hypoxia and HDAC6 in the regulation of primary cilia. And indeed it was shown that HDAC6 can stabilise HIF-1α (Kong et al. 2006; Qian et al. 2006) and that HIF-1α regulates Aurora kinase A expression (Klein et al. 2008; Dere et al. 2015). Aurora kinase A plays not only a role in cell cycle regulation, but can induce fast primary cilia reabsorption by phosphorylation and thus activation of HDAC6 at the basal body of primary cilia. Interestingly, Aurora kinase A is not only regulated by hypoxia, but also by serum via the human enhancer of filamentation 1 (HEF1) (Pugacheva et al. 2007).

Data concerning a possible connection between primary cilia elongation and stabilisation of HIF-1α, as found in this thesis, had been rarely described by others. It had been shown, that in mice upon renal injury and under the resulting hypoxic condition, primary cilia in the proximal and distal tubule/collecting duct undergo an increase in length (Verghese et al.

2008). In Madin Darby canine kidney cells those findings could be confirmed by stabilising HIF-1α via treatment with cobalt chloride (Verghese et al. 2011). Our data on primary cilia in cardiac fibroblasts and HIF-1α stabilisation upon hypoxic conditions resemble the findings of Verghese et al. Nevertheless, further investigations are required, to clarify how HIF-1α facilitates the elongation of primary cilia in cardiac fibroblasts. One explanation for a HIF-1α-dependent elongation of primary cilia could lie in its inhibition of GSK-3β. In line with this hypothesis, Lal and colleagues demonstrated that isolated cardiac fibroblasts from ischemic mouse hearts showed a 2-fold increase in GSK-3β phosphorylation at its inhibitory serine 9 (Lal et al. 2014). In summary, it can be considered as possible that there are overlaps in the effects of lithium chloride and hypoxia. But since we found, that under hypoxic conditions lithium chloride still leads to an elongation of primary cilia in comparison to primary cilia of cardiac fibroblasts under hypoxic control conditions, it is likely that the underlying mechanism is not identical.

5.3 Primary cilia and cardiac fibroblast proliferation

The formation of primary cilia is restricted to cells in cell cycle phase G1/G0, since they originate from the mother-centriole (Marshall 2007). The latter is part of the spindle-apparatus formed during mitosis and therefore not available for primary cilia formation when cells divide. Surprisingly, we could not determine a difference in the fraction of ciliated cells in NRCF in the absence or presence of 10% serum, which had been shown to be a proliferation stimulus for those cells (Jatho et al. 2015).

We found that lithium chloride has an impact on primary cilia and on proliferation in cardiac fibroblasts, which raises the question if a correlation between both can be determined. The effect of lithium chloride treatment was restricted to the length of primary cilia, whereas the fraction of ciliated cells did not change significantly. Based on these data we do not expect that the antiproliferative effect of lithium chloride treatment is based on its influence on primary cilia. It is more likely that either the increased tubulin acetylation or another mechanism underlies the impaired proliferation rate of cardiac fibroblasts treated with lithium chloride. In human Tenon's capsule fibroblasts lithium chloride has been shown to inhibit TGF-β1-induced expression of α-smooth muscle actin (Chung et al. 2014). As described in section 1.1, TGF-β1 is involved in the activation of fibroblasts to α-smooth muscle actin expressing myofibroblasts, which have a considerably higher proliferation capacity than quiescent fibroblasts. In inhibiting the TGF-β1-mediated activation, the antiproliferative effect of lithium chloride could be founded, too.

In addition, the effects of tubastatin A and lithium chloride in cardiac fibroblasts were similar concerning their effect on cell proliferation, but different concerning primary cilia length. Those findings argue for different mechanisms underlying the effects of the treatments on primary cilia and proliferation.

Even though we did not show a direct interaction between primary cilia in cardiac fibroblasts and the proliferation rate of those cells, primary cilia and proliferation cannot be assessed independently. In various other cell types a connection has been shown, such as the uncontrolled proliferation of kidney cells of patients affected by the ciliopathy polycystic kidney disease (PKD) (Nauli et al. 2003). Other examples are the loss of primary cilia in pancreatic cancer cells (Seeley et al. 2009) or in cholangiocarcinoma cells (Gradilone et al. 2013). Thus, further investigations concerning the influence of primary cilia in cardiac fibroblasts on proliferation and fibrosis development are needed.

5.4 The potential function of primary cilia in cardiac fibroblasts

The function of primary cilia in cardiac fibroblasts is far from being defined. Nevertheless, reasonable hypotheses can be proposed. In the beating heart, cardiac fibroblasts are exposed to a cyclic strain and possess the ability to react to relative changes of strain in the cardiac wall. To assess whether primary cilia as sensory organelles play a role in the perception of those changes, a method to subject cardiac fibroblasts to cyclic strain could be used.

To this end, in the chondrocytes system, flexible-bottomed culture plates have been used and a cyclic tensile strain of 10% and 20% at 0.33 Hz has been applied. This experiment revealed that primary cilia in chondrocytes are shortened under application of cyclic tensile strain (Thompson et al. 2014). Another published example of the influence of tensile stress on cilia length is the elongation of tendon cell cilia upon stress-deprivation (Gardner et al. 2011). We suggest to investigate the effect of strain on primary cilia in cardiac fibroblasts in 2D by the use of the flexible-bottomed culture plates and in 3D by stretching engineered tissue (ECT and EHM) with different amplitudes and different frequencies of cyclic strain and visualising the changes in primary cilia performance by immunofluorescence.

In addition, a chemosensory function of primary cilia in cardiac fibroblasts is possible. The entry of proteins at the base of the cilium in a concentration- and size-dependent manner has been demonstrated (Lin et al. 2013). The entry was impeded with increasing protein size. In the development of fibrosis several cytokines play an important role, such as TGF-β, which is relatively small with only a size of 13kDa. Cardiac fibroblasts activation is

triggered by cytokines and it is possible, that primary cilia are involved in the process of detecting and reacting to cytokine stimuli.

5.5 Limitations and perspectives

The investigations concerning cardiac fibrosis and its key player, the cardiac fibroblast, have been limited in the past *inter alia* by the lack of a specific fibroblast marker. With the availability of new, more specific markers such as TCF21 (Acharya et al. 2012) and PDGFRα (Moore-Morris et al. 2014), novel approaches will be facilitated, including studies not only of engineered, but of natural heart muscle. Hence, in order to complete the evaluation of the presence of primary cilia in cardiac fibroblasts, sections of healthy and diseased hearts should be examined by the help of these marker proteins.

This project revealed that primary cilia length in cardiac fibroblasts can be regulated by lithium chloride and hypoxia. So far, the mechanisms behind the effects of lithium chloride and of HIF-1α on primary cilia length are not fully understood. A role of GSK-3β in both regulations is however likely, as discussed above. Therefore, specific GSK-3β inhibitors should be included in future studies for verification. Moreover, the role of HDAC6 in primary cilia regulation differs from otherwise published data. One explanation could lie in a different localisation of HDAC6 in cardiac fibroblasts compared to other cells. Detailed immunofluorescence analyses could help to shed light on this contradictory result.

Finally, independent of their impact on primary cilia number and shape, both lithium chloride and HDAC6 inhibition resulted in a compete suppression of cardiac fibroblast proliferation. The remaining question is whether HDAC6 inhibition or lithium chloride could potentially prevent cardiac fibroblast proliferation in the diseased heart and thus prevent cardiac fibrosis. Tubastatin A has not been tested in humans yet. In animal models the data are so far not conclusive. In mice a general knockout of HDAC6 was found to improve the cardiac contractile function after chronic angiotensin II administration, however, cardiac fibrosis was strongly increased compared to wild type mice (Demos-Davies et al. 2014). In contrast, in rats the inhibition of HDAC6 with tubastatin A led to a reduction in kidney fibrosis after angiotensin II administration (Choi et al. 2015).

Lithium on the other hand is a well-known neuro-psychiatric drug, which has been used for many years including today, as a mood-stabiliser in the treatment and prophylaxis of bipolar disease (Shaldubina et al. 2001). Even though lithium has a narrow therapeutic index, a lot of clinical experience in its use already exists. Nevertheless, one potential side effect of long-term therapy with lithium was described to be kidney function impairments, which goes

along with remodelling of the tissue including interstitial kidney fibrosis (Walker et al. 1982). Moreover, lithium was shown to have the propensity to induce arrhythmias. Contraindications for lithium treatment are therefore e.g. changes in the ECG like QT-prolongations as well as heart failure, disqualifying lithium as a suitable therapy for cardiac fibrosis.

5.6 Conclusion

The data obtained in this study provide evidence, that primary cilia are present in cardiac fibroblasts from different origins in homogenous 2D as well as in rat homo- and heterogenous 3D cultures. The fraction of cells carrying primary cilia are reduced by HDAC6 inhibition with tubastatin A and primary cilia length was increased by lithium chloride and hypoxia. An increase in tubulin acetylation induced by tubastatin A or lithium chloride led in both cases to a blockade of proliferation.

6 Summary

Cardiac fibroblasts and their activation upon cardiac damage play a key role in pathological cardiac remodelling and the development of cardiac fibrosis. This thesis investigates the role of α-tubulin acetylation in cardiac fibroblasts with a special focus on formation and regulation of primary cilia. The primary cilium is a microtubule-based, immotile sensory structure, that contains acetylated α-tubulin.

First, the presence of primary cilia in cardiac fibroblasts in 2D culture of neonatal rat cardiac fibroblasts (NRCF), neonatal and adult mouse cardiac fibroblasts (NMCF, AMCF) and human ventricular cardiac fibroblasts (HVCF) was shown by immunofluorescence. This leads to the conclusion that cardiac fibroblasts from different species and maturation states possess primary cilia.

Two 3D models were used to assess primary cilia: engineered connective tissue, in which cardiac fibroblasts are embedded in collagen I, as well as engineered heart muscle, which are composed of all cardiac cells surrounded by a collagen I matrix. Primary cilia were found in cardiac fibroblasts in immunostainings of sections of ECT and EHM.

In a next step the regulation of primary cilia in cardiac fibroblasts was examined by the use of two substances, which had been shown to increase the acetylation of α-tubulin; tubastatin A (TubA) and lithium chloride (LiCl). Tubastatin A is a specific inhibitor of HDAC6, the main deacetylase of α-tubulin. Lithium chloride leads to elevated levels of α-tubulin-acetylation by a mechanism that is not fully elucidated, but which probably involves the mobilisation of the α-tubulin-N-acetyltransferase (ATAT1), which catalyses the transfer of acetyl groups on α-tubulin. In immunoblot analysis the increased α-tubulin-acetylation following both treatments (TubA, LiCl) could be shown in NRCF, NMCF and AMCF.

It was found, that treatment with lithium chloride significantly increases the length of primary cilia. The exact mechanism by which lithium chloride leads to an elongation of primary cilia is not clear but it is likely that this effect is mediated via inhibition of the glycogen synthase kinase 3 β (GSK-3β).

One condition to which cells in the heart are exposed to during pathological processes such as myocardial infarction, is hypoxia. Hypoxic conditions were successfully induced in neonatal rat cardiac fibroblasts, as shown by the stabilisation of hypoxia inducible factor 1α (HIF-1α). Under hypoxic conditions the cells were treated with tubastatin A and lithium

chloride and it was found that hypoxia increases primary cilia length under control conditions, as well as in the presence of lithium chloride.

Finally, the impact of both treatments on proliferation of NRCF and AMCF was investigated and it could be shown, that the proliferation capacity of cells with an increased α-tubulin acetylation was impaired.

7 Zusammenfassung

Kardiale Fibroblasten und ihre durch kardiale Schädigung hervorgerufene Aktivierung spielen eine Schlüsselrolle im Prozess des kardialen Umbaus und der Entwicklung kardialer Fibrose.

Die vorliegende Dissertation befasst sich mit der Rolle der Acetylierung von α-Tubulin in kardialen Fibroblasten mit besonderem Augenmerk auf die Bildung und Regulation von Primärzilien. Die Primärzilie ist eine aus Mikrotubuli bestehende, unbewegliche sensorische Struktur, die acetyliertes α-Tubulin enthält.

Zunächst wurde mittels Immunfluoreszenz gezeigt, dass 2D-Kulturen kardialer Fibroblasten von neonatalen Ratten (NRCF), neonatalen und adulten Mäusen (NMCF, AMCF) ebenso wie 2D-Kulturen humaner ventrikulärer kardialer Fibroblasten (HVCF) Primärzilien enthalten.

Zusätzlich wurden zwei 3D-Modelle genutzt, um Primärzilien zu untersuchen: Engineered Connective Tissue, in dem die kardialen Fibroblasten in Kollagen I eingebettet sind, sowie Engineered Heart Muscle, welcher aus allen kardialen Zellen besteht, die ebenfalls in einer Matrix aus Kollagen I eingebettet sind. Primärzilien konnten mittels Immunfluoreszenz in Schnitten beider künstlicher Gewebe detektiert werden.

Im nächsten Schritt wurde die Regulation der Primärzilien in kardialen Fibroblasten unter Einsatz zweier Substanzen betrachtet, die nachweislich die Acetylierung von α-Tubulin erhöhen: Tubastatin A (TubA) und Lithiumchlorid (LiCl). Tubastatin A ist ein spezifischer Inhibitor von HDAC6, der wichtigsten Deacetylase von α-Tubulin. Bei Lithiumchlorid handelt es sich um eine Substanz, die die α-Tubulin-Acetylierung durch einen bisher noch unvollständig verstandenen Mechanismus erhöht, welcher wahrscheinlich die Mobilisation der α-Tubulin-N-Acetyltransferase (ATAT1) involviert, die den Transfer von Acetylgruppen auf α-Tubulin katalysiert. Beide Behandlungen (TubA, LiCl) erhöhten die α-Tubulin-Acetylierung sowohl in NRCF, NMCF als auch in AMCF, wie mittels Immunoblot-Analyse gezeigt werden konnte.

Des Weiteren wurde festgestellt, dass die Behandlung mit Lithiumchlorid die Länge der Primärzilien erhöht. Obwohl der genaue Mechanismus, der zu dieser Verlängerung der Primärzilien führt, noch nicht geklärt ist, kann es als wahrscheinlich angesehen werden, dass der Effekt durch die Inhibition der Glykogen-Synthase-Kinase 3β vermittelt wird.

Während pathologischer Prozesse, wie beispielsweise einem Myokardinfarkt, ist das Herz einem Sauerstoffmangel ausgesetzt. Hypoxische Bedingungen wurden erfolgreich in kardialen Fibroblasten neonataler Ratten induziert, wie die Stabilisierung des hypoxia inducible factor 1α (HIF-1α) zeigt. Unter den hypoxischen Bedingungen wurden die Zellen wiederum mit Tubastatin A und Lithiumchlorid behandelt, und es konnte festgestellt werden, dass Hypoxie sowohl unter Kontrollbedingungen als auch unter Lithiumchlorid-Behandlung zu einer Verlängerung der Primärzilien führt.

Schließlich wurden die Auswirkungen beider Behandlungen auf die Zellproliferation von NRCF und AMCF untersucht, und es konnte gezeigt werden, dass die Proliferationsfähigkeit von Zellen mit einer erhöhten Acetylierung von α-Tubulin-Acetylierung eingeschränkt war.

8 Bibliography

Acharya A, Baek ST, Huang G, Eskiocak B, Goetsch S, Sung CY, Banfi S, Sauer MF, Olsen GS, Duffield JS, et al. (2012): The bHLH transcription factor Tcf21 is required for lineage-specific EMT of cardiac fibroblast progenitors. Dev Camb Engl 139, 2139–2149

Ansley SJ, Badano JL, Blacque OE, Hill J, Hoskins BE, Leitch CC, Chul Kim J, Ross AJ, Eichers ER, Teslovich TM, et al. (2003): Basal body dysfunction is a likely cause of pleiotropic Bardet–Biedl syndrome. Nature 425, 628–633

Antal MC, Bénardais K, Samama B, Auger C, Schini-Kerth V, Ghandour S, Boehm N (2017): Adenylate Cyclase Type III Is Not a Ubiquitous Marker for All Primary Cilia during Development. PLoS ONE 12, e0170756

Barra HS, Rodriguez JA, Arce CA, Caputto R (1973): A Soluble Preparation from Rat Brain That Incorporates into Its Own Proteins [14c]arginine by a Ribonuclease-Sensitive System and [14c]tyrosine by a Ribonuclease-Insensitive System. J Neurochem 20, 97–108

Berbari NF, O'Connor AK, Haycraft CJ, Yoder BK (2009): The Primary Cilium as a Complex Signaling Center. Curr Biol 19, R526

Berk BC, Fujiwara K, Lehoux S (2007): ECM remodeling in hypertensive heart disease. J Clin Invest 117, 568–575

Blacque OE, Reardon MJ, Li C, McCarthy J, Mahjoub MR, Ansley SJ, Badano JL, Mah AK, Beales PL, Davidson WS, et al. (2004): Loss of C. elegans BBS-7 and BBS-8 protein function results in cilia defects and compromised intraflagellar transport. Genes Dev 18, 1630–1642

Bochaton-Piallat ML, Gabbiani G, Hinz B (2016): The myofibroblast in wound healing and fibrosis: answered and unanswered questions. F1000Research 5

Brown RD, Ambler SK, Mitchell MD, Long CS (2005): THE CARDIAC FIBROBLAST: Therapeutic Target in Myocardial Remodeling and Failure. Annu Rev Pharmacol Toxicol 45, 657–687

Butler KV, Kalin J, Brochier C, Vistoli G, Langley B, Kozikowski AP (2010): Rational Design and Simple Chemistry Yield a Superior, Neuroprotective HDAC6 Inhibitor, Tubastatin A. J Am Chem Soc 132, 10842–10846

Chalecka-Franaszek E, Chuang D-M (1999): Lithium activates the serine/threonine kinase Akt-1 and suppresses glutamate-induced inhibition of Akt-1 activity in neurons. Proc Natl Acad Sci 96, 8745–8750

Choi SY, Ryu Y, Kee HJ, Cho S-N, Kim GR, Cho JY, Kim H-S, Kim I-K, Jeong MH (2015): Tubastatin A suppresses renal fibrosis via regulation of epigenetic histone modification and Smad3-dependent fibrotic genes. Vascul Pharmacol 72, 130–140

Chu P-Y, Mariani J, Finch S, McMullen JR, Sadoshima J, Marshall T, Kaye DM (2010): Bone Marrow-Derived Cells Contribute to Fibrosis in the Chronically Failing Heart. Am J Pathol 176, 1735–1742

Chung EJ, Sohn YH, Kwon SH, Jung S-A, Lee JH (2014): Lithium chloride inhibits TGF-β1-induced myofibroblast transdifferentiation via PI3K/Akt pathway in cultured fibroblasts from Tenon's capsule of the human eye. Biotechnol Lett 36, 1217–1224

Clement CA, Kristensen SG, Møllgård K, Pazour GJ, Yoder BK, Larsen LA, Christensen ST (2009): The primary cilium coordinates early cardiogenesis and hedgehog signaling in cardiomyocyte differentiation. J Cell Sci 122, 3070–3082

Conway DE, Schwartz MA (2013): Flow-dependent cellular mechanotransduction in atherosclerosis. J Cell Sci 126, 5101–5109

Davis EE, Brueckner M, Katsanis N (2006): The emerging complexity of the vertebrate cilium: new functional roles for an ancient organelle. Dev Cell 11, 9–19

Deane JA, Verghese E, Martelotto LG, Cain JE, Galtseva A, Rosenblum ND, Watkins DN, Ricardo SD (2013): Visualizing renal primary cilia. Nephrology Carlton Vic 18, 161–168

Demos-Davies KM, Ferguson BS, Cavasin MA, Mahaffey JH, Williams SM, Spiltoir JI, Schuetze KB, Horn TR, Chen B, Ferrara C, et al. (2014): HDAC6 contributes to pathological responses of heart and skeletal muscle to chronic angiotensin-II signaling. Am J Physiol - Heart Circ Physiol 307, H252–H258

Dere R, Perkins AL, Bawa-Khalfe T, Jonasch D, Walker CL (2015): β-catenin links von Hippel-Lindau to aurora kinase A and loss of primary cilia in renal cell carcinoma. J Am Soc Nephrol 26, 553–564

Edde B, Rossier J, Caer JL, Desbruyeres E, Gros F, Denoulet P (1990): Posttranslational glutamylation of alpha-tubulin. Science 247, 83–85

Edwards NC, Moody WE, Yuan M, Warfield AT, Cramb R, Paisey RB, Geberhiwot T, Steeds RP (2015): Diffuse left ventricular interstitial fibrosis is associated with sub-clinical myocardial dysfunction in Alström Syndrome: an observational study. Orphanet J Rare Dis 10, 83

Egeberg DL, Lethan M, Manguso R, Schneider L, Awan A, Jørgensen TS, Byskov AG, Pedersen LB, Christensen ST (2012): Primary cilia and aberrant cell signaling in epithelial ovarian cancer. Cilia 1, 15

Ehnert S, Sreekumar V, Aspera-Werz RH, Sajadian SO, Wintermeyer E, Sandmann GH, Bahrs C, Hengstler JG, Godoy P, Nussler AK (2017): TGF-β1 impairs mechanosensation of human osteoblasts via HDAC6-mediated shortening and distortion of primary cilia. J Mol Med 95, 653–663

Eipper BA (1974): Properties of rat brain tubulin. J Biol Chem 249, 1407–1416

Elbedour K, Zucker N, Zalzstein E, Barki Y, Carmi R (1994): Cardiac abnormalities in the Bardet-Biedl syndrome: echocardiographic studies of 22 patients. Am J Med Genet 52, 164–169

Esteban MA, Harten SK, Tran MG, Maxwell PH (2006): Formation of primary cilia in the renal epithelium is regulated by the von Hippel-Lindau tumor suppressor protein. J Am Soc Nephrol 17, 1801–1806

Gao Y, Chu M, Hong J, Shang J, Xu D (2014): Hypoxia induces cardiac fibroblast proliferation and phenotypic switch: a role for caveolae and caveolin-1/PTEN mediated pathway. J Thorac Dis 6, 1458–1468

Gardner K, Arnoczky SP, Lavagnino M (2011): Effect of in vitro stress-deprivation and cyclic loading on the length of tendon cell cilia in situ. J Orthop Res 29, 582–587

Gerdes JM, Davis EE, Katsanis N (2009): The Vertebrate Primary Cilium in Development, Homeostasis, and Disease. Cell 137, 32–45

Gradilone SA, Radtke BN, Bogert PS, Huang BQ, Gajdos GB, LaRusso NF (2013): HDAC6 inhibition restores ciliary expression and decreases tumor growth. Cancer Res 73, 2259–2270

Gradilone SA, Pisarello MJL, LaRusso NF (2017): Primary Cilia in Tumor Biology: The Primary Cilium as a Therapeutic Target in Cholangiocarcinoma. Curr Drug Targets 18, 958-963

Horiuchi K, Amizuka N, Takeshita S, Takamatsu H, Katsuura M, Ozawa H, Toyama Y, Bonewald LF, Kudo A (1999): Identification and Characterization of a Novel Protein, Periostin, with Restricted Expression to Periosteum and Periodontal Ligament and Increased Expression by Transforming Growth Factor β. J Bone Miner Res 14, 1239–1249

Hubbert C, Guardiola A, Shao R, Kawaguchi Y, Ito A, Nixon A, Yoshida M, Wang X-F, Yao T-P (2002): HDAC6 is a microtubule-associated deacetylase. Nature 417, 455–458

Jatho A, Hartmann S, Kittana N, Mügge F, Wuertz CM, Tiburcy M, Zimmermann W-H, Katschinski DM, Lutz S (2015): RhoA Ambivalently Controls Prominent Myofibroblast Characteritics by Involving Distinct Signaling Routes. PLoS ONE 10(10): e0137519.

Kalebic N, Sorrentino S, Perlas E, Bolasco G, Martinez C, Heppenstall PA (2013): αTAT1 is the major α-tubulin acetyltransferase in mice. Nat Commun 4, ncomms2962

Kang GM, Han YM, Ko HW, Kim J, Oh BC, Kwon I, Kim M-S (2015): Leptin Elongates Hypothalamic Neuronal Cilia via Transcriptional Regulation and Actin Destabilization. J Biol Chem 290, 18146–18155

Kim J, Lee JE, Heynen S, Suyama E, Ono K, Lee K, Ideker T, Aza-Blac P, Gleeson JG (2010): Functional genomic screen for modulators of ciliogenesis and cilium length. Nature 464, 1048–1051

Kim S, Dynlacht BD (2013): Assembling a primary cilium. Curr Opin Cell Biol 25, 506–511

Klein A, Flügel D, Kietzmann T (2008): Transcriptional Regulation of Serine/Threonine Kinase-15 (STK15) Expression by Hypoxia and HIF-1. Mol Biol Cell 19, 3667–3675

Klein PS, Melton DA (1996): A molecular mechanism for the effect of lithium on development. Proc Natl Acad Sci U S A 93, 8455–8459

Koefoed K, Veland IR, Pedersen LB, Larsen LA, Christensen ST (2014): Cilia and coordination of signaling networks during heart development. Organogenesis 10, 108–125

Kollman JM, Polka JK, Zelter A, Davis TN, Agard DA (2010): Microtubule nucleating γTuSC assembles structures with 13-fold microtubule-like symmetry. Nature 466, 879–882

Kong P, Christia P, Saxena A, Su Y, Frangogiannis NG (2013): Lack of specificity of fibroblast-specific protein 1 in cardiac remodeling and fibrosis. Am J Physiol - Heart Circ Physiol 305, H1363–H1372

Kong P, Christia P, Frangogiannis NG (2014): The Pathogenesis of Cardiac Fibrosis. Cell Mol Life Sci 71, 549–574

Kong X, Lin Z, Liang D, Fath D, Sang N, Caro J (2006): Histone Deacetylase Inhibitors Induce VHL and Ubiquitin-Independent Proteasomal Degradation of Hypoxia-Inducible Factor 1α. Mol Cell Biol 26, 2019–2028

Koulen P, Cai Y, Geng L, Maeda Y, Nishimura S, Witzgall R, Ehrlich BE, Somlo S (2002): Polycystin-2 is an intracellular calcium release channel. Nat Cell Biol 4, 191–197

Kozminski KG, Johnson KA, Forscher P, Rosenbaum JL (1993): A motility in the eukaryotic flagellum unrelated to flagellar beating. Proc Natl Acad Sci 90, 5519–5523

Lal H, Ahmad F, Zhou J, Yu JE, Vagnozzi RJ, Guo Y, Yu D, Tsai EJ, Woodgett J, Gao E, Force T (2014): Cardiac Fibroblast Glycogen Synthase Kinase-3β Regulates Ventricular Remodeling and Dysfunction in Ischemic HeartCLINICAL PERSPECTIVE. Circulation 130, 419–430

L'Hernault SW, Rosenbaum JL (1983): Chlamydomonas alpha-tubulin is posttranslationally modified in the flagella during flagellar assembly. J Cell Biol 97, 258–263

Li G, Vega R, Nelms K, Gekakis N, Goodnow C, McNamara P, Wu H, Hong NA, Glynne R (2007): A Role for Alström Syndrome Protein, Alms1, in Kidney Ciliogenesis and Cellular Quiescence. PLoS Genet 3

Li L, Yang X-J (2015): Tubulin acetylation: responsible enzymes, biological functions and human diseases. Cell Mol Life Sci 72, 4237–4255

Lieu DK, Liu J, Siu C-W, McNerney GP, Tse H-F, Abu-Khalil A, Huser T, Li RA (2009): Absence of Transverse Tubules Contributes to Non-Uniform Ca2+ Wavefronts in Mouse and Human Embryonic Stem Cell–Derived Cardiomyocytes. Stem Cells Dev 18, 1493–1500

Lin Y-C, Niewiadomski P, Lin B, Nakamura H, Phua SC, Jiao J, Levchenko A, Inoue T, Rohatgi R, Inoue T (2013): Chemically-inducible diffusion trap at cilia (C-IDTc) reveals molecular sieve-like barrier. Nat Chem Biol 9, 437-443

Mann L, Heldman E, Bersudsky Y, Vatner SF, Ishikawa Y, Almog O, Belmaker RH, Agam G (2009): Inhibition of specific adenylyl cyclase isoforms by lithium and carbamazepine, but not valproate, may be related to their antidepressant effect. Bipolar Disord 11, 885–896

Marshall JD, Bronson RT, Collin GB, Nordstrom AD, Maffei P, Paisey RB, Carey C, MacDermott S, Russell-Eggitt I, Shea SE, et al. (2005): New Alström Syndrome Phenotypes Based on the Evaluation of 182 Cases. Arch Intern Med 165, 675–683

Marshall WF (2007): What is the function of centrioles? J Cell Biochem 100, 916–922

Marshall WF, Rosenbaum JL (2001): Intraflagellar transport balances continuous turnover of outer doublet microtubules. J Cell Biol 155, 405–414

Matthijs Blankesteijn W (2015): Has the search for a marker of activated fibroblasts finally come to an end? J Mol Cell Cardiol 88, 120–123

McGlashan SR, Knight MM, Chowdhury TT, Joshi P, Jensen CG, Kennedy S, Poole CA (2010): Mechanical loading modulates chondrocyte primary cilia incidence and length. Cell Biol Int 34, 441–446

McGrath J, Brueckner M (2003): Cilia are at the heart of vertebrate left-right asymmetry. Curr Opin Genet Dev 13, 385–392

Mcguane JT, Parry LJ (2005): relaxin and the extracellular matrix: molecular mechanisms of action and implications for cardiovascular disease. Expert Rev Mol Med 7, 1–18

Metzen E, Ratcliffe PJ (2004): HIF hydroxylation and cellular oxygen sensing. Biol Chem 385, 223–230

Miyoshi K, Kasahara K, Miyazaki I, Asanuma M (2009): Lithium treatment elongates primary cilia in the mouse brain and in cultured cells. Biochem Biophys Res Commun 388, 757–762

Miyoshi K, Kasahara K, Miyazaki I, Asanuma M (2011): Factors that influence primary cilium length. Acta Med Okayama 65, 279–285

Möllmann H, Nef HM, Kostin S, von Kalle C, Pilz I, Weber M, Schaper J, Hamm CW, Elsässer A (2006): Bone marrow-derived cells contribute to infarct remodelling. Cardiovasc Res 71, 661–671

Montorfano I, Becerra A, Cerro R, Echeverría C, Sáez E, Morales MG, Fernández R, Cabello-Verrugio C, Simon F (2014): Oxidative stress mediates the conversion of endothelial cells into myofibroblasts via a TGF-β1 and TGF-β2-dependent pathway. Lab Investig J Tech Methods Pathol 94, 1068–1082

Moore-Morris T, Guimarães-Camboa N, Banerjee I, Zambon AC, Kisseleva T, Velayoudon A, Stallcup WB, Gu Y, Dalton ND, Cedenilla M, et al. (2014): Resident fibroblast lineages mediate pressure overload–induced cardiac fibrosis. J Clin Invest 124, 2921–2934

Muneer A (2017): Wnt and GSK3 Signaling Pathways in Bipolar Disorder: Clinical and Therapeutic Implications. Clin Psychopharmacol Neurosci 15, 100–114

Myklebust R, Engedal H, Saetersdal TS, Ulstein M (1977): Primary 9 + 0 cilia in the embryonic and the adult human heart. Anat Embryol (Berl) 151, 127–139

Naito H, Melnychenko I, Didié M, Schneiderbanger K, Schubert P, Rosenkranz S, Eschenhagen T, Zimmermann W-H (2006): Optimizing Engineered Heart Tissue for Therapeutic Applications as Surrogate Heart Muscle. Circulation 114, I-72-I-78

Nakakura T, Asano-Hoshino A, Suzuki T, Arisawa K, Tanaka H, Sekino Y, Kiuchi Y, Kawai K, Hagiwara H (2015): The elongation of primary cilia via the acetylation of α-tubulin by the treatment with lithium chloride in human fibroblast KD cells. Med Mol Morphol 48, 44–53

Nauli SM, Alenghat FJ, Luo Y, Williams E, Vassilev P, Li X, Elia AEH, Lu W, Brown EM, Quinn SJ, et al. (2003): Polycystins 1 and 2 mediate mechanosensation in the primary cilium of kidney cells. Nat Genet 33, 129–137

Nauli SM, Kawanabe Y, Kaminski JJ, Pearce WJ, Ingber DE, Zhou J (2008): Endothelial Cilia Are Fluid Shear Sensors That Regulate Calcium Signaling and Nitric Oxide Production Through Polycystin-1. Circulation 117, 1161–1171

Olson LE, Soriano P (2009): Increased PDGFRα Activation Disrupts Connective Tissue Development and Drives Systemic Fibrosis. Dev Cell 16, 303–313

Ou Y, Ruan Y, Cheng M, Moser JJ, Rattner JB, van der Hoorn FA (2009): Adenylate cyclase regulates elongation of mammalian primary cilia. Exp Cell Res 315, 2802–2817

Ou Y, Zhang Y, Cheng M, Rattner JB, Dobrinski I, Hoorn FA van der (2012): Targeting of CRMP-2 to the Primary Cilium Is Modulated by GSK-3β. PLOS ONE 7, e48773

Peng H, Sarwar Z, Yang X-P, Peterson EL, Xu J, Janic B, Rhaleb N, Carretero OA, Rhaleb N-E (2015): Profibrotic Role for Interleukin-4 in Cardiac Remodeling and DysfunctionNovelty and Significance. Hypertension 66, 582–589

Pinto AR, Ilinykh A, Ivey MJ, Kuwabara JT, D'Antoni ML, Debuque R, Chandran A, Wang L, Arora K, Rosenthal NA, Tallquist MD (2016): Revisiting Cardiac Cellular CompositionNovelty and Significance. Circ Res 118, 400–409

Piperno G, Fuller MT (1985): Monoclonal antibodies specific for an acetylated form of alpha-tubulin recognize the antigen in cilia and flagella from a variety of organisms. J Cell Biol 101, 2085–2094

Plotnikova OV, Pugacheva EN, Golemis EA (2009): Primary cilia and the cell cycle. Methods Cell Biol 94, 137–160

Praetorius HA (2015): The primary cilium as sensor of fluid flow: new building blocks to the model. A Review in the Theme: Cell Signaling: Proteins, Pathways and Mechanisms. Am J Physiol - Cell Physiol 308, C198–C208

Praetorius HA, Spring KR (2001): Bending the MDCK cell primary cilium increases intracellular calcium. J Membr Biol 184, 71–79

Privratsky JR, Newman PJ (2014): PECAM-1: regulator of endothelial junctional integrity. Cell Tissue Res 355, 607–619

Proulx-Bonneau S, Annabi B (2011): The Primary Cilium as a Biomarker in the Hypoxic Adaptation of Bone Marrow-Derived Mesenchymal Stromal Cells: A Role for the Secreted Frizzled-Related Proteins. Biomark Insights 2011, 107–118

Pugacheva EN, Jablonski SA, Hartman TR, Henske EP, Golemis EA (2007): HEF1-dependent Aurora A activation induces disassembly of the primary cilium. Cell 129, 1351–1363

Qian DZ, Kachhap SK, Collis SJ, Verheul HMW, Carducci MA, Atadja P, Pili R (2006): Class II Histone Deacetylases Are Associated with VHL-Independent Regulation of Hypoxia-Inducible Factor 1α. Cancer Res 66, 8814–8821

Ran J, Yang Y, Li D, Liu M, Zhou J (2015): Deacetylation of α-tubulin and cortactin is required for HDAC6 to trigger ciliary disassembly. Sci Rep 5, srep12917

Redeker V, Levilliers N, Schmitter JM, Caer JL, Rossier J, Adoutte A, Bre MH (1994): Polyglycylation of tubulin: a posttranslational modification in axonemal microtubules. Science 266, 1688–1691

Resnick A, Hopfer U (2007): Force-Response Considerations in Ciliary Mechanosensation. Biophys J 93, 1380–1390

Rieder CL, Jensen CG, Jensen LC (1979): The resorption of primary cilia during mitosis in a vertebrate (PtK1) cell line. J Ultrastruct Res 68, 173–185

Ryves WJ, Harwood AJ (2001): Lithium inhibits glycogen synthase kinase-3 by competition for magnesium. Biochem Biophys Res Commun 280, 720–725

Saggese T, Young AA, Huang C, Braeckmans K, McGlashan SR (2012): Development of a method for the measurement of primary cilia length in 3D. Cilia 1, 11

Sánchez de Diego A, Alonso Guerrero A, Martínez-A C, van Wely KHM (2014): Dido3-dependent HDAC6 targeting controls cilium size. Nat Commun 5, 3500

Satir P, Pedersen LB, Christensen ST (2010): The primary cilium at a glance. J Cell Sci 123, 499–503

Schimmack S, Kneller S, Dadabaeva N, Bergmann F, Taylor A, Hackert T, Werner J, Strobel O (2016): Epithelial to Stromal Re-Distribution of Primary Cilia during Pancreatic Carcinogenesis. PLoS ONE 11, e0164231

Secrist JP, Zhou X, Richon VM (2003): HDAC inhibitors for the treatment of cancer. Curr Opin Investig Drugs 2000 4, 1422–1427

Seeley ES, Carrière C, Goetze T, Longnecker DS, Korc M (2009): Pancreatic Cancer and Precursor PanIN Lesions Are Devoid of Primary Cilia. Cancer Res 69, 422–430

Segura AM, Frazier OH, Buja LM (2014): Fibrosis and heart failure. Heart Fail Rev 19, 173–185

Shaldubina A, Agam G, Belmaker RH (2001): The mechanism of lithium action: state of the art, ten years later. Prog Neuropsychopharmacol Biol Psychiatry 25, 855–866

Sharma N, Kosan ZA, Stallworth JE, Berbari NF, Yoder BK (2011): Soluble levels of cytosolic tubulin regulate ciliary length control. Mol Biol Cell 22, 806–816

Shida T, Cueva JG, Xu Z, Goodman MB, Nachury MV (2010): The major α-tubulin K40 acetyltransferase αTAT1 promotes rapid ciliogenesis and efficient mechanosensation. Proc Natl Acad Sci U S A 107, 21517–21522

Snider P, Hinton RB, Moreno-Rodriguez RA, Wang J, Rogers R, Lindsley A, Li F, Ingram DA, Menick D, Field L, et al. (2008): Periostin Is Required for Maturation and Extracellular Matrix Stabilization of Noncardiomyocyte Lineages of the Heart. Circ Res 102, 752–760

Song KS, Scherer PE, Tang Z, Okamoto T, Li S, Chafel M, Chu C, Kohtz DS, Lisanti MP (1996): Expression of caveolin-3 in skeletal, cardiac, and smooth muscle cells. Caveolin-3 is a component of the sarcolemma and co-fractionates with dystrophin and dystrophin-associated glycoproteins. J Biol Chem 271, 15160–15165

Soppina V, Herbstman JF, Skiniotis G, Verhey KJ (2012): Luminal Localization of α-tubulin K40 Acetylation by Cryo-EM Analysis of Fab-Labeled Microtubules. PLoS ONE 7, e48204

Souders CA, Bowers SLK, Baudino TA (2009): Cardiac Fibroblast: The Renaissance Cell. Circ Res 105, 1164–1176

Spasic M, Jacobs CR (2017): Lengthening primary cilia enhances cellular mechanosensitivity. Eur Cell Mater 33, 158–168

Stein M, Boulaksil M, Jansen JA, Herold E, Noorman M, Joles JA, Veen TAB van, Houtman MJC, Engelen MA, Hauer RNW et al. (2010): Reduction of fibrosis-related arrhythmias by chronic renin-angiotensin-aldosterone system inhibitors in an aged mouse model. Am J Physiol - Heart Circ Physiol 299, H310–H321

Szyk A, Deaconescu AM, Spector J, Goodman B, Valenstein ML, Ziolkowska NE, Kormendi V, Grigorieff N, Roll-Mecak A (2014): Molecular basis for age-dependent microtubule acetylation by tubulin acetyltransferase. Cell 157, 1405–1415

Tan PL, Barr T, Inglis PN, Mitsuma N, Huang SM, Garcia-Gonzalez MA, Bradley BA, Coforio S, Albrecht PJ, Watnick T, et al. (2007): Loss of Bardet–Biedl syndrome proteins causes defects in peripheral sensory innervation and function. Proc Natl Acad Sci 104, 17524–17529

Thoma CR, Frew IJ, Hoerner CR, Montani M, Moch H, Krek W (2007): pVHL and GSK3β are components of a primary cilium-maintenance signalling network. Nat Cell Biol 9, 588–595

Thompson CL, Chapple JP, Knight MM (2014): Primary cilia disassembly down-regulates mechanosensitive hedgehog signalling: a feedback mechanism controlling ADAMTS-5 expression in chondrocytes. Osteoarthritis Cartilage 22, 490–498

Thompson CL, Wiles A, Poole CA, Knight MM (2016): Lithium chloride modulates chondrocyte primary cilia and inhibits Hedgehog signaling. FASEB J 30, 716–726

Tillmanns J, Hoffmann D, Habbaba Y, Schmitto JD, Sedding D, Fraccarollo D, Galuppo P, Bauersachs J (2015): Fibroblast activation protein alpha expression identifies activated fibroblasts after myocardial infarction. J Mol Cell Cardiol 87, 194–203

Tobin DM, Madsen DM, Kahn-Kirby A, Peckol EL, Moulder G, Barstead R, Maricq AV, Bargmann CI (2002): Combinatorial expression of TRPV channel proteins defines their sensory functions and subcellular localization in C. elegans neurons. Neuron 35, 307–318

Troilo A, Alexander I, Muehl S, Jaramillo D, Knobeloch K-P, Krek W (2014): HIF1α deubiquitination by USP8 is essential for ciliogenesis in normoxia. EMBO Rep 15, 77–85

Ugolini GS, Pavesi A, Rasponi M, Fiore GB, Kamm R, Soncini M (2017): Human cardiac fibroblasts adaptive responses to controlled combined mechanical strain and oxygen changes in vitro. eLife 6, e22847

Van der Heiden K, Hierck BP, Krams R, de Crom R, Cheng C, Baiker M, Pourquie MJBM, Alkemade FE, DeRuiter MC, Gittenberger-de Groot AC, Poelmann RE (2008): Endothelial primary cilia in areas of disturbed flow are at the base of atherosclerosis. Atherosclerosis 196, 542–550

Veland IR, Lindbæk L, Christensen ST (2014): Linking the Primary Cilium to Cell Migration in Tissue Repair and Brain Development. Bioscience 64, 1115–1125

Verghese E, Weidenfeld R, Bertram JF, Ricardo SD, Deane JA (2008): Renal cilia display length alterations following tubular injury and are present early in epithelial repair. Nephrol Dial Transplant 23, 834–841

Verghese E, Zhuang J, Saiti D, Ricardo SD, Deane JA (2011): In vitro investigation of renal epithelial injury suggests that primary cilium length is regulated by hypoxia-inducible mechanisms. Cell Biol Int 35, 909–913

Vishwakarma S, Iyer LR, Muley M, Singh PK, Shastry A, Saxena A, Kulathingal J, Vijaykanth G, Raghul J, Rajesh N, et al. (2013): Tubastatin, a selective histone deacetylase 6 inhibitor shows anti-inflammatory and anti-rheumatic effects. Int Immunopharmacol 16, 72–78

Walker RG, Bennett WM, Davies BM, Kincaid-Smith P (1982): Structural and functional effects of long-term lithium therapy. Kidney Int Suppl 11, S13-19

Watson CJ, Collier P, Tea I, Neary R, Watson JA, Robinson C, Phelan D, Ledwidge MT, McDonald KM, McCann A, et al. (2014): Hypoxia-induced epigenetic modifications are associated with cardiac tissue fibrosis and the development of a myofibroblast-like phenotype. Hum Mol Genet 23, 2176–2188

Wu CF, Chiang WC, Lai CF, Chang FC, Chen YT, Chou YH, Wu TH, Linn GR, Ling H, Wu KD, et al. (2013): Transforming Growth Factor β-1 Stimulates Profibrotic Epithelial Signaling to Activate Pericyte-Myofibroblast Transition in Obstructive Kidney Fibrosis. Am J Pathol 182, 118–131

Xiang W, Guo F, Cheng W, Zhang J, Huang J, Wang R, Ma Z, Xu K (2017): HDAC6 inhibition suppresses chondrosarcoma by restoring the expression of primary cilia. Oncol Rep 38, 229–236

Xu J, Li H, Wang B, Xu Y, Yang J, Zhang X, Harten SK, Shukla D, Maxwell PH, Pei D, Esteban MA (2010): VHL Inactivation Induces HEF1 and Aurora Kinase A. J Am Soc Nephrol 21, 2041–2046

Xu Q, Liu W, Liu X, Liu W, Wang H, Yao G, Zang L, Hayashi T, Tashiro S-I, Onodera S, Ikejima T (2016): Silibinin negatively contributes to primary cilia length via autophagy regulated by histone deacetylase 6 in confluent mouse embryo fibroblast 3T3-L1 cells. Mol Cell Biochem 420, 53–63

Xu Q, Liu W, Liu X, Otkur W, Hayashi T, Yamato M, Fujisaki H, Hattori S, Tashiro S-I, Ikejima T (2017): Type I collagen promotes primary cilia growth through down-regulating HDAC6-mediated autophagy in confluent mouse embryo fibroblast 3T3-L1 cells. J Biosci Bioeng 125, 8-14

Yano T, Miura T, Ikeda Y, Matsuda E, Saito K, Miki T, Kobayashi H, Nishino Y, Ohtani S, Shimamoto K (2005): Intracardiac fibroblasts, but not bone marrow derived cells, are the origin of myofibroblasts in myocardial infarct repair. Cardiovasc Pathol 14, 241–246

Zhang B, Zhang T, Wang G, Wang G, Chi W, Jiang Q, Zhang C (2015): GSK3β-Dzip1-Rab8 Cascade Regulates Ciliogenesis after Mitosis. PLoS Biol 13

Zhang D, Wu C-T, Qi X, Meijering RAM, Hoogstra-Berends F, Tadevosyan A, Deniz GC, Durdu S, Akar AR, Sibon OCM, et al. (2014a): Activation of Histone Deacetylase-6 Induces Contractile Dysfunction Through Derailment of α-Tubulin Proteostasis in Experimental and Human Atrial Fibrillation CLINICAL PERSPECTIVE. Circulation 129, 346–358

Zhang L, Liu C, Wu J, Tao J, Sui X, Yao Z, Xu Y, Huang L, Zhu H, Sheng S, Qin C (2014b): Tubastatin A/ACY-1215 Improves Cognition in Alzheimer's Disease Transgenic Mice. J Alzheimers Dis 41, 1193–1205

Zhou B, Pu WT (2011): Epicardial epithelial-to-mesenchymal transition in injured heart. J Cell Mol Med 15, 2781–2783

Zimmermann W-H, Schneiderbanger K, Schubert P, Didié M, Münzel F, Heubach JF, Kostin S, Neuhuber WL, Eschenhagen T (2002): Tissue Engineering of a Differentiated Cardiac Muscle Construct. Circ Res 90, 223–230

9 Own publications

Jatho A, Hartmann S, Kittana N, **Mügge F**, Wuertz CM, Tiburcy M, Zimmermann W-H, Katschinski DM, Lutz S (2015): RhoA Ambivalently Controls Prominent Myofibroblast Characteristics by Involving Distinct Signaling Routes. PLoS ONE 10(10): e0137519.